Synthesis and Testing of diaryl sulphide based Fluorine-18 Radiotracers for Positron Emission Tomography of Hypoxic Tumours

Lee Wenn Chong

Submitted in total fulfillment of the requirements of the degree of

Doctor of Philosophy

March 2019

School of Chemistry

The University of Melbourne

Abstract

Hypoxia is a critical physiological marker demonstrated in a variety of cancers, imaging it will provide valuable insight into prognosis and treatment. However, the slow kinetics of [^{18}F]FMISO(**1.2**) means that there is a 2 hour delay between injection and imaging for patients. Fluorine-18 labelled Chloroethyl sulfoxides [^{18}F]SO101 and [^{18}F]SO201 were shown to have both faster kinetics and higher contrast compared to [^{18}F]FMISO(**1.2**) in a rat model of ischemic stroke. Perceived toxicity from the nitrogen mustard analogues in [^{18}F]SO101 and [^{18}F]SO201 lead to structural changes resulting in [^{18}F]SO501. [^{18}F]SO501 demonstrated good uptake into hypoxic SK-RC-52 tumours while also clearing from muscle, giving good contrast and therefore high-quality images, however it had a low radiochemical yield of 2.5% making it impractical for routine clinical application.

Structural changes were made to the base compound [^{18}F]SO501 in order to adapt it to a different method of radiolabelling in an attempt to increase the RCY while maintaining its selectivity for hypoxic tissue. The modifications made included the introduction of a propargyl group for click chemistry, variable length PEG groups and alterations to the ester group from an ethyl ester to an isopropyl ester and in one case doing away with it entirely. Six different diaryl-sulfoxide radiolabelled compounds were synthesised for this project **[^{18}F]2.16**, **[^{18}F]2.26**, **[^{18}F]2.36**, **[^{18}F]2.43**, **[^{18}F]2.53** and **[^{18}F]2.63** from their respective diaryl-sulfoxide precursors **2.15**, **2.25**, **2.35**, **2.42**, **2.52** and **2.62**.

After in-vivo imaging in SK-RC-52 tumours xenografted onto BALB/c nude mice the most promising tracer **[^{18}F]2.16**, which had the best tumour to muscle ratio of 1.6 at 60 minutes and 2.1 at 110min, underwent metabolism studies involving Rat S9 liver fractions.

Declaration

This is to certify that:

I. The thesis comprises only of my original work towards the Ph. D. except where indicated on the Preface

II. Due acknowledgement has been made in the text to all materials used

III. The thesis is less than 100, 000 words in length

Lee Wenn Chong

March 2019

Acknowledgments

This thesis and research project have been 6 years in the making and would not have been remotely possible if not for the support and encouragement of many people throughout the years.

First and foremost is my supervisors Jonathan White and Uwe Ackermann. Jonathan thank-you for all the support and understanding with all the trials and tribulations I've put you through. Including both this Ph.D. project and a Masters project before that. As a member of your group for 8 years and knowing you for 3 years prior to that, your patience, knowledge and tolerance have always been welcome.

Uwe Ackermann thank you for all the help and support provided out at the Austin hospital where all the radiochemistry experiments were conducted.

Special thanks to Rachel Goh whose knowledge and teaching made this all possible. None of the radiolabelling would have been done if not for the direct supervision you provided.

To the past and present members of the White group including but not limited to Christian Wichmann, Alex Macdonald, Jesse Roth-Barton, Ben Harris, Andrew Tilley, Asimo Karnezis, David Tso, Kim Kwan, Rebecca Szabai, Evelyn Laurens, John Li and Sacha Novakovic thanks for all the help throughout the years and for all the awesome fun. Something to note here is that Evelyn Laurens was my demonstrator when I started chemistry as a fresh first year and it is in her path I have followed into the wonderful world of radiochemistry.

Thank-you to my parents and sister for always been there by me with their love and support and to my girlfriend Ming who has been a wonder in my life so far.

Finally thank-you for taking the time and effort to read this labour of 6 years, I won't say love because it's had its ups and downs but at least it is more or less finished.

Table of Contents

List of Figures

List of Schemes

List of Tables

List of abbreviations

δ	chemical shift
µL	micro litre
ACN	acetonitrile
aq.	Aqueous
β^+	Positron Emission
β^-	Beta Decay
cpm	counts per minute
CT	computed tomography
d	doublet
dd	doublet of doublets
DCM	dichloromethane
DMF	dimethylformamide
dt	doublet of triplets
EC	Electron capture
ESI	electrospray ionisation
eq	equivalents
Et	Ethyl
EtOH	Ethanol
FDG	fluorodeoxyglucose
FMISO	fluoromisonidazole
GBq	gigabecquerel
HPLC	high performance liquid chromatography
h	hours
IR	infrared

M	molar concentration
m	multiplet
mCi	millicurie
Me	methyl
MeV	mega electron volt
meslyate	methanesulfonate
mL	millilitre
mm	millimetre
mm^3	millimetres cubed
mmHg	millimetre mercury
min	minutes
NADP	nicotinamide adenine dinucleotide phosphate
NADPH	nicotinamide adenine dinucleotide phosphate-oxidase
nm	nanometre
NMR	nuclear magnetic resonance
PEG	Polyethylene glycol
PET	positron emission tomography
Ph	phenyl
ppm	parts per million
pO_2	partial pressure of oxygen
PVP	Polyvinyl pyridine 2% crosslinked
QC	quality control
RCY	radiochemical yield
rt	room temperature
sat.	saturated
t	triplet
TAC	time activity curve
t/m	tumour to muscle ratio

triflate	trifluoromethanesulfonate
UV	ultraviolet

1 Introduction

1.1 Hypoxia

Hypoxia is a physiological condition that is characterised by a critically low partial pressure of intercellular oxygen (pO_2) in tissue.[2-4] There are 4 primary types of hypoxia; hypoxic hypoxia, anaemic hypoxia, ischemic hypoxia and histotoxic hypoxia. Hypoxic hypoxia is a reduction in the amount of arterial oxygen available to the body, arising from oxygen failing to reach the lungs through blocked airways or a lack of environmental oxygen, such as high altitudes or drowning.

Anaemic hypoxia is a failure in the proper transportation of oxygen in the blood supply, with causes including defects in haemoglobin or low haemoglobin levels. Histotoxic hypoxia is a deficiency in the cells that prevents them from utilising available oxygen, cyanide poisoning is one possible cause for this. Ischemic hypoxia is when inadequate blood supply reaches tissue with causes including tissue damage or embolic events. [2, 5]

Tissue hypoxia is a form of ischemic hypoxia; it occurs in a localised region and can detrimentally affect surrounding tissue and organs.[3-4] It plays an important role in many diseases such as stroke, diabetes and cancer.[6]

1.1.1 Hypoxia in tumours

Hypoxia can be found in many varieties of human tumours, and are a result of tissue growth outstripping the development of new blood vessels, depriving the local region of adequate oxygen due to the reduced blood supply.[6-12]

The level of oxygenation in tissue is measure in terms of partial pressure (pO_2) where a pO_2 of between 40mmHg and 60mmHg is typical for normoxic cells.[4-5, 13] When a pO_2 of less than 20mmHg is observed the tissue is considered hypoxic; tumours can have a pO_2 ranging from 2.5mmHg to 20mmHg depending on their type.[5, 13-14]

Treating hypoxic tumours is significantly more difficult due to their increased resistance to the effects of radiotherapy and chemotherapy compared to non-hypoxic cancer cells. [9, 11, 13, 15-16] Oxygen is believed to act as a radiosensitiser during radiotherapy, enhancing the cell kill rate, however since hypoxic cells have lower levels of oxygen the lethal effect of radiation is decreased.[2, 13, 17] Oxygen's electron affinity allows it to participate in

chemical reactions that would lead to DNA damage within the cell, leading to cell death, after the absorption of ionising radiation. [18] An example of this could be through the formation of superoxides, O_2^-, through chemically incapable of causing damage to DNA, it is believed that it can participate in release of iron by damaging dehydratases. The increase in free iron then increases the rate of DNA damage by exogenous or endogenous H_2O_2 through the Fenton reaction. The damage caused could be directly to the DNA, causing strand breakage, and/or to the DNA repair mechanisms .[19]

The radiation dose required for a hypoxic cell kill level is 2-3 times that of normoxic cells.[20-21] Additionally, hypoxia can cause changes in the cell environment, which can negatively impact on the cell killing ability of chemotherapeutic agents.[22] Highly aggressive tumours are often associated with high levels of tumour hypoxia leading to a poor prognosis.[9, 23-25] Hypoxia has an important role in the malignant progression of solid tumours as illustrated in Figure 1-1.[26]

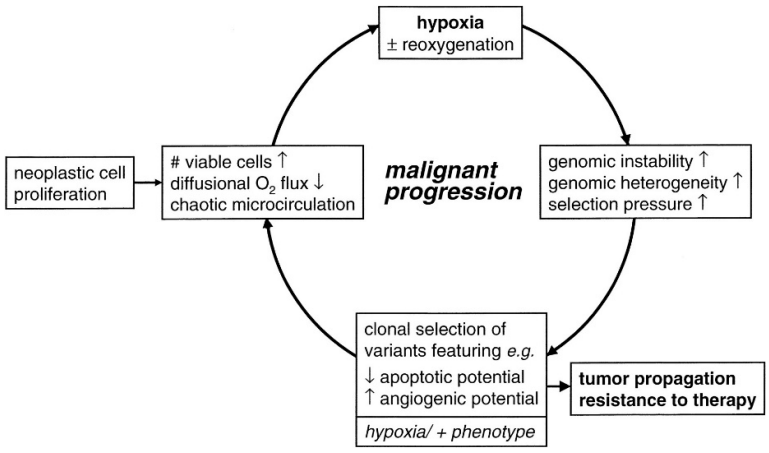

Figure 1-1: The Role of hypoxia in malignant tumour progression[26]

Even if standard treatment methods have lower effectiveness, hypoxia itself is an attractive physiological target that can be exploited for treatment using 2 different

strategies. The first strategy is to utilise prodrugs for chemotherapy which are activated by hypoxia.[6, 10, 27] This means that to non-hypoxic regions the prodrug will be benign causing no noticeable effect but when localised into a hypoxic region they will undergo chemical changes causing them to become cytotoxic. The second strategy for tumour control is to use a hypoxia-activated radiosensitiser. Radiosensitisers are compounds designed to enhance the damaging effects of radiotherapy, for hypoxic radiosensitisers this would act in chemically similar way to oxygen.[28] Additionally, several of the cytotoxic prodrugs have the potential to also act as radiosensitisers, although this is still subject to further investigation. [29-30]

Previous technologies for measuring the level of oxygenation in tissue include the polarographic oxygen electrode.[2, 9, 14, 31-32] While the method provided a detailed quantitative measure of hypoxia it had several short comings.[13] It is highly invasive and does not provide a detailed map of the tumour; a specialist is also required to perform the procedure and interpret the results, and therefore it was unsuitable for routine clinical applications.[7, 9, 13, 16, 20]

A more suitable technique was therefore required to assess tumour hypoxia. Ideally this technique would be straight forward, non-invasive and quick. It also had to be reliable and to be adaptable into routine clinical settings.[33-34]

1.1.2 Hypoxia and positron emission tomography (PET)

Positron Emission Tomography (PET) is a non-invasive imaging technique that provides a possibility for the imaging of hypoxic tumours.[2, 13] PET is routinely used in the clinical management of cancer patients having emerged as a powerful diagnostic tool for hypoxia.[16, 35-36]

Given the importance of the role hypoxia plays in tumour growth and control, assessing the hypoxic fraction of the tumour will play a part in properly understanding tumour stages. New advances in PET imaging technology also allow for the possibility of hypoxia targeted radiotherapy through the use of conformal radiotherapy and imaging directed radiotherapy. This will allow for not only the diagnosis of hypoxia in tumours but will also aid in the planning for proper tumour treatment.

1.1.3 Application of PET

PET is a non-invasive nuclear medicine imaging technology that utilises biologically relevant radiotracers, labelled with relatively short-lived positron emitting radionuclide, to measure and quantify physiological processes in-vivo.[12, 37] PET has been used to measure processes including but not limited to: metabolism, blood flow, signal transduction, gene expression, proliferation and drug pharmacokinetics.[16, 38] The use of a radioactive tracer which is applied either orally, intravenously or by inhalation allows the construction of a PET image.[39] This provides the possibility of in-vivo mapping showing the regional locations of tumour hypoxia with a high sensitivity and at high resolution.[35, 40]

1.2 Basic principles of PET

PET utilises short-lived radionuclides that emit positrons for in-vivo imaging using biologically relevant biomarker molecules and the resulting positron emission and annihilation event.[2, 41] This is demonstrated in Figure 1-2 where a positron emitting radio nuclide undergoes decay resulting in the formation of a neutron with a radiated positron, the positron generally travels a distance of 3-5mm before colliding with an electron from the surrounding tissue.[39, 42-43] The collision results in the annihilation of both particles, producing a pair of gamma rays (photons) at 511 KeV emitted in opposite directions. [44-45]

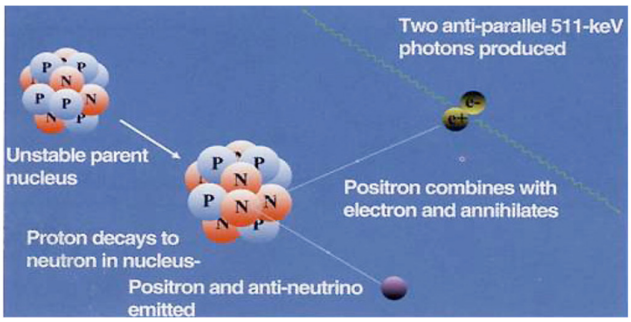

Figure 1-2: Illustration of the annihilation process involved in PET[39]

The PET scanner uses circular detectors to observe coincidence events; if 2 gamma rays are detected 180° apart with a delay of less than 12ns then it is registered as a positive event. Detected events then lead to the localisation of the origin of the event and mapping these events forms the image for the PET scan.

1.2.1 Instrumentation in PET

1.2.1.1 PET scanner

A typical PET scanner will include a detector ring with multiple layers of detector rings; each detector consists of scintillator crystals coupled to a photomultiplier.[42] A typical PET scanner will have 20,000 scintillator crystals coupled to hundreds of photomultipliers.

The scintillator crystals are chosen for their ability to absorb the high energy 511 keV photons emitted during PET imaging. They are excited by the photons and then de-excite by emitting visible scintillation light that can be detected by a photomultiplier.[39]

The signals are sent from the photomultiplier to a computer where it is used to calculate and map coincident events with strikes to the detector rings only counting if the strikes are at a 180° angle and within 12ns of each other. An image can then be constructed from the coincidence events to map the local aggregations of the radiotracer within the body.[39]

The PET scanners available at the Austin Health, where all imaging will be carried out for this thesis, are Philips Allegro PET and Philips Gemini PET/CT scanners. The combination of a PET system with a CT system provides a distinct advantage as it allows a correlation between the PET image and anatomical location generated by the CT scan.[13] This aids in the interpretation of the PET data providing biologically relevant data. CT can also aid in the reconstruction of the images allowing for quicker and more detailed PET images. Animal PET is used to generate similar images within small animal models. Small animal PET will be discussed further in chapter 4.

1.2.1.2 Cyclotron

Cyclotrons are particle accelerators able to generate radioisotopes through the bombardment of stable isotopes. Austin Health has 2 cyclotrons: an IBA cyclone 10/5 and 18/9 (Louvain-la-Neuve, Belgium). The IBA cyclone 10/5 is capable of accelerating H^- ions to 10 MeV and D^- ions to 5 MeV and the IBA cyclone 18/9 can accelerate H^- ions to 18 MeV and D^- ions to 9 MeV. Cyclotrons work by accelerating particles using a high frequency alternating voltage between 2 D shaped metal sheet electrodes. As the speed of the particle increases, they are forced to the outside until they eventually pass through the stripper foil, which is a thin carbon foil where they are stripped of electrons, resulting in the formation of the positively charged H^+ or D^+ ions.[46] The change in the charge causes ions to spin in the opposite direction due to the magnetic field, directing them into a gap between the sheets towards the target. These charged ions then bombard the stable isotopes contained inside the target.

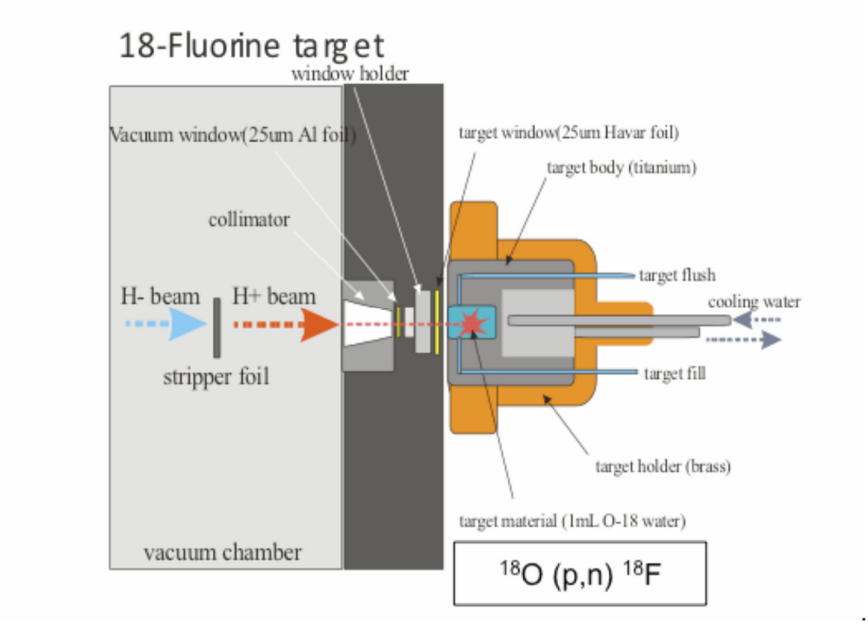

Figure 1-3: Diagram of Fluorine-18 production in a Cyclotron[1]

1.2.1.3 Targetry

The cyclone 10/5 and cyclone 18/9 located at Austin Health have 8 targets, which are attached directly to the vacuum chamber surrounding the cyclotrons located inside the return yoke of the magnetic field. Gas pressure is utilised for the loading and unloading of the targets, from where the produced radioisotopes are transported to shielded hot cells for radiolabelling experiments.

1.2.2 PET radioisotopes

Commonly used PET radioisotopes include oxygen-15 (^{15}O), nitrogen-13 (^{13}N), carbon-11 (^{11}C) and fluorine-18(^{18}F). These and a few more radioisotopes are listed on Table 1-1.[47-48] The most important feature of these radioisotopes is that their decay process is via positron emission (β^+ decay), however not all the listed radioisotopes in Table 1-1 undergo positron emission as their major mode of decay.[16, 49] Radioisotopes with

different decay types are useful for different purposes, they must be selected appropriately. Using the correct isotope is important as there are limits to the amount of radiation that can be used depending on the task. A PET scan for example requires a high β^+ decay, using an incorrect radioisotope will have high dosimetry leading to excess irradiation without providing useful imagery. In the same vain, these isotopes cannot also be used for treatment. Lu-177 is an isotope that can be used for therapeutical treatments but not in a PET scan as it has no positron emission.

Table 1-1: List of Radioisotopes, their respective half-lives and percent of decay types[49]

Radioisotopes	Half-Life	% (Decay Mode)
Oxygen-15	2.07 minutes	β^+ 100%
Nitrogen-13	10.0 minutes	β^+ 100%
Carbon-11	20.4 minutes	β^+ 100%
Gallium-68	68 minutes	β^+ 87%
Fluorine-18	109.8 minutes	β^+ 97%
Iron-52	8.3 hours	β^+ 57%
Copper-64	12.7 hours	β^+ 19% β^- 39% EC 43%
Zirconium-89	3.3 days	β^+ 23% EC 77%
Iodine-124	4.2 days	β^+ 25% EC 74%
Lutetium-177	6.6 days	B^- 100%
Rubidium-84	33 days	β^+ 96.2% β^- 3.8%

Radioisotopes such as C-11, N-13, O-15 and F-18 are useful for the evaluation of cell functional processes because they can be introduced into the structure of a molecule without altering the chemical structure radically and thereby preserving most of its biological properties. The radioisotopes therefore allow the tracing of the molecule upon its introduction to the body along with the distribution studies for the molecule's metabolism.[41]

1.2.2.1 Production of PET radioisotopes

PET radioisotopes are generated via a nuclear reaction in a cyclotron, it involves the collision of a high energy particles typically either deuterons or protons with the nucleus of a stable atom. The result of the collision is the generation of a radioactive nucleus. Table 1-2 shows the production method for commonly used radionuclides.[45, 47]

Table 1-2: Commonly used radioisotopes with their respective production methods and positron energy[47]

Radionuclides	Nuclear Reaction	MeV
Oxygen-15	$^{14}N(d,n)^{15}O$	1.70
Nitrogen-13	$^{16}O(p,\alpha)^{13}N$	1.19
Carbon-11	$^{14}N(p,\alpha)^{11}C$	0.96
Fluorine-18	$^{18}O(p,n)^{18}F$	0.635

The nuclear reactions shown have 4 vital components; the stable nucleus, the incoming charged particle, the particle emitted upon collision and the resulting radionuclide. Taking carbon-11 for example, in this case it is denoted as $^{14}N(p,\alpha)^{11}C$, the first chemical is the starting stable isotope, the particles denoted in the parenthesis are the particle accelerated and then the particle emitted and finally the last isotope is the radionuclide formed. The formation of Carbon-11 starts with inert Nitrogen-14, a proton is accelerated into the nitrogen nucleus. The resulting collision causes the emission of an alpha particle (a nucleus with 2 protons and 2 neutrons with no surrounding elections) resulting in Carbon-11 being formed. Once the desired radionuclide is formed in the cyclotron, it is then moved into a hot cell for radiolabelling the desired precursor molecule.

1.2.3 Fluorine-18 radioisotope

For this study Fluorine-18 was chosen as the radionuclide for labelling the compounds involved in PET. The reasons for choosing Fluorine-18 include its low positron energy, lack of side emissions and a half-life of 109.8 minutes.[50-52]

Fluorine-18 has a relatively low positron energy emission of 0.635MeV when compared to other common radionuclides such as carbon-11 (0.96MeV) and nitrogen-13 (1.19meV). The lower positron energy means that the positron will on average travel a shorter distance before losing sufficient kinetic energy so that a collision with an electron results in an annihilation process. This means that there will be a lower spatial area for the events from the source, resulting in high-resolution PET images.[50]

Fluorine-18 also has a high percentage of decay (97%) via positron emission, therefore making it suitable for PET imaging as no gamma rays are produced, reducing possible noise. The lack of side emissions also benefits the patient as they are not exposed to excess radiation dosage.[50]

The half-life of 109.8 minutes is considerably longer than some other radioisotopes shown in Table 1-1 but shorter than others.[53] Its relatively long half-life is ideal because it provides sufficient time for both the labelling process of the radiotracer and for bio-distribution of the radiotracer in the body. Conversely the half-life is short enough to minimise negative effects from radiation exposure.

Carbon-11 would be ideal for integration for radiopharmaceuticals because it can be added in as a methyl group, which are commonly present on pharmaceuticals and could therefore easily convert them into a tracer however, its short half-life and the fact it requires an air-sealed system make handling time extremely short, about 40minutes, and technically complex. It's reaction pathways therefore need to be straight forward with minimal reaction times. While there is a Carbon-11 module at the Austin Health it is for clinical production and therefore cannot be used for research purposes.

Despite all the advantages of Fluorine-18 there are still challenges incorporating it into organic molecules. A high amount of energy is required to produce Fluorine-18 in the cyclotron, limiting its availability for radiochemistry.[50] Due to the high amount of radioactivity involved remote handling and transport of the Fluorine-18 is required in addition to the automation of the radiosynthetic processes.

1.2.3.1 Production of Fluorine-18

The production of Fluorine-18 can be accomplished through several different nuclear processes listed in table 1-3.[50] The cyclotron is able to produce Fluorine-18 radioisotopes as both the [^{18}F]anion and [^{18}F]fluorine gas.

Table 1-3: Production methods of Fluorine-18

Nuclear reaction
$^{20}Ne(d,\alpha)^{18}F$
$^{20}Ne(p,2pn)^{18}F$
$^{16}O(3He,p)^{18}F$
$^{16}O(\alpha,pn)^{18}F$
$^{18}O(p,n)^{18}F$
$^{20}Ne(3He,\alpha n)^{18}Ne$, ^{18}Ne decays to ^{18}F
$^{6}Li(n,\alpha)^{3}H$, ^{3}H reacts in a following nuclear reaction $^{16}O(^{3}H,n)^{18}F$

Oxygen-18 enriched water is the primary source for the [^{18}F]anion, which can then be introduced into organic molecules via a nucleophilic substitution reaction.[54] The [^{18}F]fluorine gas is produced from Neon-20 and is introduced into organic molecules using electrophilic reactions.[50, 52, 55] The drawback of [^{18}F]fluorine gas is that it requires fluorine-19 carrier gas, therefore limiting its availability, resulting in low specific activity.[50] The [^{18}F]anion can be obtained with higher specific activity using a no carrier

added method, therefore it was chosen for radiochemistry synthesis in the work described in this thesis.

The Fluorine-18 radioisotope was produced using Oxygen-18 enriched water via the $^{18}O(p,n)^{18}F$ nuclear reaction within either the IBA cyclotron 10/5 or IBA cyclotron 18/9 located at Austin Health.

Formation of Fluorine-18 begins with the acceleration of H^- ions which pass through the stripper foil, converting them into a proton beam. The enriched water containing the stable Oxygen-18 radioisotope is then bombarded with the high energy protons to give radioactive Fluorine-18.[46, 56] Once sufficient activity is built up the Fluorine-18 radioisotope is transferred into shielded hot cells for radiolabelling experiments.

1.3 Hypoxic tracers

Radiotracers are compounds containing radioisotopes they are used in PET imaging for the evaluation of in-vivo processes. Combined with a radiation detection device the location of the radiotracer can be tracked by its decay, allowing for the study of metabolism, distribution and uptake of the tracer from its introduction into the body.

Hypoxic radiotracers are biological markers that accumulate upon uptake into hypoxic tissue. To be considered an effective hypoxia radiotracer certain criterion must be met. The radiotracer should show specific uptake for tumour hypoxia and the rate of uptake should ideally correlate directly with the low intracellular pO_2 of the hypoxic tissue.[34, 57]

To meet these criteria the hypoxic radiotracer requires certain attributes. The first of these is lipophilicity. The radiotracer needs to be lipophilic enough to allow quick uptake into hypoxic tumour cells, while retaining a fast clearance rate from the circulatory system and normoxic tissue.[57] This will yield a high-resolution image with minimal post injection delay.[34, 57-58]

Added to this the radiotracer needs to be metabolised in a specific way under hypoxic conditions, limiting it metabolism from non-hypoxic pathways. This will allow for selective uptake into hypoxic tissues compared to normoxic tissue.[57]

Once a new radiotracer is discovered it undergoes in-vivo and in-vitro testing. Assessment of new radiopharmaceuticals can be undertaken by using animal models and a small animal PET scanner, allowing for non-invasive in-vivo imaging. This allows for direct correlation with in-vitro data.[59]

1.3.1 Cu-ATSM

Diacetylbis(4-methylthiosemicarbazonato)copper^{II} (Cu-ATSM), shown in Figure 1-4, is a metal chelate that was shown to have hypoxic selectivity by Fujibayashi and co. relying on the Copper-64 positron emitting radionuclide [^{64}Cu]Cu-ATSM (**1.1**) can be used for PET.[60-61] [^{64}Cu]Cu-ATSM enters cells entirely through passive diffusion. In normoxic cells no reduction happens allowing it to move freely across cell membranes. Under hypoxic conditions the Cu(II) is reduced to Cu(I) resulting in the degradation of the complex and retention of the radioisotope.[62-64] While Cu-ATSM meets all the criteria for a hypoxic tracer being: lipophilic, small in size and having hypoxia selective bioreduction, Cu-ATSM is not used routinely because of the lack of facilities that produce copper-64.

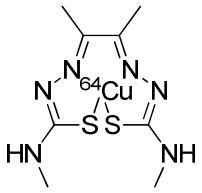

[^{64}Cu]Cu-ATSM (**1.1**)

Figure 1-4: Structure of [^{64}Cu]Cu-ATSM

1.3.2 FMISO

Currently the most popular hypoxic radiotracer is [^{18}F]fluoromisonidazole (FMISO) as depicted in Figure 1-5.[7, 65-69] It utilises a nitroimidazole group, which had been scrutinised as an oxygen mimetic for increasing the cytotoxicity of ionising radiation in tissue with low intracellular oxygen. [21]

[^{18}F]FMISO (**1.2**) Misonidazole (**1.3**)

Figure 1-5: Structures of [18F]FMISO and Misonidazole

One nitroimidazole, misonidazole (**1.3**) shown in Figure 1-5, was used as a sensitizer for hypoxic cells, increasing the efficacy of ionising radiation on tumours. Misonidazole is metabolised through the bioreduction of the nitroimidazole group by several intracellular nitroreductase enzymes resulting in its irreversible trapping in hypoxic cells.[17, 33, 37] It was proposed that FMISO undergoes metabolism through a similar pathway as misonidazole.[33] Therefore [^{18}F]FMISO depends on the sequential reduction of the nitro group located on the imidazole ring for its mechanism of uptake.[16, 43, 67] The proposed stepwise reduction for the process is illustrated in Scheme 1-1.[1]

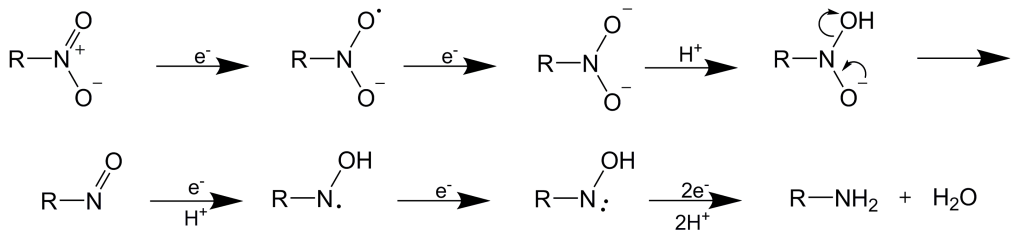

Scheme 1-1: Possible reduction process of the nitro group contained in nitroimidazole under hypoxic conditions[1]

The bioreduction of [^{18}F]FMISO is initialised with the transfer of an electron to the nitro group, resulting in its conversion into a high energy radical anion intermediate. Under normoxic conditions this intermediate is re-oxidised however, under hypoxic conditions the radical anion accepts a second electron forming another intermediate which is sequentially reduced into an amino derivative upon protonation.[16, 21, 33] Each of the subsequent steps is assisted by addition of proton to the variously charged negative intermediates.[5, 70] The proton-coupled electron transfer could possibly occur through the involvement of acids in the process. The amino derivative is capable of binding to macromolecules in the cell, resulting in its retention within hypoxic cells; the mechanism of retention is demonstrated in Scheme 1-2.[5, 17, 37, 41, 70]

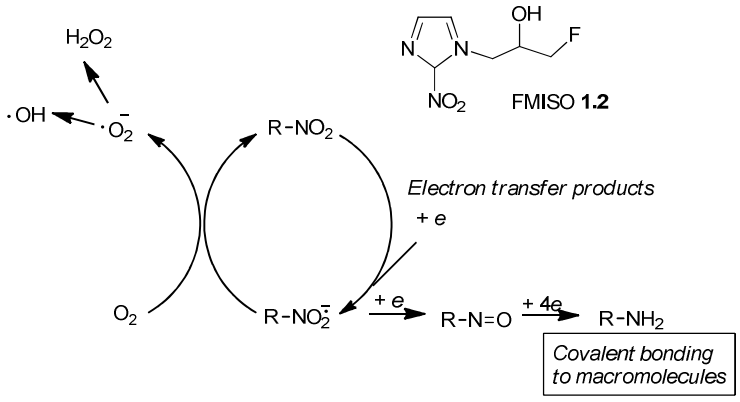

Scheme 1-2: Mechanism of retention for [^{18}F]FMISO[5, 70]

It is possible that the retention of [^{18}F]FMISO in hypoxic cells may simply be a consequence of the strongly basic amino-imidazole, this can be converted to its positively charged conjugate acid form shown in Scheme 1-3.[70] This charged species would be trapped in the cell as diffusion would no longer be possible across the lipophilic membrane.[67]

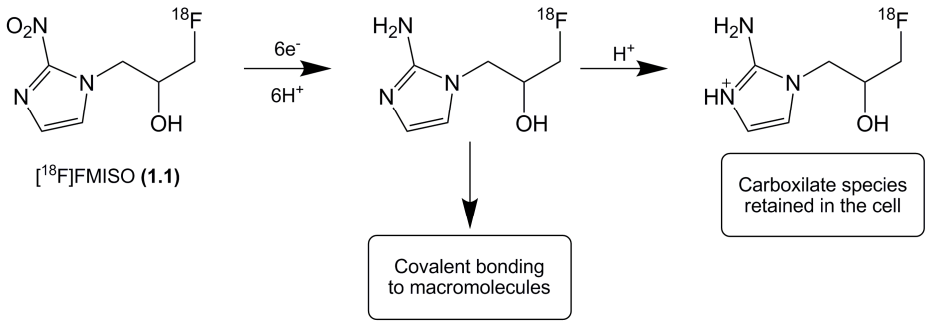

Scheme 1-3: Possible mechanisms of retention for [^{18}F]FMISO in hypoxic cells

While [^{18}F]FMISO is a stable radiopharmaceutical that shows uptake into hypoxic tumours with a pO_2 value of less the 10 mmhg, it has some drawbacks.[5, 21, 41] [^{18}F]FMISO displays slow accumulation in hypoxic tissue and slow clearance from normoxic tissue resulting in a low target to background ratio and therefore low contrast images.[23, 71] Additionally patients must wait 2 hours between administration of the tracer and the PET scan.[71] These shortcomings have led to a desire for improved hypoxia imaging agents that would exhibit more favourable pharmacokinetics and radiopharmaceutical properties.

1.4 Research background

Nitrogen mustard moieties have been incorporated into a range of potential chemotherapeutic agents for cancer chemotherapy, the characteristic bis-(chloroethyl)amine functional groups for these nitrogen mustards is shown in Figure 1-6.[22, 72-74]

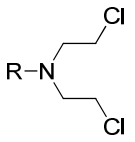

Figure 1-6: bis-(chloroethyl)amine functional group in the nitrogen mustards

It's thought that nitrogen mustards exert their cytotoxic effects though their ability to alkylate DNA and other biological nucleophiles. Neighbouring group participation from the nitrogen allows the displacement of the chloride leaving group forming the reactive aziridine intermediate giving the nitrogen mustards their high reactivity as alkylating agents.[75-76] Sun Z. et al developed and tested several sulfoxide nitrogen mustards **1.4-1.8** shown in Table 1-4.[27]

Table 1-4: Structures of Sulfoxides 1.4-1.8

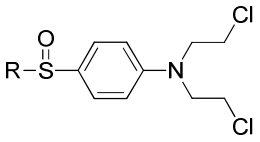

Sulfoxide	R
1.4	CH_3
1.5	$CH_3CH_2CH_2$
1.6	Ph
1.7	$(ClCH_2CH_2)_2NPh$
1.8	O_2NPh

Studies originally carried out by Sun Z. et al highlighted the potential of diaryl sulfoxides to act as hypoxia selective cytotoxins, as they exhibited hypoxia directed bioreduction. Under normal conditions these molecules are stable due to the electron withdrawing effects exhibited by para-sulfoxides resulting in low nitrogen reactivity. Under hypoxic conditions the sulfoxide is believed to undergo bioreduction, as shown in Figure 1-7, to the reactive thioether. The sulphide then activates the nitrogen allowing for the formation of the azridinium ion. Presumably the ion then undergoes reaction with biological nucleophiles resulting in the irreversible retention in the cell, although extensive research into the exact mechanism of action has not been carried out yet. [27]

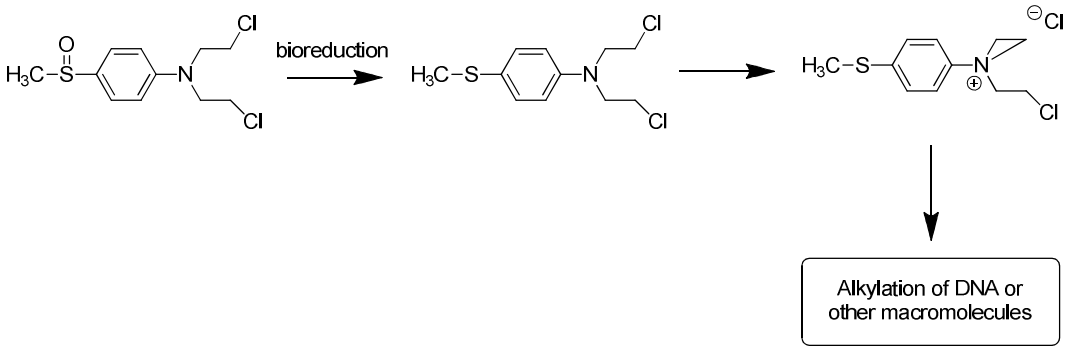

Figure 1-7: Mechanism of retention for the Sulfoxide containing nitrogen mustard 1.4

They also reported the hypoxia selective cytotoxicity of the sulfoxides **1.4-1.8** shown in Table 1-5.[27] A previous PhD student chose the methyl sulfoxide **1.4** and 4-nitrophenyl sulfoxide **1.8** as the basis of a potential imaging agent for hypoxic tissue.[77] Despite the methyl sulfoxide **1.4** having a lower hypoxic selectivity of 3; however its relative ease of synthesis makes it an appealing target. The 4-nirophenyl sulfoxide **1.8** was chosen due to its much higher hypoxia selectivity of 20.

Table 1-5: Hypoxia-selective cytotoxicity for the nitrogen mustards 1.4-1.8

Compound	IC_{90}(μM)-air[a]	IC90(μM)-N_2[a]	Hypoxic Selectivity[b]
1.4	944	370	3
1.5	953	319	3
1.6	2012	189	11
1.7	3094	184	17
1.8	3680	182	20

[a]IC_{90}: drug concentration (μM) required to reduce cell survival to 10% of controls using V-79 cells in the clonogenic assay. [b]Hypoxia selectivity is expressed as a ratio of IC_{90} values in air and N_2 [IC_{90}(air)/IC_{90}(N_2)]

As nitrogen mustards have been previously covered by other members of the White group please refer to the theses "Synthesis and biological analysis of novel Fluorine-18 positron emission tomography (PET) imaging agents for hypoxic tissues in tumours"[1] and "Synthesis, Radiolabelling and Evaluation of Novel Imaging Agents for Hypoxic Tissue"[55] for more details.

1.4.1 Previous Studies

Dr Cheryl Falzon was the first member of the White group in association with Austin Health to prepare a new class of hypoxia selective imaging agent based on the sulfoxides **1.4** and **1.8**.[55] The two resulting radiotracers [^{18}F]SO101(**1.9**) and [^{18}F]SO201(**1.10**) are presented in Figure 1-8.

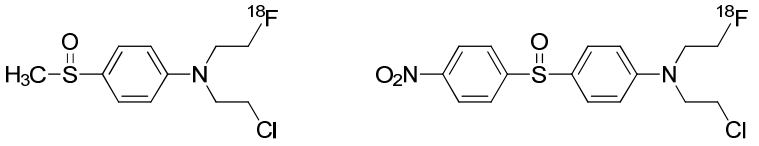

[^{18}F]SO101 (**1.9**) [^{18}F]SO201 (**1.10**)

Figure 1-8: structures of the radiotracers [18F]1.9 and [18F]1.10

Both radiotracers [18F]**1.9** and [18F]**1.10** were prepared through a halogen exchange Fluorine-18 radiolabelling technique from their nitrogen mustard precursors, N,N-bis-chloroethylamino-phenylsufoxides **1.4** and **1.8** as outlined in Scheme 1.4. Both reactions were performed at 100^{o}C for 15 minutes using noncarrier added F-18, they had radiochemical yields of 40% and 27% respectively, however it is not stated as to whether this is decay corrected or not.

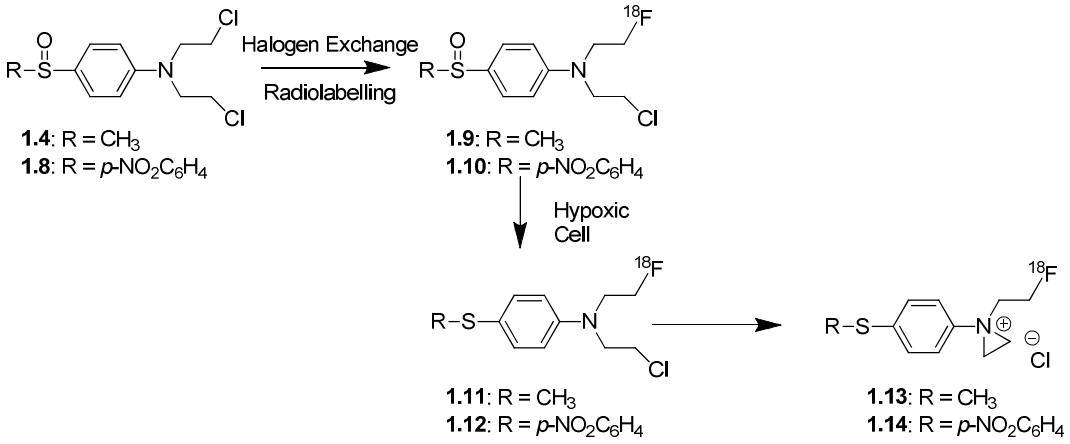

Scheme 1-4: Synthesis of the radiotracers [18F]1.9 and [18F]1.10 and their corresponding mechanism of retention in hypoxic cells.

The proposed mechanism for retention of the radiotracers [^{18}F]**1.9** and [^{18}F]**1.10** in hypoxic cells is also illustrated in Scheme 1-4. The mechanism of retention for the

sulfoxides [^{18}F]**1.9** and [^{18}F]**1.10** is believed to follow a similar pathway to the original sulfoxide moieties **1.4** and **1.8** respectively.[77] Firstly, the radiotracer undergoes bioreduction under hypoxic conditions at the sulfoxide group reducing it to a sulfide. [^{18}F]**1.9** and [^{18}F]**1.10** are reduced to the sulfides [^{18}F]**1.11** and [^{18}F]**1.12** respectively. Sulfides [^{18}F]**1.11** and [^{18}F]**1.12** are then able to form their highly reactive azridinium ions [^{18}F]**1.13** and [^{18}F]**1.14**, which can alkylate molecules within the hypoxic cells resulting in cell retention.[76]

Lipophilicity studies performed in-vitro for both [^{18}F]SO101(**1.9**) and [^{18}F]SO201(**1.10**) are shown in Table 1-6 comparing their results to [^{18}F]FMISO(**1.2**). The study was conducted with the lipophilicity defined as the partition coefficient value (logP value). The radiotracers [^{18}F]SO101(**1.9**) and [^{18}F]SO201(**1.10**) exhibit higher lipophilicity than [^{18}F]FMISO(**1.2**) shown through their respective logP values.[55]

Table 1-6: LogP values of [^{18}F]SO101, [^{18}F]SO201 and [^{18}F]FMISO

Radiotracer	LogP values
[^{18}F]FMISO (**1.1**)	0.054
[^{18}F]SO101 (**1.9**)	1.210
[^{18}F]SO201 (**1.10**)	1.734

Further studies performed *in-vivo* using a induced stroke rat model validated the *in-vitro* findings with both [^{18}F]SO101(**1.9**) and [^{18}F]SO201(**1.10**) displaying faster uptake in hypoxic tissue compared to [^{18}F]FMISO(**1.1**).[55] With the combination of both the animal and lipophilicity studies it can be assumed that the new class of sulfoxide tracers have

better pharmacokinetics for crossing the blood brain barrier compared to [^{18}F]FMISO(**1.1**) due to their more favourable LogP values.

Despite the initial potential that [^{18}F]SO101(**1.9**) and [^{18}F]SO201(**1.10**) exhibited as hypoxia imaging agents in the stroke model rats, the compounds were deemed unsuitable for routine use; this was due to its structural similarities to those of highly toxic nitrogen mustards. Structural modifications were required for the sulfoxides to remove the similarities while retaining their hypoxia selectivity.[1]

Dr Evelyn Laurens continued on the project synthesising several potential hypoxia radiotracers including a structural derivative of [^{18}F]SO201(**1.10**), [^{18}F]SO501(**1.15**) shown in Figure 1-9. The major structural change between [^{18}F]SO501(**1.15**) and [^{18}F]SO201(**1.10**) was the addition of ester functionality through the addition of an ethyl acetate group replacing the chloroethyl group. [1]

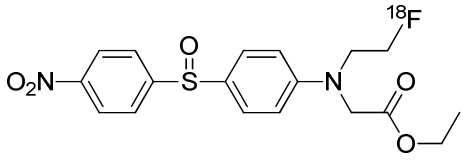

[^{18}F]SO501 (**1.15**)

Figure 1-9: Structure of [^{18}F]SO501 (1.15)

The radiotracer [^{18}F]SO501(**1.15**) is prepared from the precursor sulfoxide **2.04** via halogen exchange as illustrated in Scheme 1-5. The proposed mechanism of retention involves its introduction to a hypoxic environment where the sulfoxide is reduced to a sulphide; this will allow activation of the amino moiety leading to the formation of a

highly reactive α-lactone ion. This α-lactone has the ability to alkylate DNA or other intracellular molecules leading to its retention in the cell.[1]

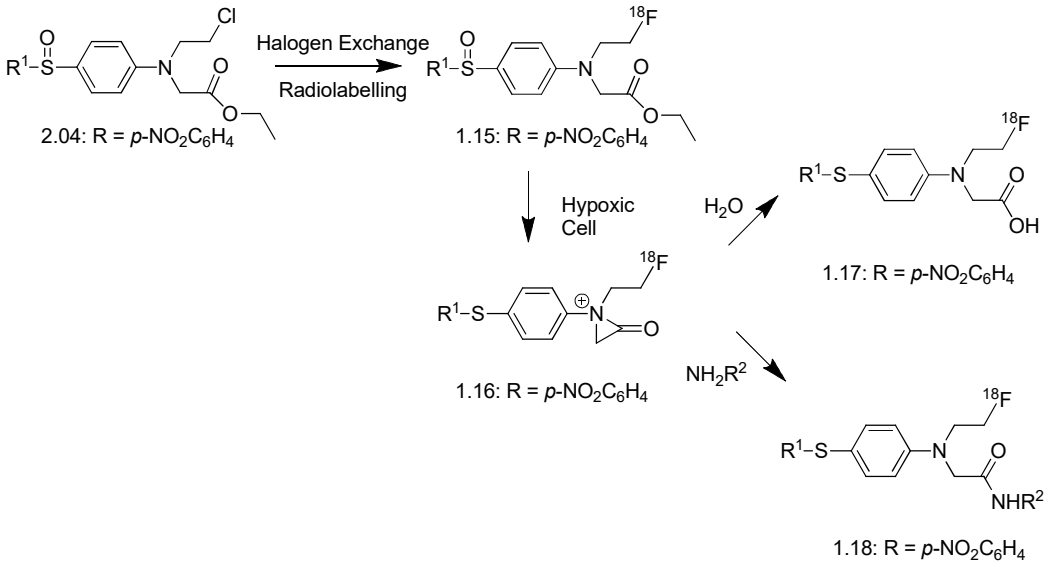

Scheme 1-5: Synthesis of the radiotracer [^{18}F]1.15 and its proposed mechanism of retention in hypoxic cells.[1]

In-vitro studies performed on [^{18}F]SO501(**1.15**) calculated that it has a LogP value of 2.45, indicating that its lipophilicity is suitable for crossing cell membranes. It was also found to be stable during its metabolism study in the presence of a cytochrome p450 assay with more than 80% intact after a 2 hour period and no defluorination.[1]

[^{18}F]SO501(**1.15**) showed solid results during it's in-vivo mouse studies with SK-RC-52 tumours, which are shown to become hypoxic when they surpass 300mm^3.[1] The time activity curves are shown in Figure 1-10, [^{18}F]SO501(**1.15**) had an average tumour to muscle ratio of 2.27, while [^{18}F]FMISO(**1.1**) has a ratio of 2.59. However,

[^{18}F]SO501(**1.15**) reaches a 1:1 ratio of tumour to muscle after 20minutes post injection compared to [^{18}F]FMISO(**1.1**), where it wasn't observed until 60 minutes post injection.[1]

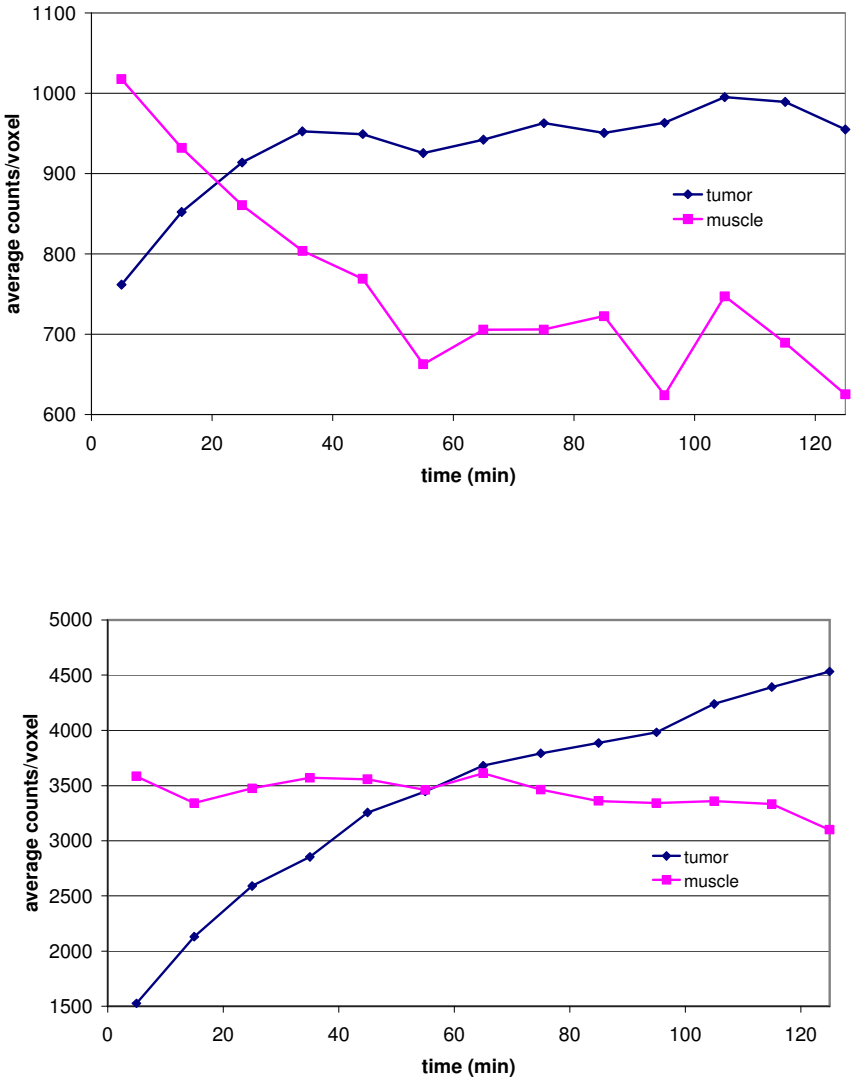

Figure 1-10: TACs for tumour and muscle for [^{18}F]1.15 (top) and [^{18}F]1.1 (bottom)[1]

The advantage of the quicker uptake time of [^{18}F]SO501(**1.15**) is demonstrated in Figure 1-11 where the tumours are clearly visible at 50 minutes but imaging [^{18}F]FMISO(**1.1**) at the same post injection time showed little contrast between tumours and muscle.

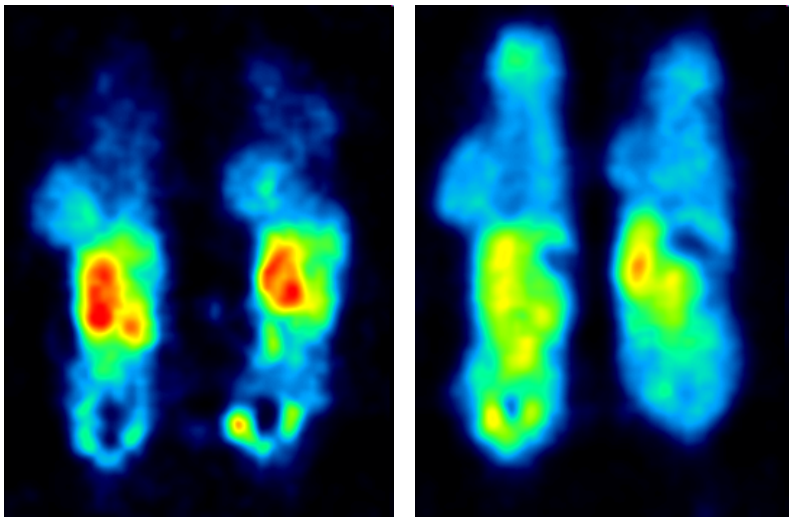

Figure 1-11: Coronal positron emission tomography (PET) images of [^{18}F]1.15 (left) and [^{18}F]1.1 (right) at 50 minutes post injection

Although [^{18}F]SO501(**1.15**) displayed good imaging quality and favourable uptake values it suffered from low labelling yields with non-decay corrected yields of 1.18% (decay corrected radiochemical yield 2.5%) making it unlikely to ever be used in a clinical application.[1] This was due to the method of radiolabelling which was via halogen exchange of the chloride; therefore a different method of radiolabelling would be required.

1.5 Project aim

The aim of this project was to create new radiolabelled tracers through new precursors in order to find a radiotracer with an increased radiochemical yield compared to that of SO501(**1.15**) while maintaining the sulfoxide moiety. This proposal involved replacing the chloride halogen in SO501(**1.15**) with a terminal alkyne group, therefore allowing the use of click chemistry as the radiolabelling method instead of halogen exchange.

Click chemistry was chosen due to the ease of synthesis of the fluoroethyl azide prosthetic group allowing for the automation of the radiosynthesis. Fluoroethyl azide is ideal as a prosthetic group as its synthesis starts from tosylethyl azide allowing for easy fluorination, distillation allows for separation from the remaining free fluoride. This can then be reacted with an appropriate precursor to form its respective radiotracer under relatively mild conditions, one of the advantages of click chemistry.

Table 1-7: List of proposed precursors and their corresponding Fluorine-18 radiotracers

Precursor	Radiotracer
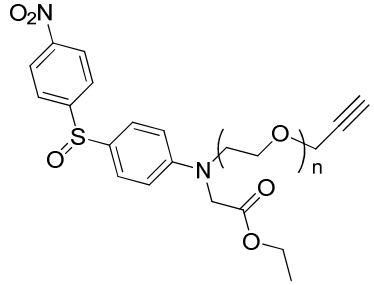 2.15; n = 1 2.25; n = 2 2.35; n = 3	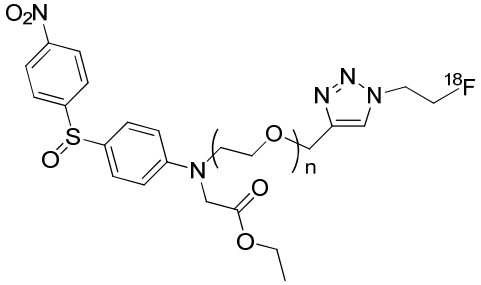 [^{18}F]2.16; n = 1 [^{18}F]2.26; n = 2 [^{18}F]2.36; n = 3
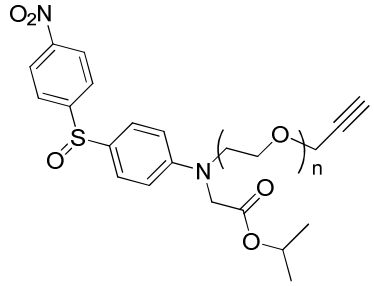 2.42; n = 1 2.52; n = 2	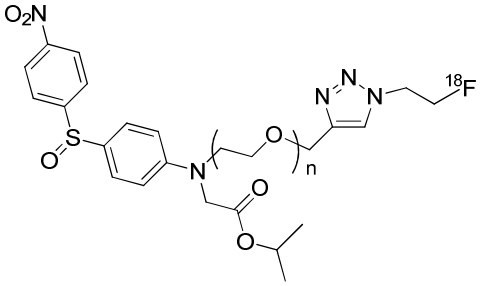 [^{18}F]2.43; n = 1 [^{18}F]2.54; n = 2
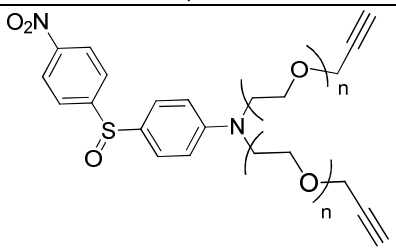 2.62; n = 2	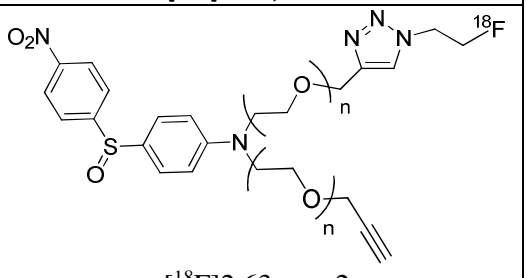 [^{18}F]2.63, n = 2

In-vivo imaging utilising SK-RC-52 tumours implanted into BALB/c Nude mice was used to test the synthesised radiotracers in a pre-clinical small animal model. SK-RC-52 Tumours become hypoxic after they grow to a certain size, determined

2 Synthesis of Precursors and Cold Standards

2.1 Rationale of target precursor compounds.

The lead compound [^{18}F]SO501(**1.15**) showed favourable uptake in hypoxic tumour cells with good clearance from normoxic tissue.[1] As such it provided a promising basis for further development. Utilising a terminal alkyne opens up the compound for click chemistry which potentially allows multiple prosthetic groups to be attached. This also allows ease of automation compared to substitution reactions streamlining production of the radiopharmaceutical. This investigation was focused on creating a series of compounds with slight structural changes to test their impact on cellular uptake and retention. To do this differing length PEG chains were used between the amine and the alkyne and in some cases the ester group was also subject to alteration with both the ethyl ester and isopropyl ester variants being synthesised.

Table 2-1: List of precursors, cold standards and radiotracers

Precursor	Cold Standard	Radiotracer
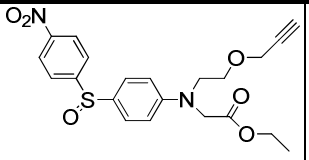	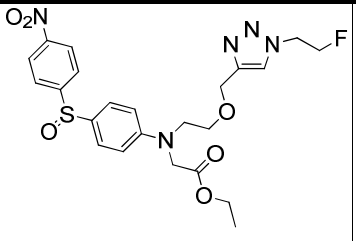	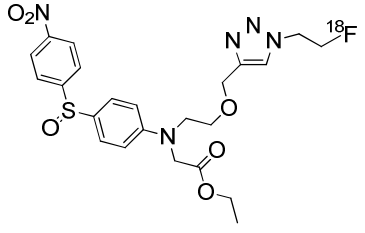
2.15	2.16	[^{18}F]2.16

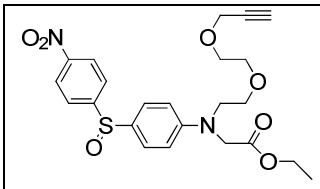 2.25	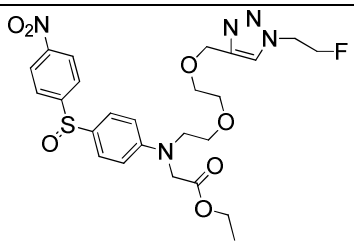 2.26	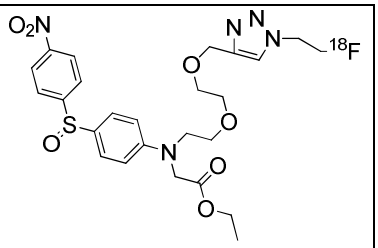 [^{18}F]2.26
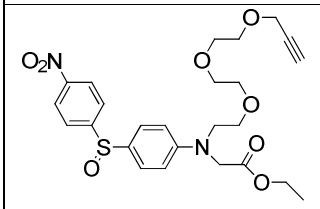 2.35	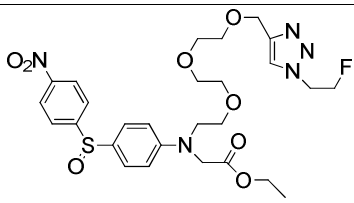 2.36	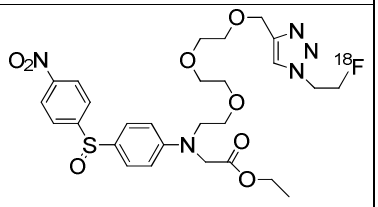 [^{18}F]2.36
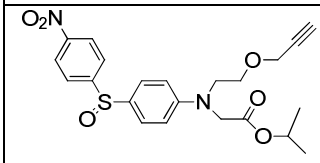 2.42	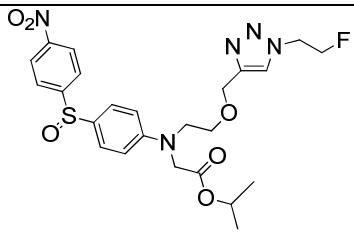 2.43	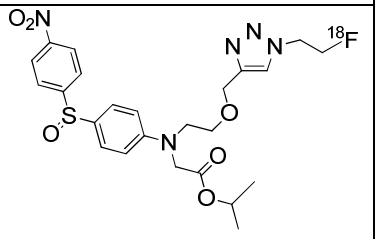 [^{18}F]2.43
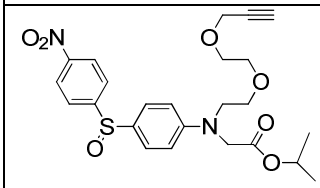 2.52	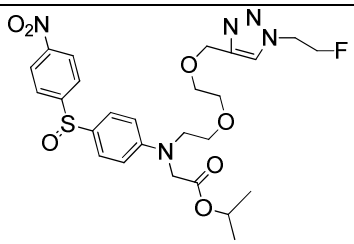 2.53	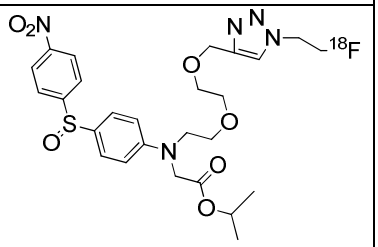 [^{18}F]2.53
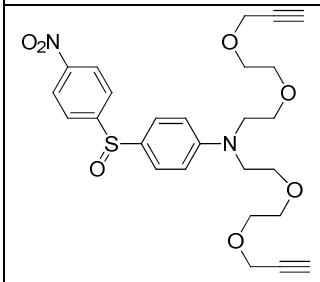 2.62	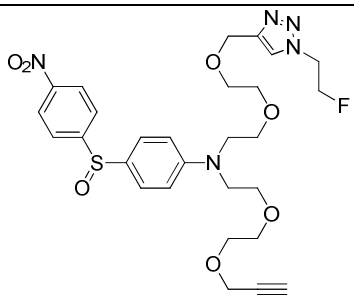 2.63	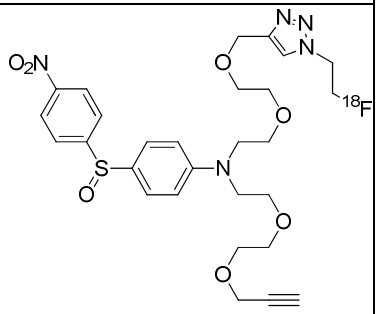 [^{18}F]2.63

2.2 Proposed synthesis approach of targeted precursor compounds

Using the synthetic route outlined from the synthesis of **SO5O1(1.15)** shown in Scheme 2-1 was used as a starting point, only slight modification to incorporate the terminal alkyne should have been required.[1]

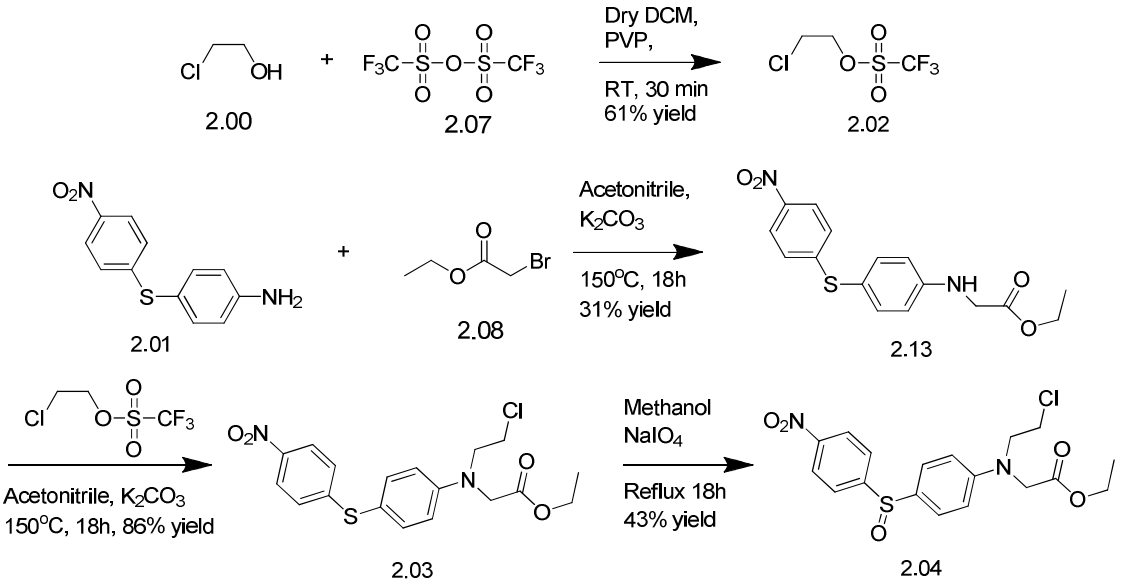

Scheme 2-1: Synthesis of the SO501 precursor

The first step was the synthesis of the alkylating agent 2-chloroethyl trifluoromethanesulfonate (**2.02**) through the reaction of 2-chloroethanol (**2.00**) and triflic anhydride (**2.07**). Parallel to this the sulphide ester was formed by an alkylation reaction between the sulphide backbone 4-nitro-4-amino-diphenylsulphide (**2.01**) and ethyl bromoacetate (**2.08**). The sulphide ester (**2.13**) and 2-chloroethyl trifluoromethanesulfonate (**2.02**) were then alkylated to give **2.03**. This was followed by oxidised with sodium periodate to give the precursor to [^{18}F]SO5O1 (**2.04**).

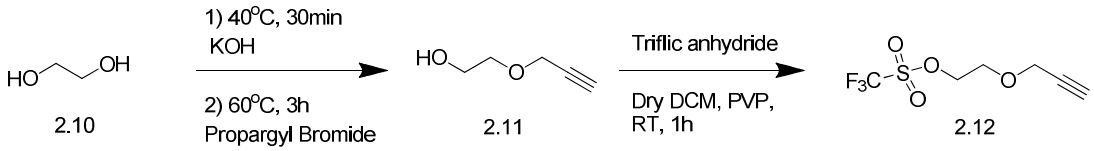

Scheme 2-2: Proposed synthesis of the triflate 2.12

The synthesis varied initially from that presented in Scheme 2-1 due to the integration of terminal alkyne onto the PEG groups. These groups were coupled to one of the hydroxyl terminal groups using a 2 step 1 pot reaction starting with the addition of KOH to PEG in a solvent free reaction. Propargyl bromide was added after 30 minutes to produce a terminal alkyne PEG. The isolated product was added to triflic anhydride to form the triflate.

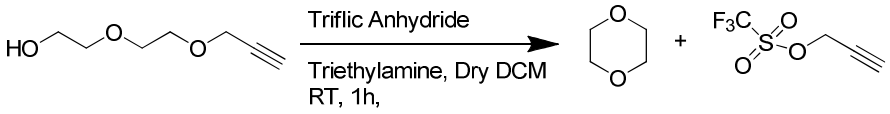

Scheme 2-3: Attempted synthesis to form a longer chain PEG triflate

The synthesis for the ethylene glycol single chain group worked using this method to produce 2-(prop-2-yn-1-yloxy)ethyl trifluoromethanesulfonate, however shown in Scheme 2-3 when the length of the ethylene glycol chain was increased to 2 or more the triflation resulted in a self-cyclisation to give propargyl triflate and dioxane. This is where the molecule has reacted internally giving 2 side products instead of the desired one and where one of the products produced is a ring.

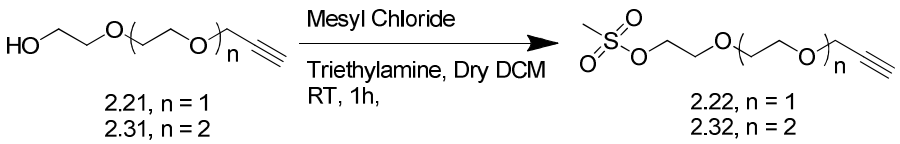

Scheme 2-4: Proposed synthesis of mesylates 2.22 and 2.32

An alternate route was therefore required for longer ethylene glycol chains. This was accomplished using Scheme 2-4 where the methylsulfonates **2.22** and **2.32** were synthesised using methanesulfonyl chloride and propargyl diethylene glycol or propargyl triethylene glycol respectively.

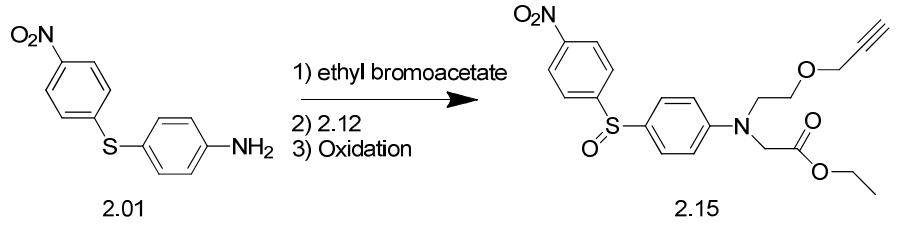

Scheme 2-5: Proposed synthesis of precursor 2.15

Formation of the ethyl ester precursor **2.15** was produced using a similar method to that presented in Scheme 2-1. Scheme 2-5 shows how the synthesis began with the alkylation of 2-ethylbromo acetate followed by reaction with the propargyl triflate **2.12** and finally oxidation with sodium periodate to give precursor **2.15**.

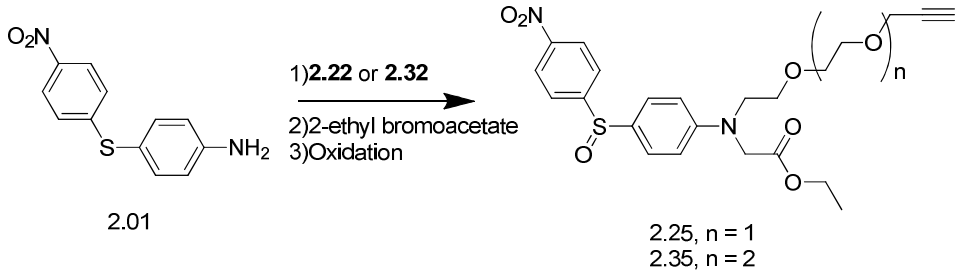

Scheme 2-6: Proposed synthesis of precursors 2.25 and 2.35

For the PEG mesylates the order of reactions was reversed with alkylation first performed with the mesylates **2.22** or **2.32** followed by addition of the 2-ethylbromo acetate and finally oxidation with sodium periodate to give the precursors **2.24** and **2.34**.

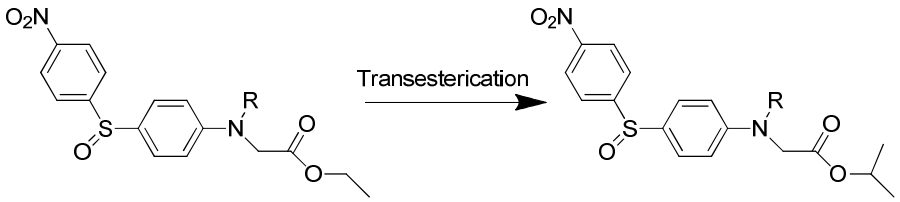

2.15 R= $(CH_2CH_2O)CH_2CCH$
2.25 R= $(CH_2CH_2O)_2CH_2CCH$

2.42 R= $(CH_2CH_2O)CH_2CCH$
2.52 R= $(CH_2CH_2O)_2CH_2CCH$

Scheme 2-7: Proposed synthetic route for transesterification of 2.15 and 2.25 respectively to the precursors 2.42 and 2.52

A one step transesterification shown in Scheme 2-7 was performed using sodium isopropanoate on precursors **2.15** and **2.25** to synthesise **2.42** and **2.52** respectively. Upon completion of the reaction however, the isolated products were not the desired ones with the phenyl groups cleaved from the sulphide linker.

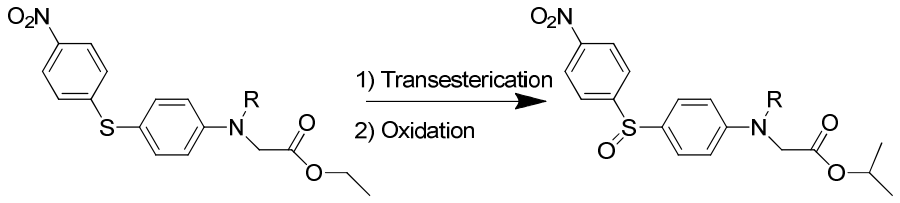

2.14 R= $(CH_2CH_2O)CH_2CCH$
2.24 R= $(CH_2CH_2O)_2CH_2CCH$

2.42 R= $(CH_2CH_2O)CH_2CCH$
2.52 R= $(CH_2CH_2O)_2CH_2CCH$

Scheme 2-8: Revised synthesis for the production of 2.42 and 2.52

To overcome this, the transesterification was performed on **2.14** and **2.24** using sodium isopropanoate followed by the oxidation with sodium periodate to give **2.42** and **2.52** as shown in Scheme 2-8.

2.2.1 Rationale of cold standard compounds.

Cold standards must be prepared before any radiolabelling experiment as they are essential for the characterisation of any radiolabelled tracers. The cold standard compounds are identical in every aspect to the radiolabelled tracers with the exception of containing fluorine-19 instead of the radioactive fluorine-18 isotope. Identification of the radio tracer can be carried out by comparing its retention time with that of its respective cold standard using a HPLC system.

As mentioned in chapter 1 the method of radiolabelling used for all compounds was click chemistry involving the [2+3] cycloaddition between an azide and alkyne. This will allow for the synthesis of the compounds **2.16**, **2.26**, **2.36**, **2.43**, **2.53** and **2.63**.[78-79]

2.2.2 Proposed Synthesis of cold standards

The production of the cold standards will start with the synthesis of 2-fluoroethyl azide from 2-fluoroethyl tosylate shown in Scheme 2-9. Then the cold standards will be synthesised with 2-fluoroethyl azide in the presence of a Cu(I) catalyst system and the respective precursor, undergoing click chemistry to form a triazole.

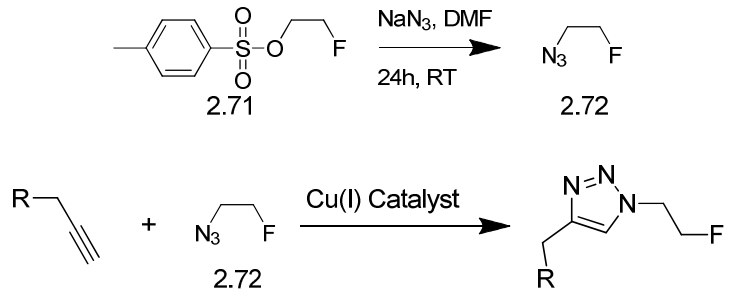

Scheme 2-9: Synthesis of 2-fluoroethyl azide followed by the 1,3 cycloaddition to form the cold standards

2.3 Results and Discussion

Table 2-2: Overall yields for precursor compounds

Precursor	Overall Yield	Precursor	Overall yield
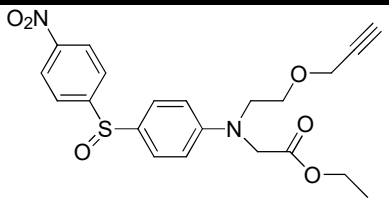 2.15	5.3%	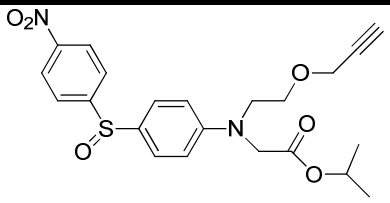 2.42	1.3%
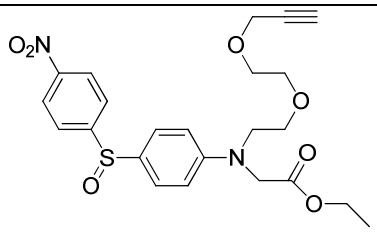 2.25	10.3%	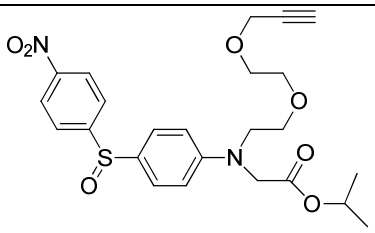 2.52	3.8%
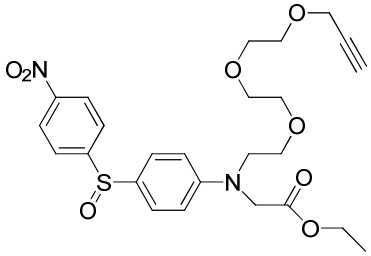 2.35	3.1%	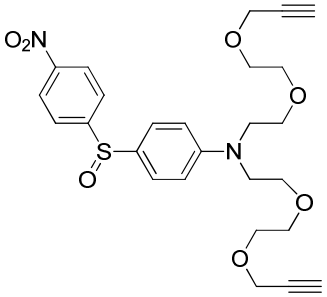 2.62	11.1%

In total 6 precursor compounds were successfully synthesised as shown in Table 2-2. The precursors 2.15, 2.25 and 2.35 vary by the length of the peg chain, while 2.42 and 2.52 are transesterifications of 2.15 and 2.25 respectively, having an isopropyl ester instead of the ethyl ester. The final precursor 2.62 was a side product from the synthesis of 2.25, a similar side product was observed during the synthesis of 2.35 however due to time constraints for later radiolabelling this product wasn't examined further.

Table 2-3: List of cold standards and their yields

Cold Standard	Yield	Cold Standard	Yield
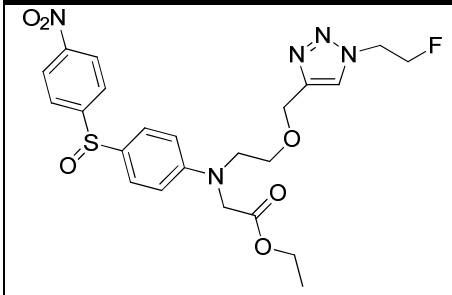 2.16	29%	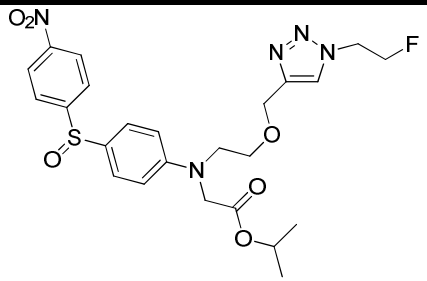 2.43	21%
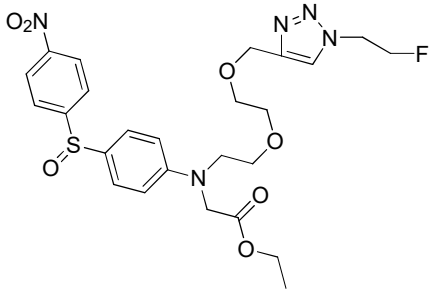 2.26	29%	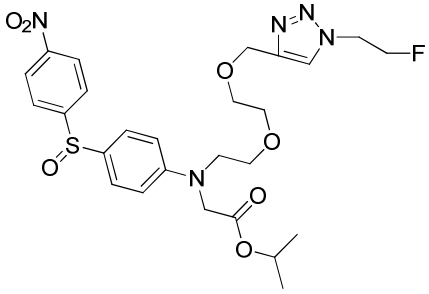 2.53	17%
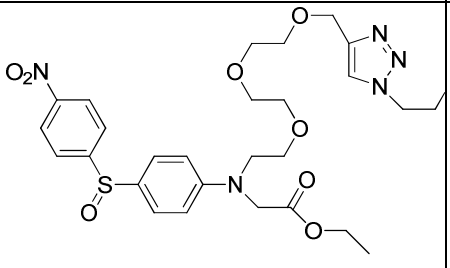 2.36	27%	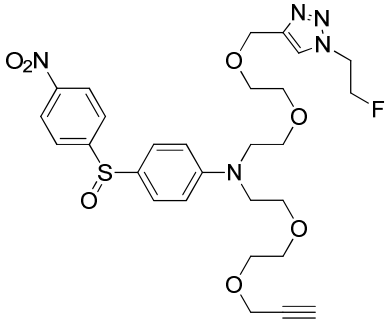 2.63	N/A

With the completion of the 6 precursor compounds the next step was the synthesis of the cold standards. The cold standards **2.16**, **2.26**, **2.36**, **2.43** and **2.53** were synthesised without issue. Cold standard 2.63 was not isolated; this will be discussed further in chapter 2.3.2.

Table 2-4: Summary of the retention times for the precursors and cold standards

Precursor	Retention Time (min)	Cold Standard	Retention Time (min)
2.15	13.946	**2.16**	13.059
2.25	13.985	**2.26**	13.032
2.35	13.867	**2.36**	13.032
2.42	14.337	**2.43**	13.357
2.52	14.215	**2.53**	13.385
2.62	13.958	**2.63**	13.206/13.465

The retention times of both the precursor and cold standards in a HPLC system were recorded, all HPLCs were carried out on a reverse phase C18 column with a water to acetonitrile gradient (0 min, 5% ACN; 0-8min 5-90% ACN; 8-12min, 90% ACN; 12-15min: 90-5% ACN; 15-18min: 5% ACN). This was primarily as a reference for their respective radiolabelled compounds because there were no practical ways to analyse them other than through retention time, this is for 2 reasons; handling radioactive compounds in a large enough quantities to do spectroscopy would be unsafe and the length of time you have to work with them is limited by the half-life of the isotope used.

2.3.1 Synthesis of precursor compounds

2.3.1.1 Preparation of precursor 2.15

Preparation of precursor **2.15** began with the formation of **2.11** through the reaction of ethylene glycol with propargyl bromide. This was a solvent free reaction started with ground potassium hydroxide added to pure ethylene glycol at 40°C followed 30 minutes later by propargyl bromide at 60°C. Flash chromatography was used to separate the products giving a 50% yield of pure product as yellow oil.

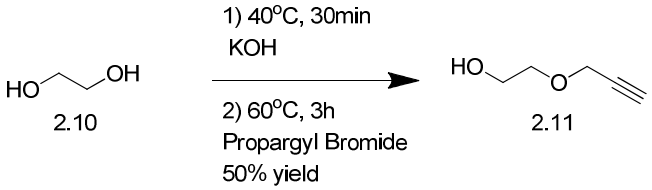

Scheme 2-10: Synthesis of 2.11 from 2.10

The purified propargyl ethylene glycol (Propargyl-PEG-1) **2.11** was characterised by ^{1}H NMR, showing a triplet at δ 2.45ppm with an integration of 1 proton and a doublet at δ 4.20 ppm with a 2 proton integration which is indicative of the propargyl group. Additionally, the peaks at δ 3.65 ppm and δ 3.77 ppm are the proton signals from the PEG group. The ^{13}C NMR showed 5 unique carbon environments in accordance with the expected compound.

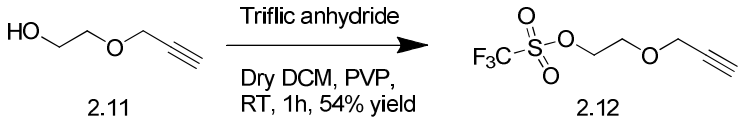

Scheme 2-11: Synthesis of the triflate 2.12

This propargyl ethylene glycol **2.11** was then added to excess triflic anhydride at 0°C before allowing the reaction to proceed at room temperature for an hour. After the

work up the propargyl-PEG-1-triflate **2.12** was obtained as a viscous pink liquid in 54% yield and used without further purification.

^{1}H NMR showed the absence of a peak where the hydroxyl proton would be expected but with the expected peaks at δ 4.65ppm, δ 4.24ppm, δ 3.87ppm and δ 2.48ppm. ^{13}C NMR indicated that there were now 6 carbon environments including a quartet at δ 118.57 consistent with the expect CF_3 environment.

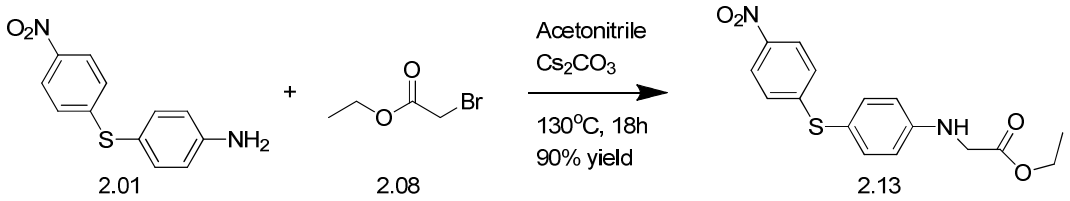

Scheme 2-12: Synthesis of 2.13

Formation of the sulphide mono ester **2.13** began with the commercially available 4-amino-4'-nitrodiphenyl sulphide **2.01** and ethyl bromoacetate heated at 130°C in a sealed tube in acetonitrile overnight. After extraction with diethyl ether, the organic phase was washed with sodium carbonate. Removal of the solvent gave the crude product as a waxy yellow solid. Flash chromatography was then used to purify the product giving the desired product **2.13** as yellow crystals in 90% yield.

Characterisation of the product **2.13** showed a quartet at δ4.29 ppm and a triplet at δ1.32 on the ^{1}H NMR, consistent with the expected splitting of the ethyl group. Doublets at δ 6.67, δ 7.09, δ 7.38 and δ 8.03 are consistent with 4 different aromatic proton environments and finally a broad singlet at δ 4.62 with a relative integration of 1 would account for the secondary amine proton.

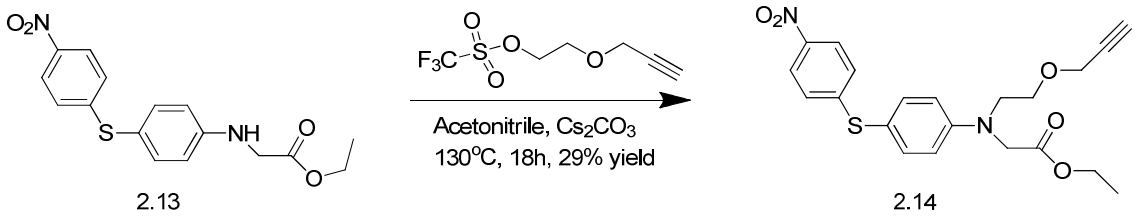

Scheme 2-13: Synthesis of 2.14

With the synthesis of **2.12** and **2.13** complete, the next step was the reaction to form **2.14**. This was accomplished using a sealed tube with acetonitrile at 130°C. Using the same work up as the previous step, the crude product was isolated as brown oil. Purification was performed using flash chromatography giving 2.14 as yellow oil in 29% yield. When chilled the yellow oil crystallised into sharp yellow crystals.

The ^{1}H NMR of **2.14** showed a few changes from that of 2.13, namely the addition of the alkyne triplet at δ 2.44 and the absence of the amine proton that was at δ 4.62.

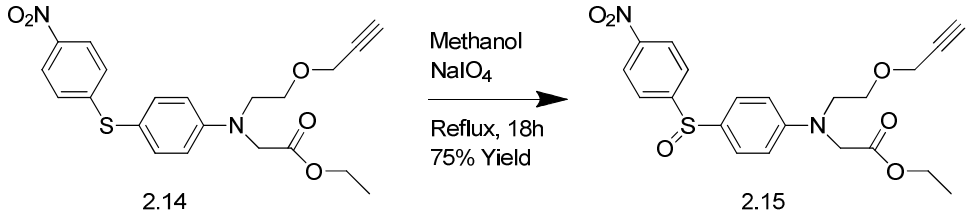

Scheme 2-14: Oxidation of 2.14 to form the precursor 2.15

The final step for the formation of the precursor **2.15** was the oxidation of **2.14**; this was accomplished by refluxing **2.14** in the presence of $NaIO_4$. 0.8 equivalents of $NaIO_4$ were used to prevent over-oxidation of the compound, given that it was more convenient to isolate and re-oxidise any remaining **2.14** then it would be to reduce any sulfone produced because of over oxidation due to the presence of the nitro group, which would most likely also undergo reduction. After refluxing overnight, the resultant mixture was

diluted with water, extracted with dichloromethane and then washed with water. After purification by flash chromatography the final product was yellow oil in 89% yield.

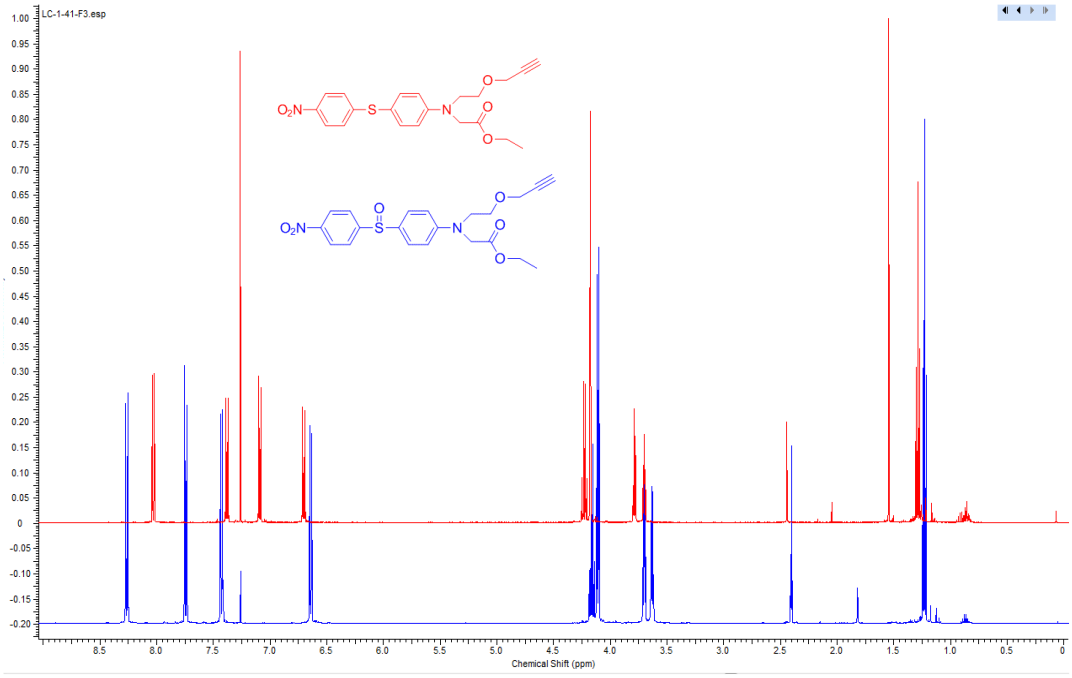

Figure 2-1: ^{1}H NMR comparing 2.14 (red) and 2.15 (blue)

The aromatic regions ortho to the sulfoxide were characterised by downfield shifts in the ^{1}H NMR spectra relative to those in the sulphide precursor. This is illustrated in Figure 2-1 where the change in aromatic regions is shown with peaks shifting from δ8.02, δ7.37, δ7.08 and δ6.70 for **2.14** to δ8.27, δ7.74, δ7.43 and δ6.64 in **2.15**.

2.3.1.2 Preparation of precursor 2.25

The preparation of the precursor **2.25** started with the synthesis of **2.21** from the reaction of commercially available diethylene glycol **2.20** with propargyl bromide. This was accomplished in two steps by first combining **2.20** with potassium hydroxide at 40°C for 30 minutes followed by the addition of propargyl bromide and stirred for a further 3

hours at 60°C. The crude product was brown oil which upon purification via flash chromatography gave light yellow oil in 48% yield.

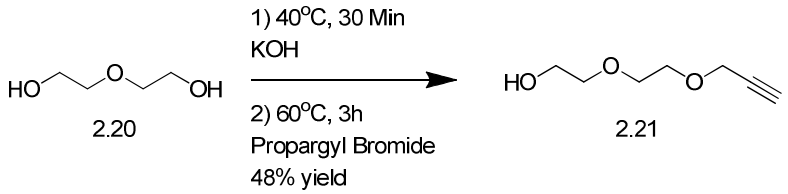

Scheme 2-15: Synthesis of the propargyl PEG-2 2.21

Purified propargyl diethylene glycol 2.21 exhibits a similar ^{1}H NMR spectra to **2.11**. The characteristic alkyne triplet was shown at δ2.44 with the corresponding doublet at δ4.21. The main difference is the relative integration of the PEG chain protons that had increased to a total of 8 as expected from the previous 4.

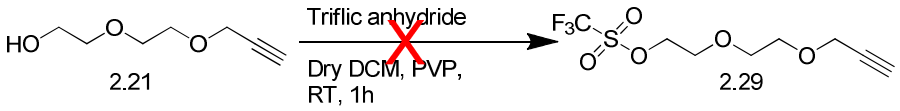

Scheme 2-16: Failed Synthesis of the triflate 2.29

As explained in the chapter 2.2 the initial attempt to make precursor **2.25** was synthesis the triflate **2.29**. This involved the reaction of propargyl 2.21 with triflic anhydride in the presence of polyvinyl pyridine. The resulting product was washed and the solvent removed to give a dark brown liquid.

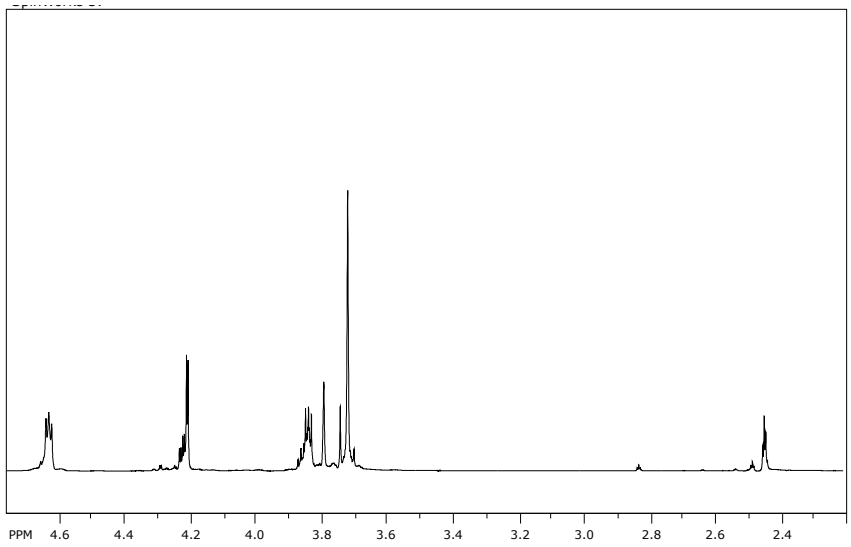

Figure 2-2: ^{1}H NMR of crude triflate 2.29

NMR analysis of the product triflate 2.29 shown in Figure 2-2 has a peak around δ3.71 which could account for the PEG group protons, however 1,4-dioxane also has a peak at δ3.71 in $CDCl_3$. An important note is that this was carried to the next step because it was actually one of first reactions that was performed during the experimental work of this thesis, so there was very little operational knowledge with what the NMRs should look like for these compounds. Had this been carried out later, the product formed from this reaction would not have been carried through to the next step as it would have been clear that PEG groups do not show a singlet at δ3.71.

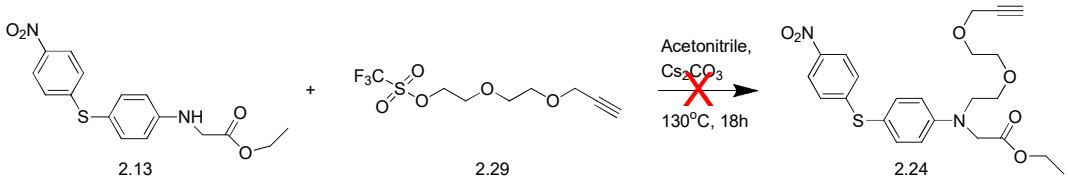

Scheme 2-17: Attempted synthesis of 2.24

The product was moved on the next step where it was reacted with the ethyl ester **2.13**. This was performed in a sealed tube at 130°C overnight in the presence of acetonitrile. The product was washed and purified using flash chromatography giving yellow oil.

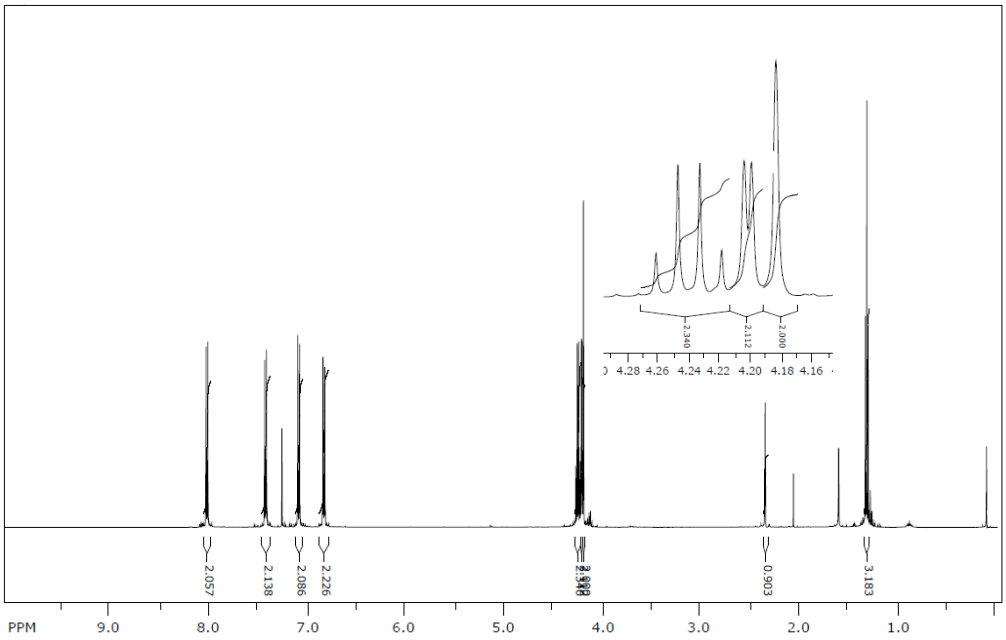

Figure 2-3: ^{1}H NMR from the attempted synthesis of 2.24 from 2.29

^{1}H NMR analysis of the product **2.24** shown in Figure 2-3 lacked the expected PEG peaks around δ3.70ppm. This indicates that it is unlikely that the triflate 2.29 was synthesised correctly.

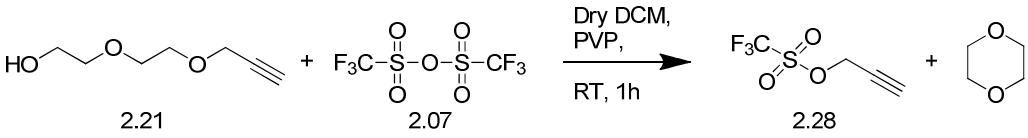

Scheme 2-18: Proposal for the actual reaction of 2.29

The more likely products that were formed from the reaction of the propargyl **2.21** and triflic anhydride **2.07** would be propargyl triflate **2.28** and 1,4-dioxane. Both the ^{1}H NMR and the following reaction with **2.13** support this conclusion.

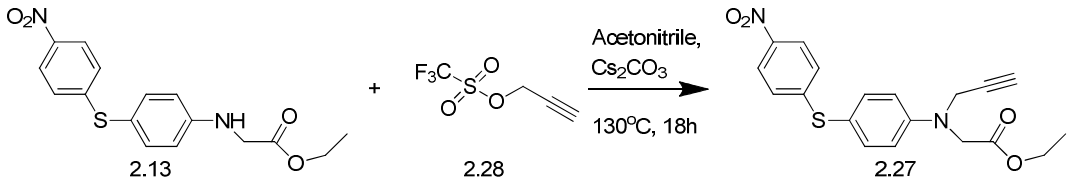

Scheme 2-19: Synthesis of 2.27

The product **2.27** was therefore synthesised from the reaction of **2.13** and the triflate **2.28**. Unfortunately, this product had already been tested as a precursor for radiolabelling by Austin Health so it was not taken any further and another route was required for the synthesis of precursor **2.25**.

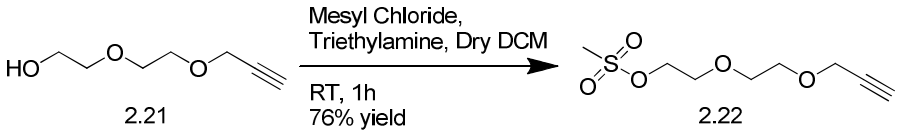

Scheme 2-20: Synthesis of the PEG-2-mesylate 2.22

Due to the initial failure of adapting the triflation method for the synthesis of **2.22** an alternate route was used. This utilised the less reactive methyl sulfonate leaving group. This reaction was performed under an inert atmosphere. The methanesulfonyl chloride was diluted into dichloromethane and chilled to 0°C. Compound **2.21** and triethylamine were combined in dichloromethane and added dropwise to the mesyl chloride solution, the solution was then reacted for a further hour at 25°C. Purification of the product was performed using a work up followed by flash chromatography to give brown oil in 79% yield.

^{1}H NMR characterisation was consistent with the expected product. The alcohol proton has been replaced with a singlet at δ 3.08ppm with a relative integration of 3, accounting for the methyl group on the methylsulfonate.

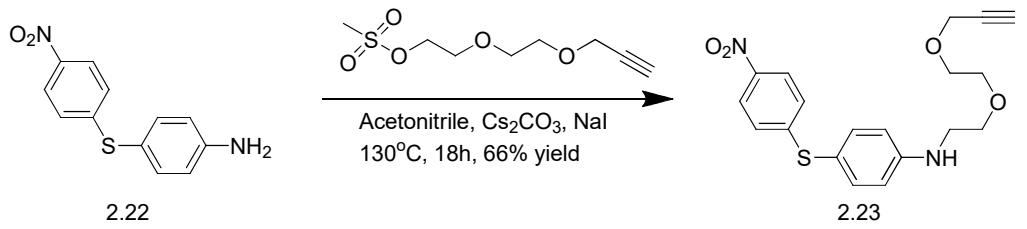

2.22 2.23

Scheme 2-21: Alkylation with 2.22 to form 2.23

Utilising the newly formed PEG2-mesylate **2.22** an alkylation reaction was performed with the diphenyl sulphide starting material **2.01** in a sealed tube to form **2.23**. The reaction was carried out in acetonitrile at 130°C overnight. Purification of the product was done via extraction followed by flash chromatography to give viscous brown oil in 66% yield. ^{1}H NMR characterisation of **2.23** showed the typical terminal alkyne proton triplet at δ 2.41ppm. It is important to note that the acetonitrile used was AR grade and not anhydrous. This was due to the use of freshly distilled acetonitrile (anhydrous) resulting in only small amounts of product and starting material. A test was conducted to make sure that it was the acetonitrile that was the issue where the reaction was spiked with 0.5mL of water, the reaction proceeded normally, showing that the small amount of water in AR grade acetonitrile was required for the reaction to work.

The PEG group protons integrated for 8 at δ 3.74ppm with the amine proton showing a broad singlet at δ 4.47 ppm.

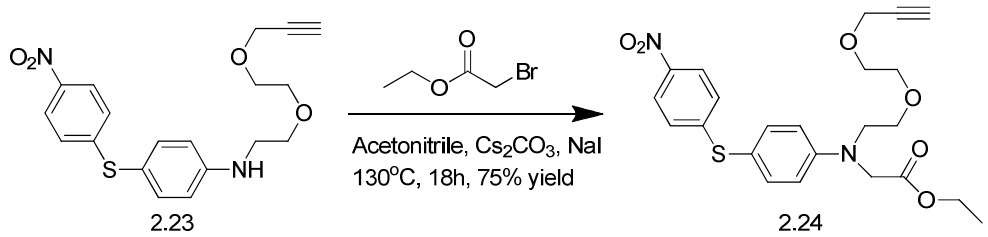

2.23 2.24

Scheme 2-22: Formation of the ethyl ester 2.24

With the synthesis of **2.23** complete the next step performed was the addition of the ethyl ester group. The reaction was carried out at 130°C overnight in a sealed tube with acetonitrile as the solvent combining **2.23** with ethyl bromoacetate **2.05** in the presence of Cs_2CO_3 and NaI. After cooling to room temperature, the reaction mixture was diluted with diethyl ether and washed with saturated sodium bicarbonate. Purification was performed using flash chromatography yielding the pure product as brown oil in 75% yield.

^{1}H NMR analysis showed a loss of the NH proton from the previous compound as expected. The addition of the ester group was characterised by the triplet located at δ 1.30ppm with a relative integration of 3.

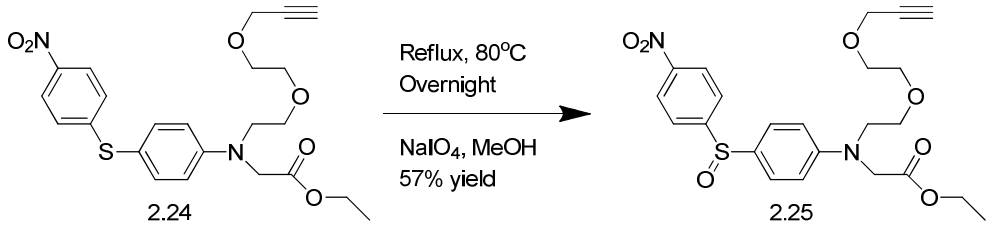

Scheme 2-23: Oxidation to form the precursor 2.25

The final step for the preparation of precursor **2.25** was the oxidation of **2.24**. This was performed by refluxing **2.24** in methanol in the presence of $NaIO_4$. Only 0.8 equivalents of the oxidising agent were used to prevent over oxidation of the product. Upon completion of the reaction the mixture was diluted with water before it was extracted with dichloromethane. The organic phase was then washed with water, the solvent removed and flash chromatography was performed on the crude product. The final pure product was yellow oil in 57% yield.

The ^{1}H NMR shows shifts in the aromatic region consistent with the oxidation of the sulfide to a sulfoxide. The aromatic peaks have shifted from δ8.04ppm, δ7.38ppm, δ7.10ppm and δ6.71ppm to δ8.31ppm, δ7.78ppm, δ7.45ppm and δ6.66ppm.

2.3.1.3 Preparation of precursor 2.35

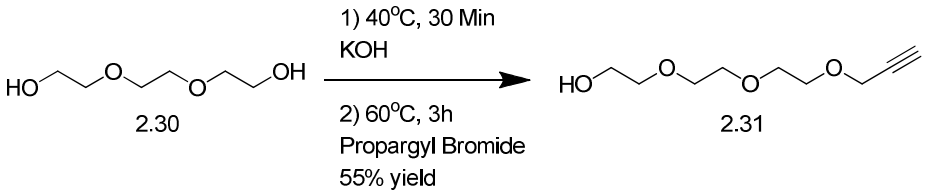

Scheme 2-24: Synthesis of the PEG-3 Propargyl 2.31

Synthesis of the third precursor **2.35** began with the propargylation of triethylene glycol **2.30** by first reacting it with potassium hydroxide for 30 minutes at 40°C followed by the addition of propargyl bromide with another 3 hours of stirring at 60°C. The reaction mixture was then diluted with water and acidified with HCl before it was extracted with ethyl acetate. The organic layer was then washed with further water before the solvent was removed and the crude product was purified via flash chromatography to give the pure product as light yellow oil in 55% yield.

^{1}H NMR showed the characteristic alkyne peaks with the triplet at δ2.42ppm and the doublet at δ4.22ppm. The PEG group protons all show up in the δ3.62-3.75ppm range as a multiplet.

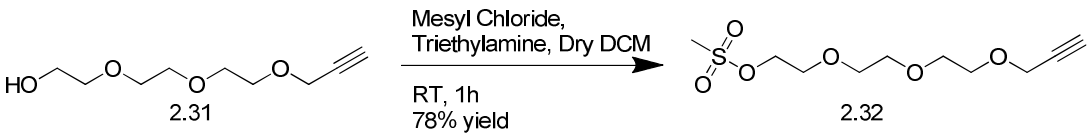

Scheme 2-25: Formation of the PEG-3 Mesylate 2.3

Similarly to the synthesis of the PEG-2 mesylate **2.22** the production of the PEG-3 mesylate **2.32** involved first diluting the mesyl chloride in dichloromethane. This mixture was cooled to 0°C and the propargyl PEG-3 **2.31** was added dropwise to the solution. Once the addition was complete the reaction was brought up to room temperature and stirred for a further hour. More dichlormethane was added to dilute the reaction before it was quenched in chilled water to remove any remaining mesyl chloride. After further washing the solvent was removed and the crude product was purified by flash chromatography to give yellow oil in 78% yield.

The distinct methyl singlet at δ3.08ppm and the proparyl triplet δ2.44ppm and doublet δ4.20ppm indicate that the target compound was made as they occupy the terminal ends of the PEG-3 chain.

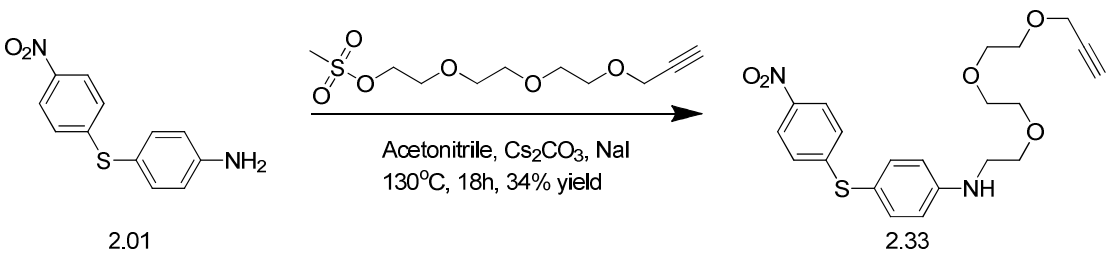

Scheme 2-26: Synthesis of 2.33

With the mesylate **2.32** the next step in the route was to alkylate the 4-amino-4'-nitrodiphenyl sulphide backbone. This was performed overnight in a sealed tube at 130°C in acetonitrile with NaI and Cs_2CO_3. The reaction was diluted with diethyl ether

and washed. After the solvent was removed and purification with flash chromatography the product was a viscous brown oil in 34% yield.

Analysis of the product by ^{1}H NMR showed a NH triplet at δ4.50ppm consistent with expectations. The characteristic alkyne peaks are at δ2.46ppm and δ4.20ppm and the 4 expected aromatic peaks are at δ8.01ppm, δ7.33ppm, δ7.07ppm and δ6.67ppm.

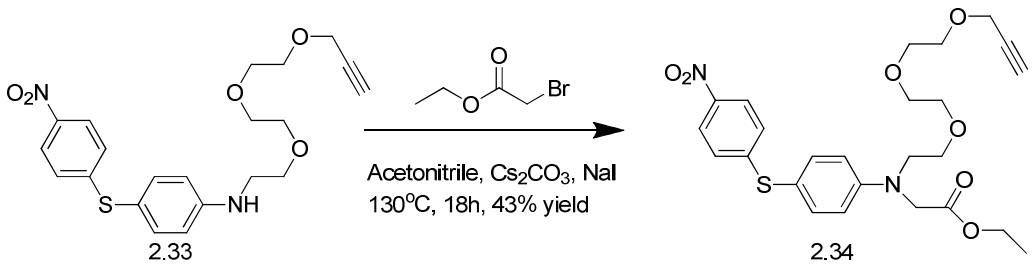

Scheme 2-27: Synthesis of 2.34

Ethyl bromoacetate **2.05** was used in conjunction with **2.33** to form 2.34. This was achieved by reacting them in a sealed tube at 130° overnight. Once the reaction was complete the mixture was diluted with diethyl ether and washed. The solvent was then removed and the crude product purified with flash chromatography giving the product as brown oil in 43% yield.

^{1}H NMR showed a loss of the NH proton that was present in **2.33** and the addition of the triplet peak at δ1.29ppm from the CH_3 group on the end of the ester moiety.

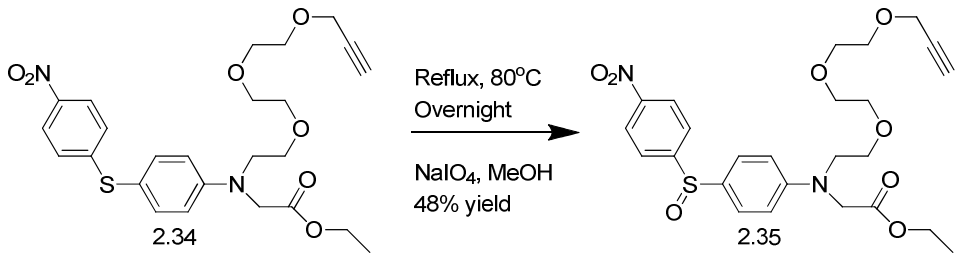

Scheme 2-28: Oxidation of 2.34 to precursor 2.35

The final step in the preparation of precursor **2.35** was oxidation of the sulphide to a sulfoxide. This was done by reacting **2.34** with 0.8 equivalents of $NaIO_4$. Once the reaction was complete the solution was diluted with water and extracted with dichloromethane. The organic phase was then washed, the solvent removed and the product was purified using flash chromatography to give yellow oil in 48% yield.

1H NMR showed the expected shifts in the aromatic region with peaks at δ8.28ppm, δ7.75ppm, δ7.43ppm and δ6.65ppm confirming the formation of the precursor **2.35**.

2.3.1.4 Preparation of precursor 2.42

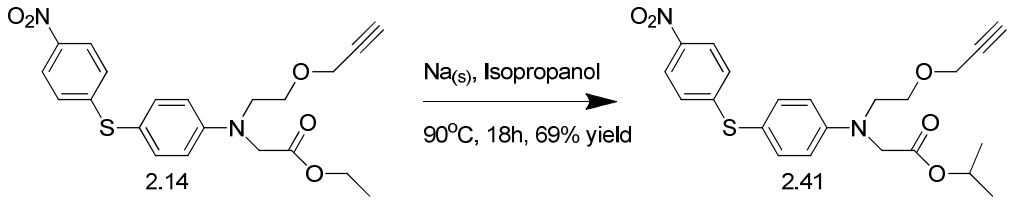

Scheme 2-29: Transesterification of 2.14 to 2.41

Precursor **2.42** was synthesised first by the transesterification of the ethyl ester to the isopropyl ester. This was achieved by first reacting sodium in distilled isopropanol allowing the formation of sodium isopropoxide. **2.14** was then added to the solution and allowed to stir overnight under reflux. The isopropanol was removed and the product was extracted using Diethyl either was in 3 aliquots. The flask was sonicated and each aliquot was transferred to another flask. Once all 3 aliquots were gathered the diethyl ether was removed in vacuo to give the product **2.41** as yellow oil in 69% yield.

The doublet peak at δ1.26ppm with a relative integration of 6 confirmed the transesterification of **2.41**.

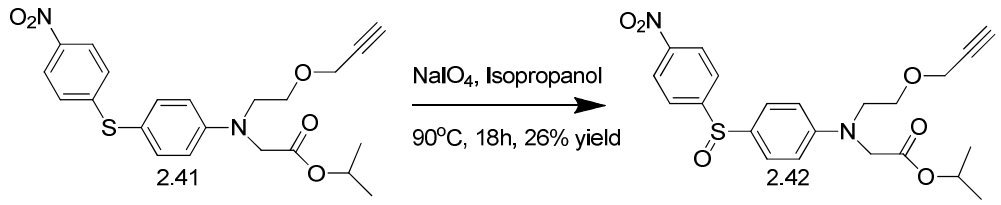

Scheme 2-30: Oxidation to form precursor 2.42

With the transesterification complete the oxidation of **2.41** was carried out using isopropanol as the solvent instead of methanol like the previous oxidations. **2.41** and 0.8 equivalents of $NaIO_4$ were reacted overnight at 90°C, then the solution was diluted with water and extracted with dichloromethane, the organic phase was washed and then the solvent was removed. After purification by flash chromatography the product **2.42** was given as yellow oil in a 26% yield.

1H NMR analysis of **2.42** shows shifts in the aromatic region when compared to 2.41 with peaks at δ8.30ppm, δ7.77ppm, δ7.45ppm and δ6.66ppm confirming the formation of the sulphoxide.

2.3.1.5 Preparation of precursor 2.52

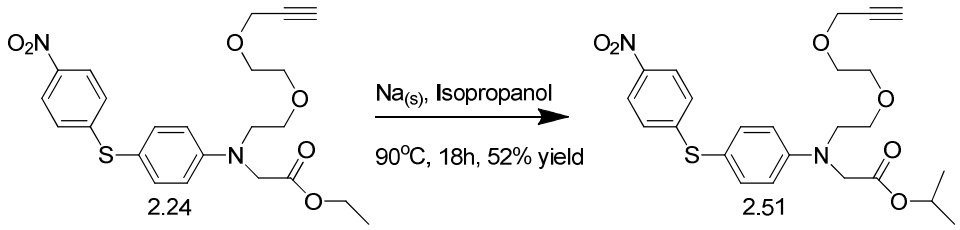

Scheme 2-31: Transesterification of 2.24 to 2.51

Synthesis of the precursor **2.52** began with formation of sodium isopropoxide by adding sodium metal to distilled isopropanol. **2.24** was then added to the solution and left to reflux overnight. The solvent was removed and the residue was extracted with diethyl ether. Isolation of the product provided yellow oil in 52% yield.

^{1}H NMR showed the transesterification with a doublet at δ1.25ppm with an integration of 6 replacing the triplet of **2.24**.

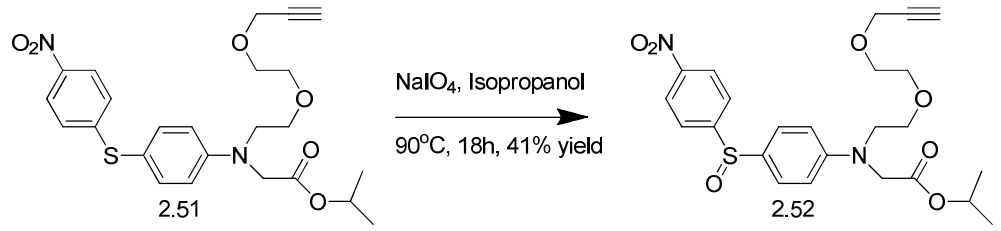

Scheme 2-32: Oxidation to synthesis the precursor 2.52

Oxidation of **2.51** was performed by combining it with 0.8 equivalents of $NaIO_4$ in isopropanol and it was reacted at 90°C overnight. The mixture was diluted with water before it was extracted with dichloromethane. The organic phase was washed and the solvent removed. Flash chromatography provided the product as yellow oil in 41% yield.

^{1}H NMR showed shifts in the aromatic regions with peaks at δ8.28ppm, δ7.75ppm, δ7.43ppm and δ6.63ppm.

2.3.1.6 Preparation of precursor 2.62

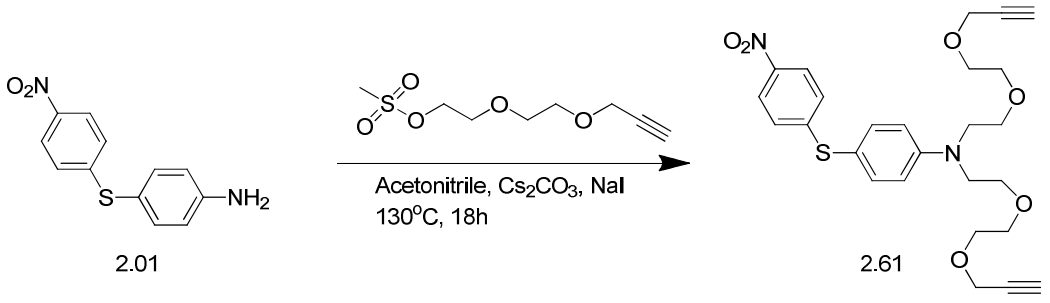

Scheme 2-33: Synthesis of 2.61

The compound **2.61** was produced as a side product for the synthesis of **2.23** however depending on the conditions it could be isolated in yields of up to 50% as brown oil from the same flash chromatography column used to purify **2.23**. This is most likely due to

the synthesis of **2.23** using 5 equivalents of **2.22** to 1 equivalent of 2.01. The same is observed with the production of **2.33**, which used the same ratio, however that product was not examined any further. The ratio was chosen just because of how easy the starting material was to make, just to ensure that product was made. Lowering the equivalents would yield less of both products

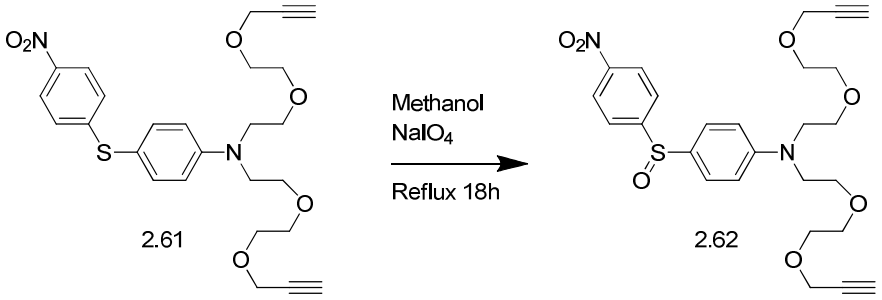

Scheme 2-34: Oxidation of 2.61 to 2.62

The synthesis of 2.62 was carried out by refluxing 2.61 in methanol with 0.8 equivalents of sodium periodate. After 18 hours the solution was cooled and diluted with water. Dichloromethane was used to perform an extraction; the solvent was removed from the combined organic phase and then the crude product was purified via flash chromatography to give **2.62** as yellow oil in 62% yield.

2.3.2 Synthesis of the Cold standards

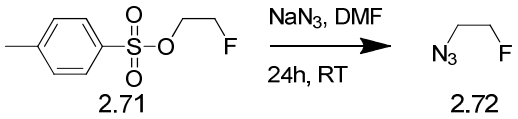

Scheme 2-35: Synthesis of 2-fluoroethyl azide 2.72

All the cold standards required 2-fluoroethyl azide 2.72 in their preparation. This was done by reacting 2-fluoroethyl tosylate with sodium azide in DMF overnight. The

product was used “as is” for the following reactions as the 2-fluoroethyl azide would be too dangerous to isolate so it was kept permanently in solution.

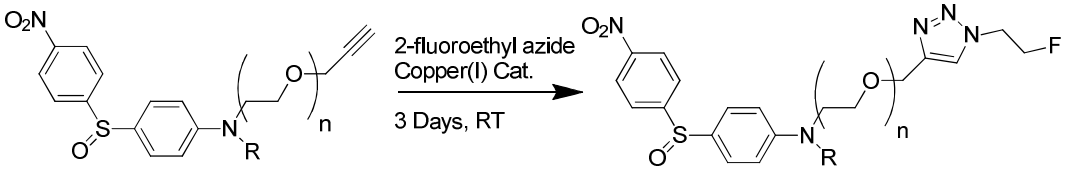

2.15: n =1, R = $CH_2COOCH_2CH_3$
2.25: n =2, R = $CH_2COOCH_2CH_3$
2.35: n =3, R = $CH_2COOCH_2CH_3$
2.42: n =1, R = $CH_2COOCH(CH_3)_2$
2.52: n =2, R = $CH_2COOCH(CH_3)_2$

2.16: n =1, R = $CH_2COOCH_2CH_3$
2.26: n =2, R = $CH_2COOCH_2CH_3$
2.36: n =3, R = $CH_2COOCH_2CH_3$
2.43: n =1, R = $CH_2COOCH(CH_3)_2$
2.53: n =2, R = $CH_2COOCH(CH_3)_2$

The 5 cold standards **2.16, 2.26**, **2.36**, **2.43** and **2.53** were all synthesised following the same route. They were reacted with 2-fluoroethyl azide in the presence of copper catalyst over 3 days at room temperature. Yields varied from 15-29% and all of them were yellow oils. The presence of the cold standard was first confirmed with a HPLC-MS, providing a retention time and a low-resolution mass spectrometry. All HPLC was carried out using a reverse phase system with Acetonitrile(solvent A) and water with 0.1% formic acid(solvent B); 0 min, 5% A; 0-8min 5-90% A; 8-12min, 90% A; 12-15min: 90-5% A; 15-18min: 5% A.

The retention time is important because it provides a reference for the later radiolabelled compounds, which cannot be identified by any other means. The successfully synthesised cold standards were analysed by ^{1}H NMR and LC-MS

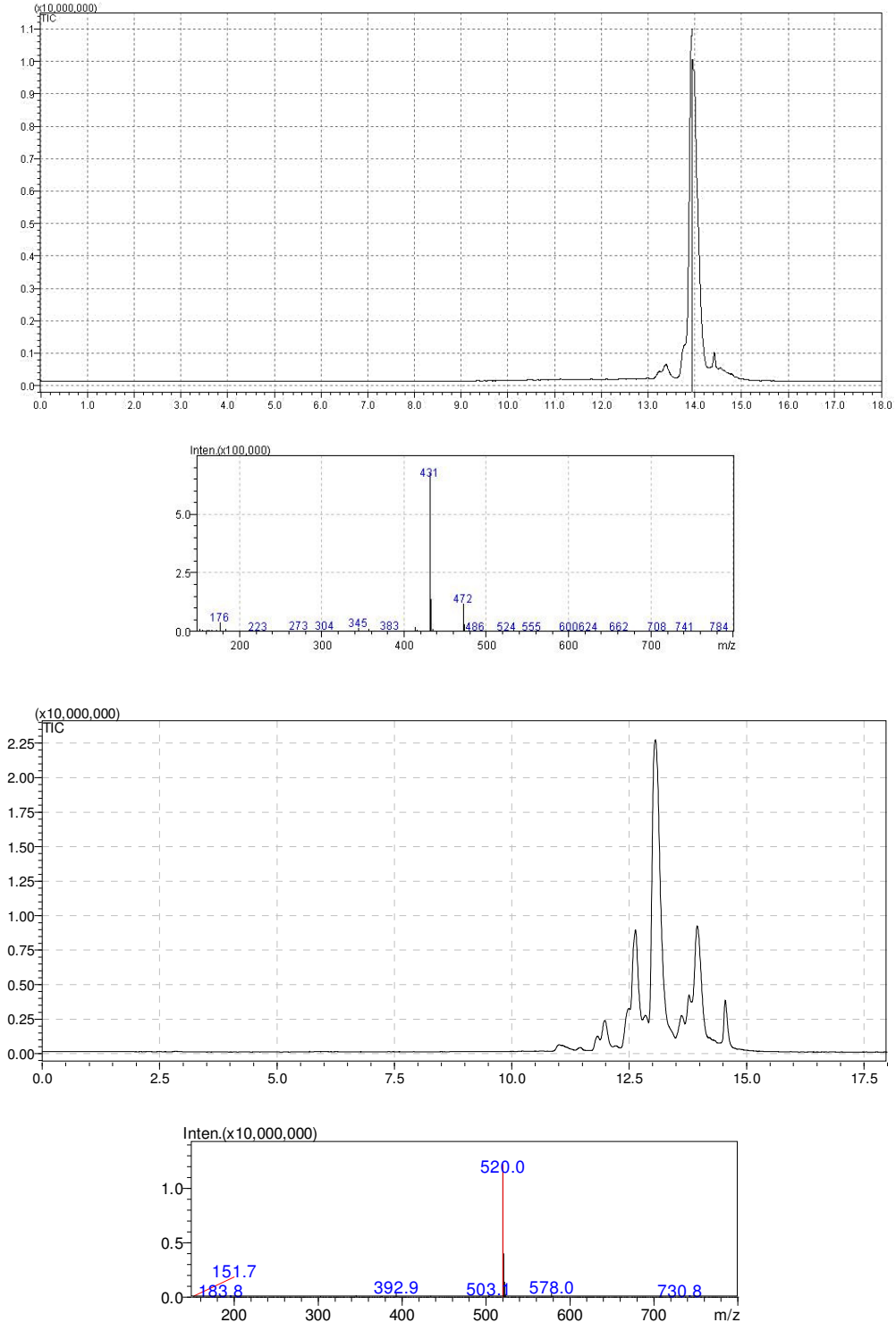

Figure 2-4: (top) graph of the total ion count of 2.15 and (top middle) the M+Z at 13.946 minutes, (bottom middle) graph of the total ion count of 2.16 and (bottom) the M+Z at 13.059 minutes

The first part of the identification of the cold standard 2.16 was to first use the LCMS on the crude product to verify that the click reaction worked. Figure 2-4 shows the LCMS total ion current chromatography (TIC) of both the precursor 2.15 and the cold standard 2.16; this is the summed intensity of the masses at the given point in time. The precursor shows up at 13.946 minutes with an M+H of 431 while the cold standard 2.16 has a retention time of 13.059 minutes and an M+H of 520. The cold standard retention time is of particular importance later as it will be used for the identification of the radiolabelled [^{18}F]2.16. LCMS serves a second important function, it allowed for the monitoring of the cold standard synthesis, for example if no product was formed with a catalyst system then there would be no product in the chromatograph; so a new catalyst system could be added. Once the precursor had formed in sufficient quantities then the cold standard would be purified and characterised.

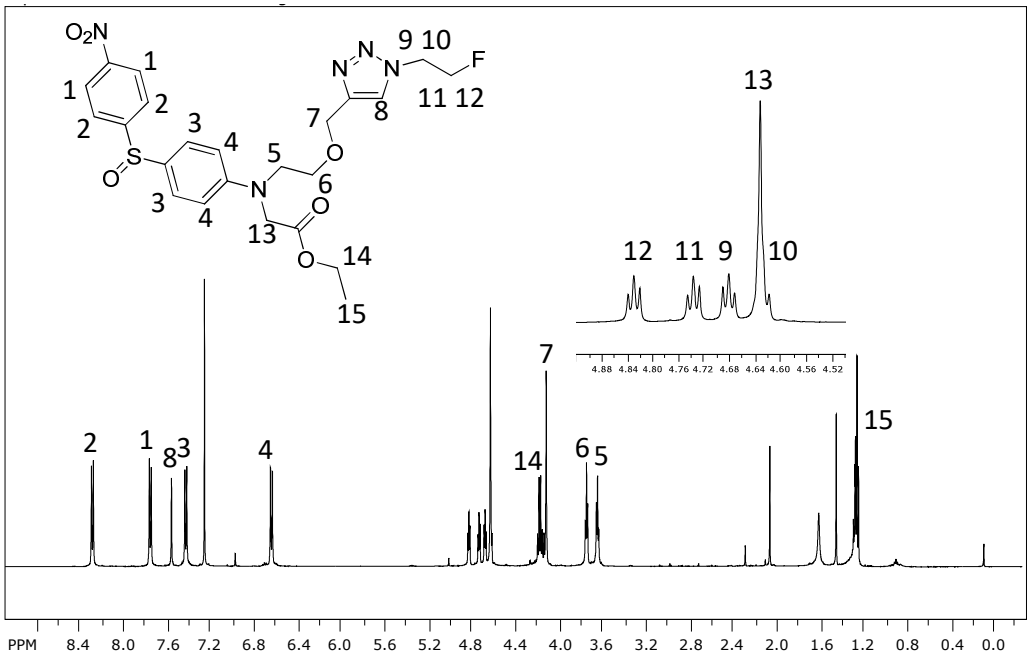

Figure 2-5: ^{1}H NMR of 2.16, inset shows a zoom of the region δ4.9-4.5ppm

Figure 2-5 shows the ^{1}H NMR of 2.16, in it 4 triplets can be seen in the region from δ4.9-4.5ppm; unfortunately, one of the peaks is obscured by another signal. This pattern is characteristic for all the cold standard ^{1}H NMRs and is thought to be the from the ethyl fluoride. The peaks are actually 2 sets of doublets of triplets due to the splitting from having 2 neighbouring protons as well as a fluoride which with a spin state of ½ also acts like an adjacent proton. Another indictor from the NMR for the successful synthesis of the cold standard is the loss of the alkyne signal from δ2.45ppm and a new aromatic peak at δ7.58ppm associated with the triazole that was formed.

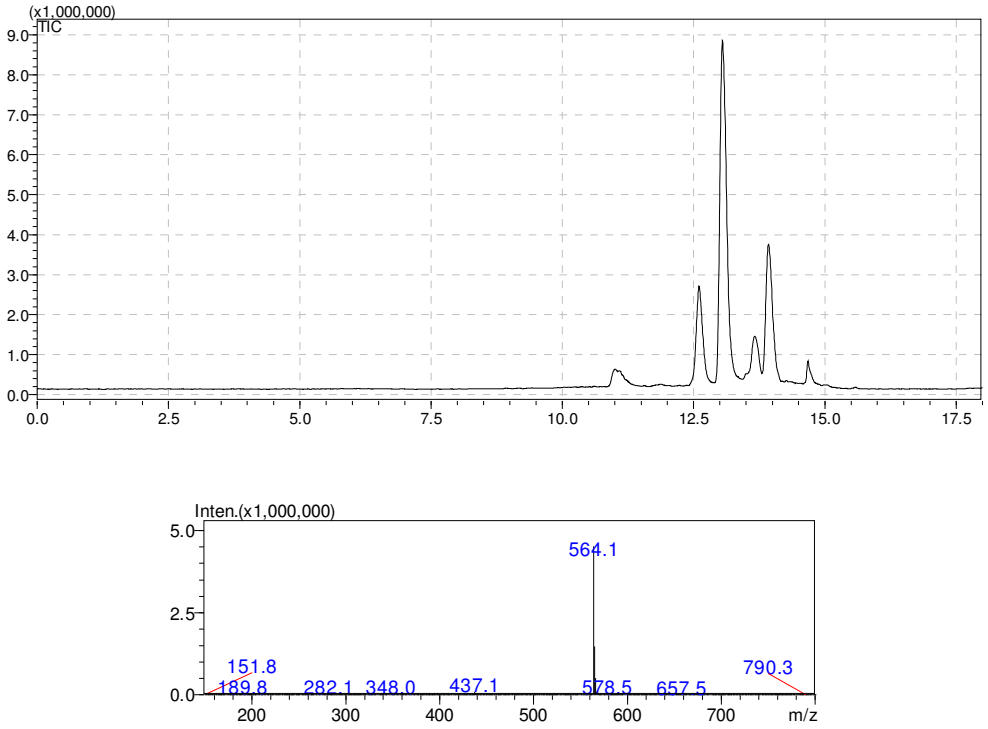

Figure 2-6: TIC of crude cold standard 2.26 and its corresponding MS at 13.032 minutes

Similarly to **2.16** the cold standard **2.26** was synthesised and characterised. Figure 2-6 shows the total ion current for 2.26 with a retention time of 13.032minutes and an M+H of 564.1. The NMR was analysed and showed the same results as that of 2.16 but with a higher proton integration due to the extra ethylene glycol group.

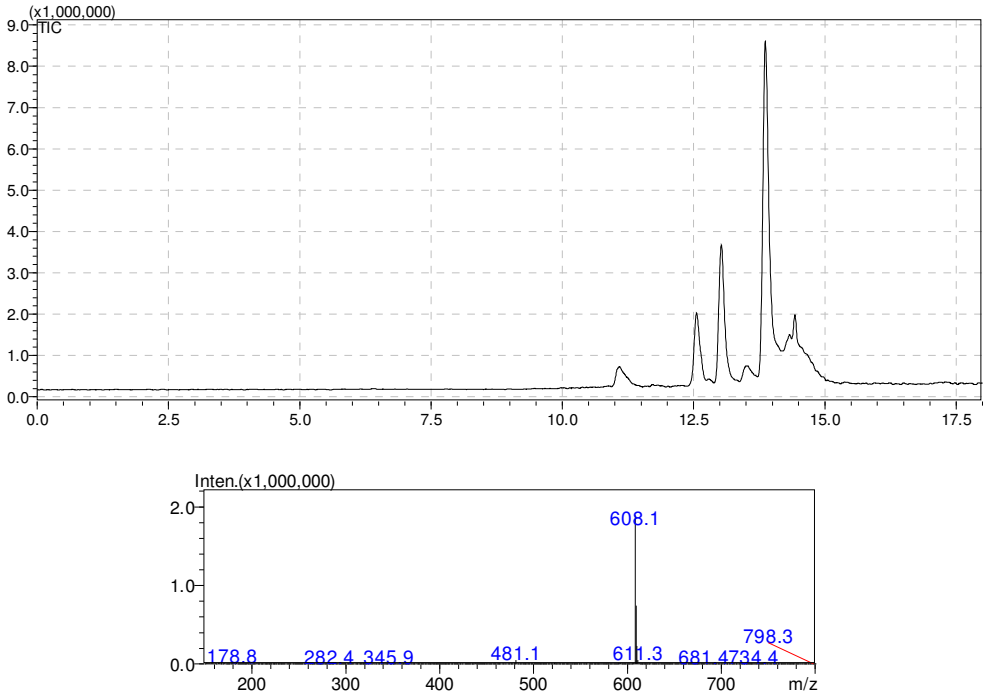

Figure 2-7: TIC of crude cold standard 2.36 and its corresponding MS at 13.032 minutes

2.36 was characterised by a retention time of 13.032 minutes, identical to that of **2.26**. This is most likely due to the very similar structure of the two cold standards with **2.36** having only one extra ethylene glycol chain. The MS however showed an M+H of 608.1 indicating the presence of the desired cold standard.

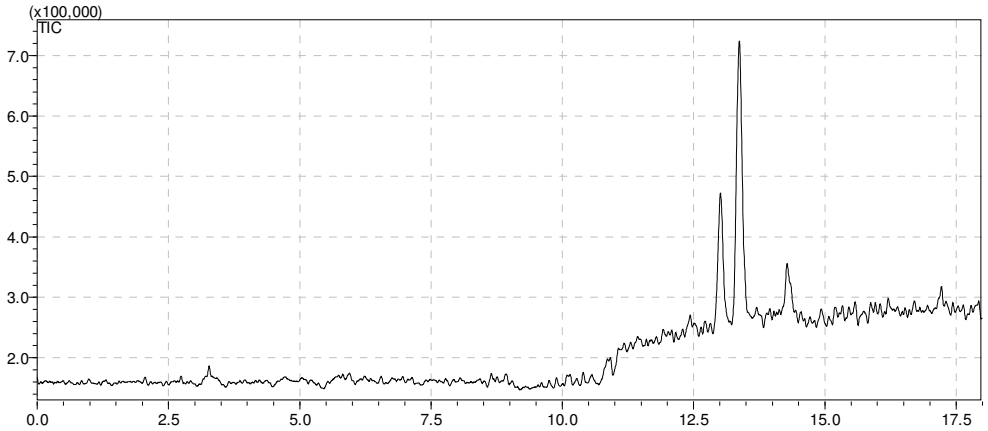

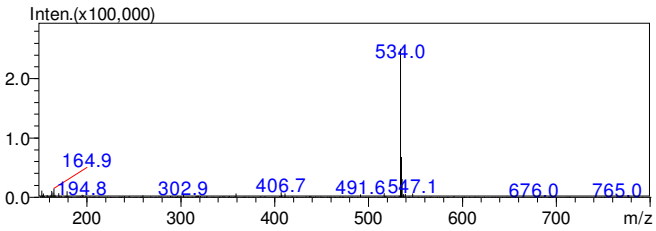

Figure 2-8: TIC of crude cold standard 2.43 and its corresponding MS at 13.357 minutes

Figure 2-8 shows the first isopropyl variant cold standard **2.43**. It has a later retention time of 13.357minutes compared to compound **2.16** which has an ethyl ester instead of the isopropyl ester of **2.43**. This is further reflected in the M+H of 534 for **2.43,** consistent with the structural differences being 14 mass units larger than the M+H of **2.16**.

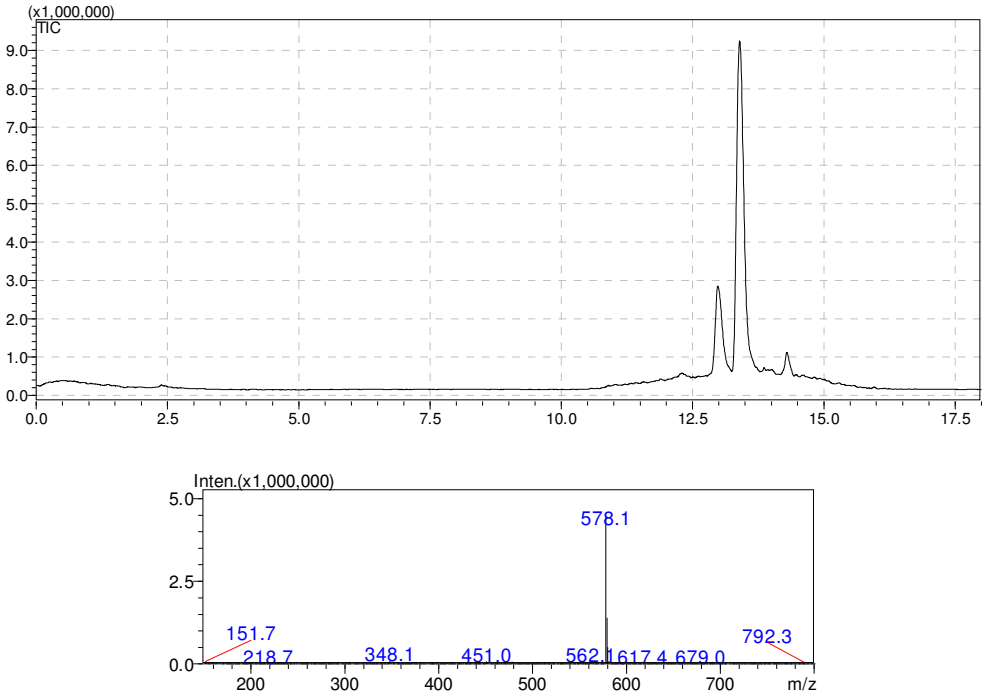

Figure 2-9: TIC of crude cold standard 2.53 and its corresponding MS at 13.385 minutes

The TIC for cold standard **2.53** is shown in Figure 2-9, it has a retention time of 13.385 minutes with an M+H of 578g/mol. It has a mass 14 units higher than its ethyl ester analogue **2.26**.

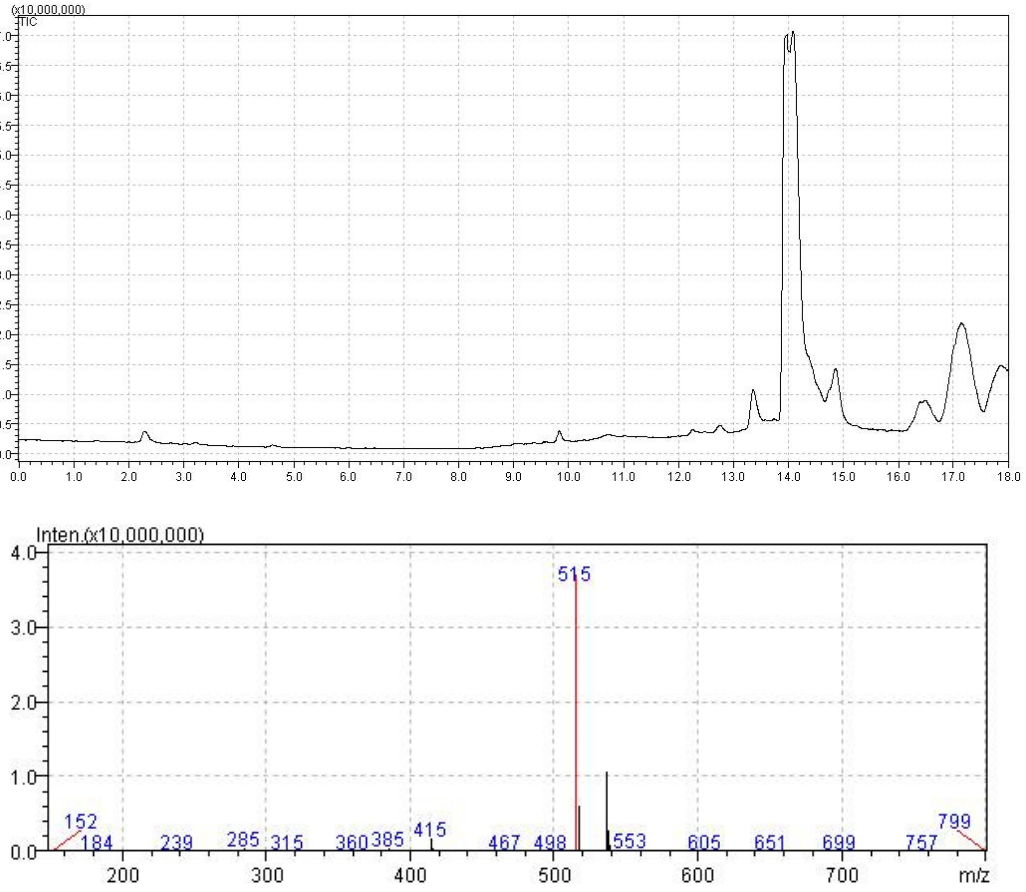

Figure 2-10: TIC of precursor 2.62 with a retention time of 13.958 min and its corresponding MS

Synthesis of the cold standard **2.63** began by HPLC analysis of the precursor 2.62 with the TIC shown in Figure 2-10, it has a retention time of 13.958 minutes with an M/Z of 515.

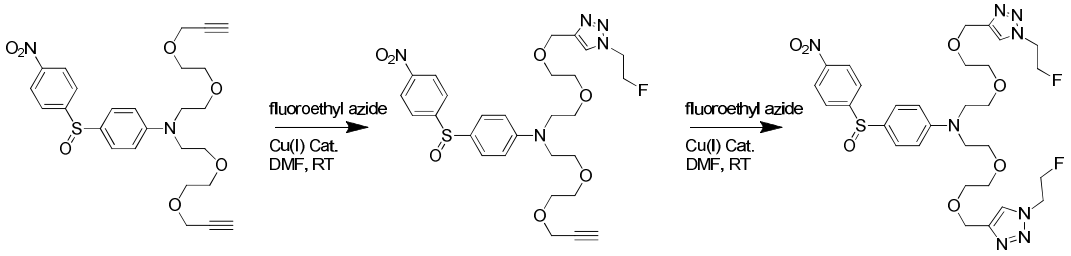

Figure 2-11: Synthesis of 2.63 and 2.64 from 2.62

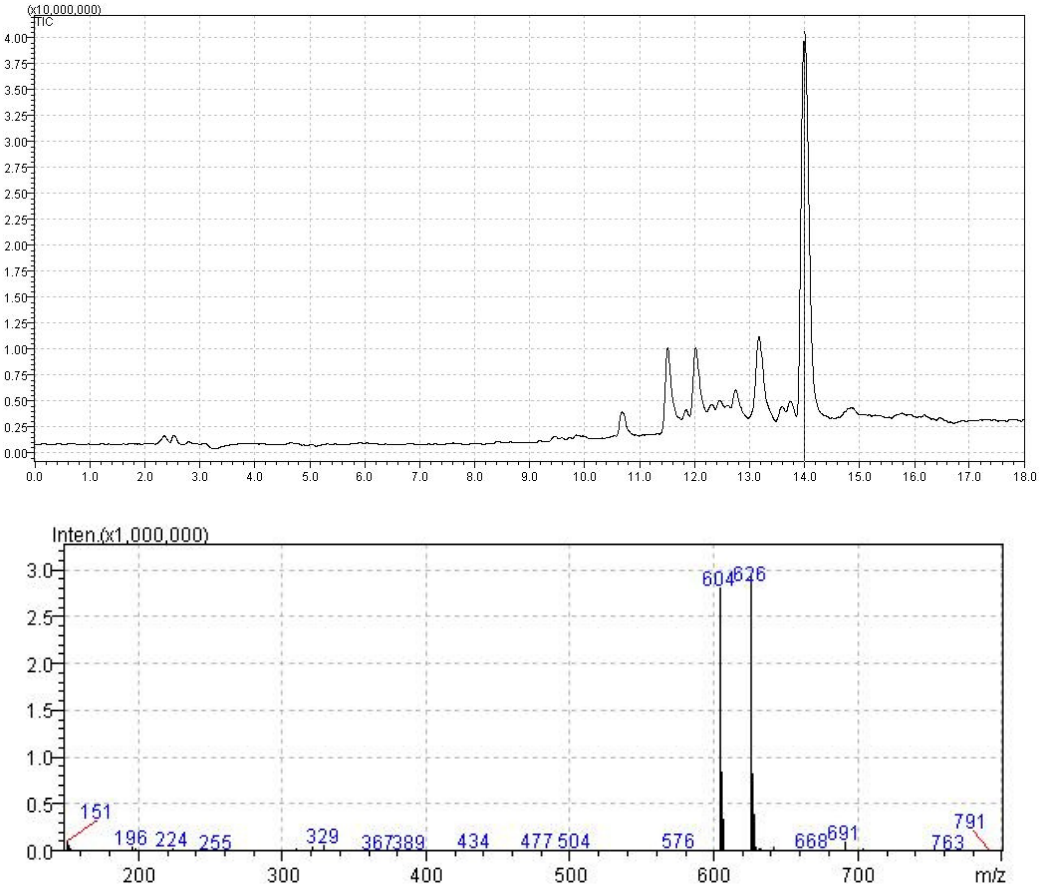

Figure 2-12: TIC of cold standard 2.63 with a retention time of 13.206 min and its corresponding MS

The cold standard reaction was set up as shown in Figure 2-11 with 2-fluoroethyl azide been added to the precursor **2.62** in the presence of the copper catalyst. After an hour of stirring at room temperate a sample was taken from the solution and tested on the HPLC system to determine if the reaction was proceeding. At 13.206 minutes a peak showing the desired product with an M+H of 604 is observed, but with the primary peak still been that of the precursor the reaction was left to react until 3 days had passed matching the reaction conditions of the previous cold standard reactions.

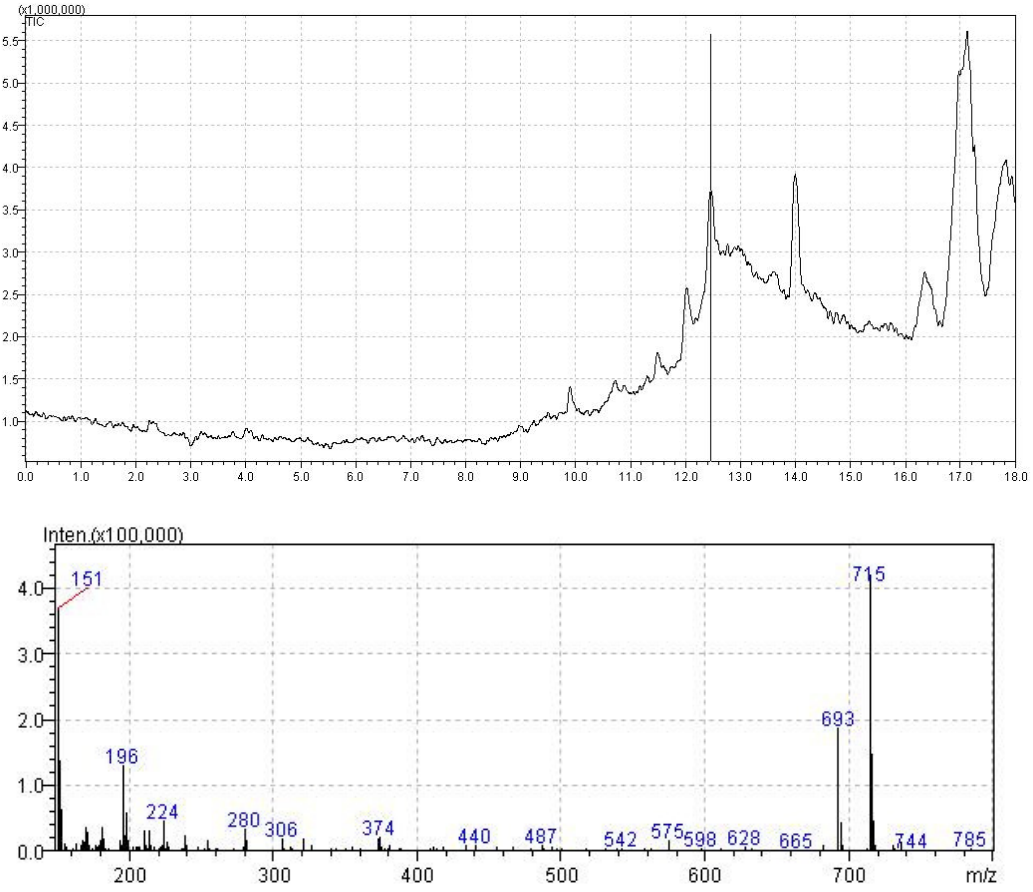

Figure 2-13: TIC at 3 days for the formation of cold standard 2.63. Compound 2.64 retention time at 12.457minutes and the corresponding MS at that time

After 3 days of reaction the peak at 13.206minutes for the cold standard 2.63 had disappeared with the corresponding M/z, instead a new peak is present in the TIC with a retention time of 12.457 minutes and a M/z of 693. This corresponded to the product that forms if both the alkyne groups from **2.62** undergo click chemistry to form the double reaction product **2.64**.

The inability to isolate the desired product meant that the quality control of [^{18}F]**2.63** would have to rely entirely on the LCMS of the crude cold standard reaction mixture. This also meant that the UV trace contained all the by-products from the reaction mixture giving multiple peaks. The only way to isolate the desired retention time was by analysing the total ion count from the corresponding mass spectrum.

2.4 Experimental

2.4.1 General

All chemicals and solvents were purchased from Sigma-Aldrich or Merck and used as received. Analytical thin layer chromatography (TLC) was carried out using aluminium backed 0.2mm thick Merck Kieselgel Silica gel 60 GF254. UV active compounds were visualised under UV 254nm light. Purification steps were carried out using automated column chromatography with either the Biotage Isolera One located at Bio21 or Reveleris located at Austin Health using either; Reveleris 80g silica 40µm, Reveleris 40g silica 40µm, Reveleris 12g silica 40µm, Reveleris 4g silica 40µm, Biotage 50g Silica Snap 40 µm, Biotage 25g Silica Snap 40 µm and Biotage 10g Silica Snap 40 µm. 2-Fluoroethyl 4-toluenesulfonate was synthesised according to literature procedures. All X-ray crystal data was collected and refined by Prof. Jonathan White.

Nuclear magnetic resonance (NMR) spectra ^{1}H and ^{13}C nuclei were recorded using a Varian Unity 500NMR operating at 500 and 125 MHz respectively. All ^{1}H NMR were obtained using deuterochloroform solution ($CDCl_3$) at 25˚C unless otherwise indicated. $CDCl_3$ run spectra were internally referenced to residual chloroform at δ 7.26ppm. 1H NMR chemical shifts (δ) are reported in parts per million (ppm) and are followed, in brackets, by integration, multiplicity (s: singlet, d: doublet, t: triplet, m: multiplet, dd: doublet of doublets, dt: doublet of triplets), coupling constant (*J*) given in Hertz (Hz) and peak assignment. Proton decoupled ^{13}C NMR chemical shifts were referenced on centre peak of $CDCl_3$ (δ 77.0ppm) and the signals reported as chemical shifts (ppm).

Synthesis of 2.11

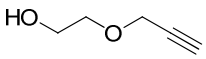

Potassium hydroxide (3.7g, 61.7mmol) was ground under $N_{2(g)}$, and then ethylene glycol (9.45mL, 167mmol) was added. The reaction mixture was stirred for 30mins at 40°C. Propargyl bromide (6mL, 55.7mmol) was added and the solution stirred at 60°C for 3hours. The mixture was diluted with 50mL of water and acidified to pH 1 with HCl (80mL, 1M). The crude product was then extracted with ethyl acetate (3x100mL) and washed with brine (2x100mL) and then dried with Na_2SO_4. The solvent was then removed *in-vacuo* to give the crude product as yellow oil. This was columned using a 0-100% hexane to ethyl acetate gradient to give the pure product as yellow oil (2.79g, 50%).

^{1}H NMR(500MHz, $CDCl_3$): 4.20 (2H, d, –C**H**$_2$C≡), 3.77 (2H, m, -OC**H**$_2$C-), 3.65 (2H, m, -CC**H**$_2$O-), 2.45 (1H, t, -CC**H**), 2.26 (1H, s, **H**O-)

^{13}C NMR(125MHz, $CDCl_3$): 80.79, 76.05, 72.54, 62.76, 59.62

Synthesis of 2.12

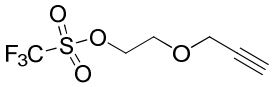

Trifluoromethanesulfonic anhydride **2.07** (5.03g, 3.00mL, 17.7mmol, 1.1eq.) was added to a stirred solution of 4-(polyvinyl) pyridine 2% crosslinked (3.5g, 32.2mmol) in dry DCM (50mL). Propargyl ethylene glycol **2.11** (1.16g, 16.1mmol) was then added dropwise at 0°C before the solution was left to stir at room temperature for 1 hour. The 4-(polyvinyl) pyridine was filtered off and washed with DCM (10mL). The organic phase was washed with $NaHCO_3$ (3 x 50mL), H_2O (3 x 50mL) and dried with $MgSO_4$. After removal of the solvent *in-vacuo* the crude product was given as yellow oil (2.02g, 54%).

^{1}H NMR(500MHz, $CDCl_3$): 4.65 (2H, m, -OC**H**$_2$C-), 4.24 (2H, d, –C**H**$_2$C≡), 3.87 (2H, m, -CC**H**$_2$O-), 2.48 (1H, t, -CC**H**)

^{13}C NMR(125MHz, $CDCl_3$): 118.57(q, CF_3), 78.39, 75.43, 75.03, 66.56, 58.43

Synthesis of 2.13

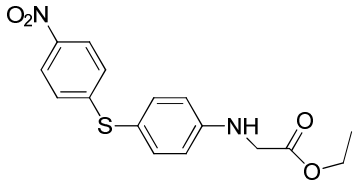

Ethyl bromoacetate **2.08** (0.85g, 0.6mL, 5.29mmol, 1.3 eq.) and anhydrous caesium carbonate (3.91g, 12.0mmol) were added to a solution of 4-nitro-4'-aminodiphenyl sulphide **2.01** (1.00g, 4.06mmol) in Acetonitrile (5mL). The reaction was left to stir overnight at 130^{o}C. After cooling to room temperature the solution was diluted with diethyl ether (90mL) and washed with $NaHCO_3$ (3 x 50mL), H_2O (3 x 50mL) and dried with $MgSO_4$. Removal of the solvent *in-vacuo* gave the crude product as a yellow solid (1.33g, 99%). The product was purified via flash chromatography to give yellow crystals (1.21g, 90%).

^{1}H NMR(500MHz, $CDCl_3$): 8.03 (2H, d, ArC**H**), 7.38(2H, d, ArC**H**), 7.09(2H, d, ArC**H**), 6.67(2H, d, ArC**H**), 4.62 (1H, br s, N**H**), 4.29 (2H, q, CC**H**$_2$CH$_3$), 3.95 (2H, br s, -NC**H**$_2$C-) 1.32 (3H, t, -CH$_2$C**H**$_3$)

^{13}C NMR(125MHz, $CDCl_3$): 170.50, 151.07, 148.47, 144.67, 137.15, 125.10, 123.80, 115.66, 113.96, 61.56, 45.20, 14.15

Synthesis of 2.14

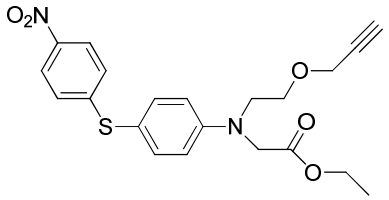

To a solution of 2.06 (0.332g, 1.0 mmol) in acetonitrile (5mL) in a sealed tube, 2.11 (1.63g, 7.0mmol) and anhydrous potassium carbonate (0.414g, 3.0mmol) were added. This was heated to 130°C and left to stir overnight. After cooling to room temperature the solution was diluted with diethyl ether (90mL) and washed with $NaHCO_3$ (3 x 50mL), H_2O (3 x 50mL) and dried with $MgSO_4$. The crude product was purified via flash chromatography to give yellow crystals (0.120g, 29%).

^{1}H NMR(500MHz, $CDCl_3$): 8.02 (2H, d, ArC**H**), 7.37(2H, d, ArC**H**), 7.08(2H, d, ArC**H**), 6.70(2H, d, ArC**H**), 4.22 (2H, q, CC**H**$_2$CH$_3$), 4.17 (4H, m),3.78 (2H, t, -NC**H**$_2$CH$_2$-), 3.69 (2H, t, -CH$_2$C**H**$_2$O-), 2.44 (1H, t, -CC**H**) 1.32 (3H, t, -CH$_2$C**H**$_3$)

^{13}C NMR(125MHz, $CDCl_3$): 189.89, 170.56, 168.77, 164.24, 156.53, 144.69, 143.32, 134.41, 132.63, 98.89, 94.24, 87.42, 80.67, 78.03, 72.37, 70.95, 33.72

Synthesis of 2.15

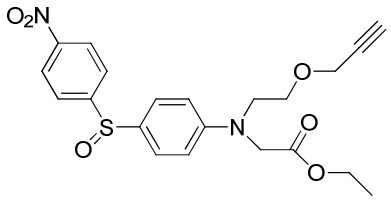

To a solution of **2.14** (0.100g, 0.24mmol) in methanol (20mL), $NaIO_4$ (0.043g, 0.20mmol) dissolved in H_2O (1mL) was added. This was reacted at 80°C under $N_{2(g)}$ overnight. The reaction was cooled to room temperature, diluted with water (30mL) and extracted with

DCM (3 x 30mL). The organic phase was the washed with water (50mL) and dried with $MgSO_4$. The solvent was removed in-vacuo to give a yellow residue which was purified via flash chromatography. The final product was a yellow oil(0.076g, 89%)

^{1}H NMR(500MHz, $CDCl_3$): 8.27 (2H, d, ArC**H**), 7.74(2H, d, ArC**H**), 7.43(2H, d, ArC**H**), 6.64(2H, d, ArC**H**), 4.16 (2H, q, CC**H**$_2$CH$_3$), 4.12 (2H, s, -NC**H**$_2$C-), 4.10(2H, d, –C**H**$_2$C≡), 3.78 (2H, t, -NC**H**$_2$CH$_2$-), 3.69 (2H, t, -CH$_2$C**H**$_2$O-), 2.44 (1H, t, -CC**H**) 1.32 (3H, t, -CH$_2$C**H**$_3$)

^{13}C NMR(125MHz, $CDCl_3$): 170.5, 153.66, 151.09, 148.99, 130.63, 128.14, 125.46, 124.20, 112.40, 79.34, 74.89, 67.81, 61.38, 58.61, 52.97, 51.57, 14.27

Synthesis of 2.21

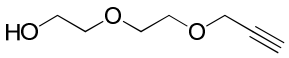

Potassium hydroxide (3.7g, 61.7mmol) was ground under $N_{2(g)}$, then diethylene glycol (15.8mL, 167mmol) was added. The reaction mixture was stirred for 30mins at 40^{o}C. Propargyl bromide (6mL, 55.7mmol) was added and the solution stirred at 60^{o}C for 3hours. The mixture was diluted with 50mL of water and acidified to pH 1 with HCl (80mL, 1M). The crude product was then extracted with ethyl acetate (3x100mL) and washed with brine (2x100mL) and then dried with Na_2SO_4. The solvent was then removed *in-vacuo* to give the crude product as yellow oil. This was columned using a 0-100% hexane to ethyl acetate gradient to give the pure product as yellow oil (3.85g, 48%).

^{1}H NMR(400MHz, $CDCl_3$): 4.21(2H, d, –C**H**$_2$C≡), 3.73(6H, m, HOCH$_2$C**H**$_2$OC**H**$_2$C**H**$_2$O), 3.61(2H, m, HOC**H**$_2$C), 2.44(1H, t, -CC**H**)

Synthesis of 2.22

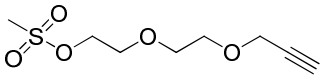

A solution of **2.14** (1.0g, 6.94mmol) and triethylamine (1.54g, 2.12mL, 15.3mmol) in dry DCM (15mL) was added drop wise to a solution of methanesulfonyl chloride (1.59g, 1.08mL, 13.9mmol) in dry DCM (35mL) at 0°C. The mixture was left to stir at room temperature for 1 hour before been diluted with DCM (50mL) and then quenched in chilled water (200mL). The organic layer was washed with water (2 x 50mL) and dried with $MgSO_4$ before the solvent was removed *in-vacuo*. The product was purified via flash chromatography to give a yellow oil (1.18g, 76%)

^{1}H NMR(500MHz, $CDCl_3$): 4.38 (2H, m, -SOC**H**$_2$C-), 4.19 (2H, d, –C**H**$_2$C≡), 3.77 (2H, m, -SOCH$_2$C**H**$_2$O-), 3.70 (4H, s, -OC**H**$_2$C**H**$_2$O-), 3.08 (3H, s, C**H**$_3$S-), 2.44 (1H, t, -CC**H**)

^{13}C NMR(125MHz, $CDCl_3$): 79.74, 75.00, 70.74, 69.54, 69.31, 58.67, 38.02

Synthesis of 2.23

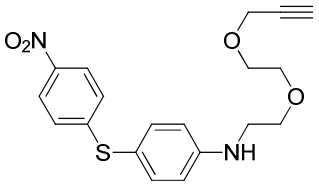

To a solution of 4-nitro-4'-aminodiphenyl sulphide **2.01** (0.30g, 1.22mmol) in Acetonitrile (15mL) in a sealed tube, **2.22** (1.35g, 6.08mmol, 5eq.), anhydrous caesium carbonate (0.91g, 2.80mmol) and sodium iodide (0.792g, 5.28mmol) were added. The reaction was left to stir overnight at 130°C. After cooling to room temperature the solution was diluted with diethyl ether (90mL) and washed with $NaHCO_3$ (3 x 50mL), H_2O (3 x 50mL) and dried with $MgSO_4$. Removal of the solvent *in-vacuo* gave the crude

product as a brown oil. The product was purified via flash chromatography to give viscous brown oil (0.30g, 66%).

^{1}H NMR(500MHz, $CDCl_3$): 8.02 (2H, d, ArC**H**), 7.34(2H, d, ArC**H**), 7.08(2H, d, ArC**H**), 6.68(2H, d, ArC**H**), 4.47 (1H, br s, N**H**), 4.17 (2H, d, –C**H**$_2$C≡), 3.74 (8H, m, -NC**H**$_2$C**H**$_2$OC**H**$_2$C**H**$_2$O-), 2.46 (1H, t, -CC**H**)

Synthesis of 2.24

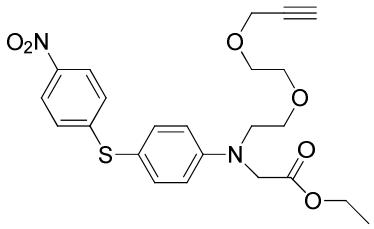

To a solution of **2.23** (0.30g, 0.81mmol) in Acetonitrile (15mL) in a sealed tube, ethyl bromoacetate **2.08** (1.34g, 0.9mL, 8.02mmol, 10eq.), anhydrous caesium carbonate (1.3g, 4.00mmol) and sodium iodide (0.60g, 4.00mmol) were added. The reaction was left to stir overnight at 130^{o}C. After cooling to room temperature the solution was diluted with diethyl ether (90mL) and washed with $NaHCO_3$ (3 x 50mL), H_2O (3 x 50mL) and dried with $MgSO_4$. Removal of the solvent *in-vacuo* gave the crude product as a brown oil. The product was purified via flash chromatography to give viscous brown oil (0.27g, 75%).

^{1}H NMR(500MHz, $CDCl_3$): 8.04 (2H, d, ArC**H**), 7.38(2H, d, ArC**H**), 7.10(2H, d, ArC**H**), 6.71(2H, d, ArC**H**), 4.22 (6H, m), 3.72 (8H, m, -NC**H**$_2$C**H**$_2$OC**H**$_2$C**H**$_2$O-), 2.45 (1H, t, -CC**H**), 1.30 (3H, t, -CH_2C**H**$_3$)

^{13}C NMR(125MHz, $CDCl_3$): 170.46, 151.08, 149.27, 144.72, 136.99, 125.15, 123.80, 114.74, 113.02, 79.48, 74.60, 70.52, 69.07, 69.04, 61.12, 58.39, 52.91, 51.50, 14.20

Synthesis of 2.25

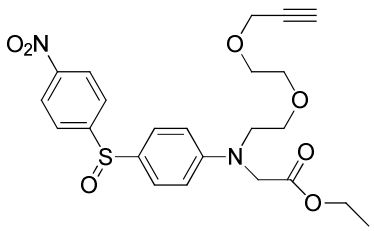

To a solution of **2.24** (0.200g, 0.44mmol) in methanol (20mL), $NaIO_4$ (0.075g, 0.35mmol) dissolved in H_2O (1mL) was added. This was reacted at 80°C under $N_{2(g)}$ overnight. The reaction was cooled to room temperature, diluted with water (30mL) and extracted with DCM (3 x 30mL). The organic phase was the washed with water (50mL) and dried with $MgSO_4$. The solvent was removed in-vacuo to give a yellow residue which was purified via flash chromatography. The final product was a yellow oil(0.117g, 57%).

^{1}H NMR(500MHz, $CDCl_3$): 8.31 (2H, d, ArC**H**), 7.78(2H, d, ArC**H**), 7.45 (2H, d, ArC**H**), 6.66(2H, d, ArC**H**), 4.18 (6H, m), 3.66 (8H, m, -NC**H**$_2$C**H**$_2$OC**H**$_2$C**H**$_2$O-), 2.44 (1H, t, -CC**H**), 1.27 (3H, t, -CH_2C**H**$_3$)

Synthesis of 2.31

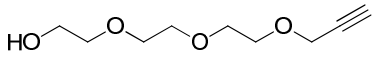

Potassium hydroxide (3.7g, 61.7mmol) was ground under $N_{2(g)}$, and then triethylene glycol (22.3mL, 167mmol) was added. The reaction mixture was stirred for 30mins at 40^{o}C. Propargyl bromide (6mL, 55.7mmol) was added and the solution stirred at 60^{o}C for 3hours. The mixture was diluted with 50mL of water and acidified to pH 1 with HCl (80mL, 1M). The crude product was then extracted with ethyl acetate (3x100mL) and washed with brine (2x100mL) and then dried with Na_2SO_4. The solvent was then removed *in-vacuo* to give the crude product as yellow oil. This was purified via flash chromatography to give the pure product as yellow oil (5.77g, 55%).

^{1}H NMR(500MHz, $CDCl_3$): 4.22 (2H, d, –C**H**$_2$C≡), 3.75 (10H, m, –OC**H**$_2$C**H**$_2$O-), 3.62 (2H, m, –OCH$_2$C**H**$_2$OCH2CCH), 2.42 (1H, t, –CC**H**)

^{13}C NMR(125MHz, $CDCl_3$): 79.5, 74.7, 72.5, 70.5, 70.19, 70.16, 68.9, 61.4, 58.2

Synthesis of 2.32

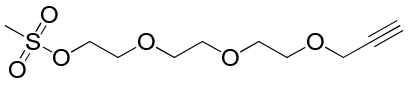

A solution of **2.31** (1.0g, 5.3mmol) and triethylamine (1.17g, 1.6mL, 11.7mmol) in dry DCM (15mL) was added drop wise to a solution of methanesulfonyl chloride (1.2g, 0.82mL, 10.6mmol) in dry DCM (35mL) at 0^{o}C. The mixture was left to stir at room temperature for 1 hour before been diluted with DCM (50mL) and then quenched in chilled water (200mL). The organic layer was washed with water (2 x 50mL) and dried with $MgSO_4$ before the solvent was removed *in-vacuo*. The product was purified via flash chromatography to give a yellow oil (1.1g, 78%)

^{1}H NMR(500MHz, $CDCl_3$): 4.38 (2H, m, -SOC**H**$_2$C-), 4.20 (2H, d, –C**H**$_2$C≡), 3.77 (2H, m, -SOCH$_2$C**H**$_2$O-), 3.70 (8H, s, -OC**H**$_2$C**H**$_2$O-), 3.08 (3H, s, C**H**$_3$S-), 2.44 (1H, t, -CC**H**)

^{13}C NMR(125MHz, $CDCl_3$): 79.46, 74.52, 70.42, 70.35, 70.20, 69.22, 68.91, 68.84, 58.19, 37.56

Synthesis of 2.33

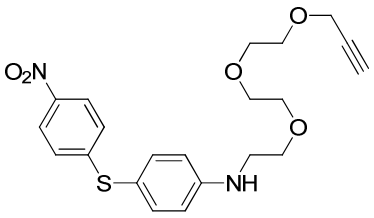

To a solution of 4-nitro-4'-aminodiphenyl sulphide **2.01** (0.30g, 1.22mmol) in Acetonitrile (15mL) in a sealed tube, **2.32** (1.6g, 6.08mmol, 5eq.), anhydrous caesium

carbonate (0.91g, 2.80mmol) and sodium iodide (0.792g, 5.28mmol) were added. The reaction was left to stir overnight at 130°C. After cooling to room temperature the solution was diluted with diethyl ether (90mL) and washed with $NaHCO_3$ (3 x 50mL), H_2O (3 x 50mL) and dried with $MgSO_4$. Removal of the solvent *in-vacuo* gave the crude product as a brown oil. The product was purified via flash chromatography to give viscous brown oil (0.174g, 34%).

^{1}H NMR(500MHz, $CDCl_3$): 8.01 (2H, d, ArC**H**), 7.33(2H, d, ArC**H**), 7.07(2H, d, ArC**H**), 6.67(2H, d, ArC**H**), 4.50 (1H, t, N**H**), 4.20 (2H, d, –C**H**$_2$C≡), 3.70 (12H, m, -NC**H**$_2$C**H**$_2$OC**H**$_2$C**H**$_2$O-), 2.46 (1H, t, -CC**H**)

^{13}C NMR(125MHz, $CDCl_3$): 151.43, 149.80, 144.72, 137.16, 125.09, 123.83, 114.66, 113.97, 79.56, 74.60, 70.58, 70.45, 70.30, 69.26, 69.10, 58.41, 43.10

Synthesis of 2.34

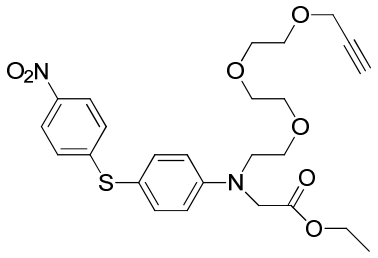

To a solution of **2.33** (0.15g, 0.36mmol) in Acetonitrile (15mL) in a sealed tube, ethyl bromoacetate **2.08** (0.60g, 0.4mL, 3.6mmol, 10eq.), anhydrous caesium carbonate (.59g, 1.8mmol) and sodium iodide (0.27g, 1.8mmol) were added. The reaction was left to stir overnight at 130°C. After cooling to room temperature the solution was diluted with diethyl ether (90mL) and washed with $NaHCO_3$ (3 x 50mL), H_2O (3 x 50mL) and dried with $MgSO_4$. Removal of the solvent *in-vacuo* gave the crude product as a brown oil. The product was purified via flash chromatography to give viscous brown oil (0.90g, 43%).

^{1}H NMR(500MHz, $CDCl_3$): 8.03 (2H, d, ArC**H**), 7.37(2H, d, ArC**H**), 7.09(2H, d, ArC**H**), 6.69(2H, d, ArC**H**), 4.21 (6H, m), 3.69 (12H, m, -NC**H**$_2$C**H**$_2$(OC**H**$_2$C**H**$_2$)$_2$O-), 2.43 (1H, t, -CC**H**), 1.29 (3H, t, -CH_2C**H**$_3$)

^{13}C NMR(125MHz, $CDCl_3$): 170.53, 151.14, 149.34, 144.75, 137.03, 125.19, 123.84, 114.71, 113.07, 79.61, 74.61, 70.71, 70.63, 70.44, 69.08, 69.06, 61.16, 58.38, 52.91, 51.54, 14.24

Synthesis of 2.35

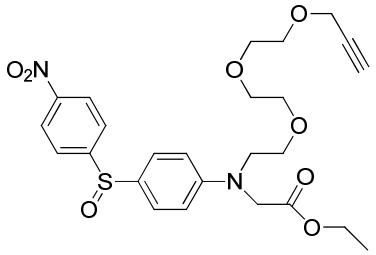

To a solution of **2.34** (0.08g, 0.16mmol) in methanol (20mL), $NaIO_4$ (0.026g, 0.12mmol) dissolved in H_2O (1mL) was added. This was reacted at 80°C under $N_{2(g)}$ overnight. The reaction was cooled to room temperature, diluted with water (30mL) and extracted with DCM (3 x 30mL). The organic phase was the washed with water (50mL) and dried with $MgSO_4$. The solvent was removed *in-vacuo* to give a yellow residue which was purified via flash chromatography. The final product was a yellow oil(0.040g, 48%).

^{1}H NMR(500MHz, $CDCl_3$): 8.28 (2H, d, ArC**H**), 7.75(2H, d, ArC**H**), 7.43(2H, d, ArC**H**), 6.65(2H, d, ArC**H**), 4.16 (6H, m), 3.63 (12H, m, -NC**H**$_2$C**H**$_2$(OC**H**$_2$C**H**$_2$)$_2$O-), 2.43 (1H, t, -CC**H**), 1.24 (3H, t, -CH_2C**H**$_3$)

^{13}C NMR(125MHz, $CDCl_3$): 170.08, 153.59, 151.08, 148.9, 130.36, 128.08, 125.39, 124.12, 112.25, 79.58, 74.60, 70.70, 70.58, 70.41, 69.05, 68.87, 61.26, 58.37, 52.92, 51.58, 14.19

Synthesis of 2.41

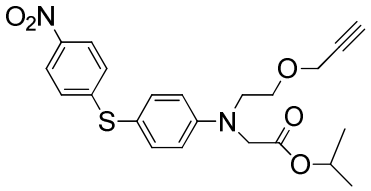

2.14 (0.100g, 0.24mmol) was dissolved in dry isopropanol (15mL) to this a solution of Sodium Isopropoxide in isopropanol was added (10%, 2mL), this was left to reflux overnight under N_2. The reaction was cooled then the solvent was removed *in-vacuo* leaving a yellow residue. Diethyl ether (3x20mL) was added and the mixture was sonicated and then filtered between each addition. The filtrates were combined and the solvent was removed to give the pure product as yellow oil (0.072g, 69%)

^{1}H NMR(500MHz, $CDCl_3$): 8.02 (2H, d, ArC**H**), 7.38(2H, d, ArC**H**), 7.08(2H, d, ArC**H**), 6.69(2H, d, ArC**H**), 5.08 (1H, m, -C**H**$(CH_3)_2$), 4.18(2H, d, -OC**H**$_2$CCH), 4.14(2H, s, -NC**H**$_2$OO-), 3.79 (2H, t, -NCH$_2$C**H**$_2$O-), 3.70(2H, t, -NC**H**$_2$CH$_2$O-), 2.44 (1H, t, -CC**H**), 1.26 (6H, d, -CH(C**H**$_3$)$_2$)

^{13}C NMR(125MHz, $CDCl_3$): 169.90, 151.08, 149.29, 144.74, 137.00, 125.17, 123.81, 114.88, 113.09, 79.362, 74.72,68.87, 67.86, 58.54, 53.15, 51.51, 21.79

Synthesis of 2.42

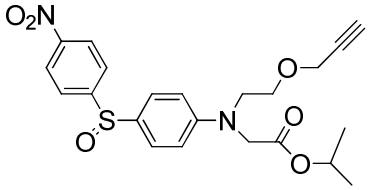

To a solution of **2.41**(0.070g, 0.16mmol) in dry isopropanol (20mL), $NaIO_4$ (0.028g, 0.13mmol) was added. This was reacted at 90°C under $N_{2(g)}$ overnight. The reaction was cooled to room temperature, diluted with water (30mL) and extracted with DCM (3 x

30mL). The organic phase was the washed with water (50mL) and dried with $MgSO_4$. The solvent was removed in-vacuo to give a yellow residue which was purified via flash chromatography. The final product was a yellow oil(0.019g, 26%).

^{1}H NMR(500MHz, $CDCl_3$): 8.30 (2H, d, ArC**H**), 7.77(2H, d, ArC**H**), 7.45(2H, d, ArC**H**), 6.66(2H, d, ArC**H**), 5.05 (1H, m, -C**H**$(CH_3)_2$), 4.14(2H, d, OC**H**$_2$CCH), 4.10(2H, s, -NC**H**$_2$OO-), 3.73 (2H, t, -NCH$_2$C**H**$_2$O-), 3.65 (2H, t, -NC**H**$_2$CH$_2$O-), 2.43 (1H, t, -CC**H**), 1.23 (6H, d, -CH(C**H**$_3)_2$)

^{13}C NMR(125MHz, $CDCl_3$): 169.44, 153.56, 151.03, 148.88, 130.49, 128.03, 125.35, 124.08, 112.26, 79.21, 74.77, 69.04, 67.65, 58.52, 53.13, 51.52, 21.74

Synthesis of 2.51

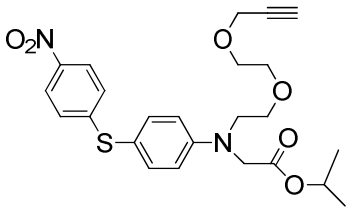

2.24 (0.076g, 0.16mmol) was dissolved in dry isopropanol (15mL) to this a solution of Sodium Isopropoxide in isopropanol was added (10%, 2mL), this was left to reflux overnight under N_2. The reaction was cooled then the solvent was removed *in-vacuo* leaving a yellow residue. Diethyl ether (3x20mL) was added and the mixture was sonicated and then filtered between each addition. The filtrates were combined and the solvent was removed to give the pure product as yellow oil (0.042g, 52%)

^{1}H NMR(500MHz, $CDCl_3$): 8.02 (2H, d, ArC**H**), 7.37(2H, d, ArC**H**), 7.08(2H, d, ArC**H**), 6.68(2H, d, ArC**H**), 5.08 (1H, m, -C**H**$(CH_3)_2$), 4.20 (2H, d, OC**H**$_2$CCH), 4.14(2H,s, -NC**H**$_2$OO-), 3.69(8H, m), 2.43 (1H, t, -CC**H**), 1.25 (6H, d, -CH(C**H**$_3)_2$)

^{13}C NMR(125MHz, $CDCl_3$): 169.97, 151.11, 149.32, 144.72, 136.98, 125.14, 123.80, 114.69, 113.00, 79.46, 74.59, 70.53, 69.04, 69.01, 68.83, 58.39, 53.19, 51.58, 21.78

Synthesis of 2.52

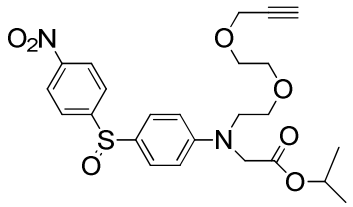

To a solution of **2.51** (0.085g, 0.18mmol) in dry isopropanol (20mL), $NaIO_4$ (0.031g, 0.14mmol) was added. This was reacted at 90°C under $N_{2(g)}$ overnight. The reaction was cooled to room temperature, diluted with water (30mL) and extracted with DCM (3 x 30mL). The organic phase was the washed with water (50mL) and dried with $MgSO_4$. The solvent was removed in-vacuo to give a yellow residue which was purified via flash chromatography. The final product was a yellow oil (0.036g, 41%).

^{1}H NMR(500MHz, $CDCl_3$): 8.28(2H, d, ArC**H**), 7.75(2H, d, ArC**H**), 7.43(2H, d, ArC**H**), 6.63(2H, d, ArC**H**), 5.03 (1H, m, -C**H**$(CH_3)_2$), 4.15(2H, d, OC**H**$_2$CCH), 4.09(2H,s, -NC**H**$_2$OO-), 3.64(8H, m), 2.42(1H, t, -CC**H**), 1.21(6H, d, -CH(C**H**$_3)_2$)

^{13}C NMR(125MHz, $CDCl_3$): 169.52, 153.56, 151.08, 148.87, 130.30, 128.04, 125.35, 124.07, 112.20, 79.42, 74.63, 70.52, 69.01, 68.83, 58.37, 53.18, 51.61 21.75

Synthesis of 2.61

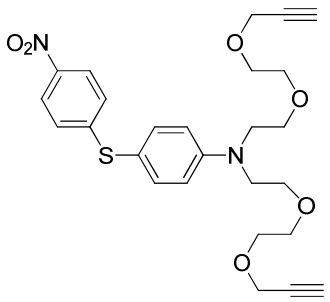

To a solution of 4-nitro-4'-aminodiphenyl sulphide **2.04** (0.30g, 1.22mmol) in Acetonitrile (15mL) in a sealed tube, **2.17** (1.35g, 6.08mmol, 5eq.), anhydrous caesium carbonate (0.91g, 2.80mmol), water (0.5mL) and sodium iodide (0.792g, 5.28mmol) were added. The reaction was left to stir overnight at 130°C. After cooling to room temperature the solution was diluted with diethyl ether (90mL) and washed with $NaHCO_3$ (3 x 50mL), H_2O (3 x 50mL) and dried with $MgSO_4$. Removal of the solvent *in-vacuo* gave the crude product as brown oil. The product was purified via flash chromatography to give 2.61 as a viscous brown oil (0.298g, 49%).

Synthesis of 2.62

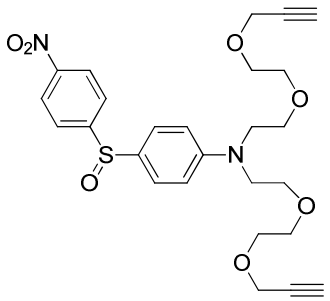

To a solution of 2.61 (0.10g, 0.2mmol) in methanol (20mL), $NaIO_4$ (0.g, 0.mmol) dissolved in H_2O (1mL) was added. This was refluxed under $N_{2(g)}$ overnight. The reaction was cooled to room temperature, diluted with water (30mL) and extracted with DCM (3 x 30mL). The organic phase was the washed with water (50mL) and dried with $MgSO_4$. The solvent was removed in-vacuo to give a yellow residue which was purified via flash chromatography. The final product was a yellow oil(0.063g, 62%)

2-[^{19}F]Fluoroethyl Azide 2.72

Sodium azide (65mg, 1 mmol) was added to a solution of 2-fluoroethyl-4-toluenesulfonate (218mg, 1mmol) in 10mL of anhydrous DMF. The mixture was stirred at room temperature for 24hours to give the crude product which was used without further purification.

Preparation of the copper catalyst for click chemistry

H_2O (250µL) was added to CuI (2.5mg, 0.013mmol) and sodium ascorbate (22.9mg, 0.13mmol). To this mixture diisopropylethylamine (25µL, 0.14mmol), DMF (250µL) and acetonitrile (250µL) were added. This mixture was used in it's entirety to catalyse each click reaction.

Synthesis of 2.16

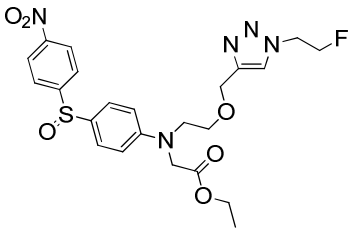

To a stirred solution of **2.15** (20mg, 0.046mmol) in acetonitrile, the prepared copper catalyst mixture was added. 2-[^{19}F]fluoroethyl azide solution (**2.72**) (3eq.) was then added and the reaction left to stir for 72 hours at room temperature. The majority of the solvent was removed in-vacuo and the remaining was diluted with water (3mL)

before it was extracted with Ethyl acetate (3x 10mL). The organic phase was diluted with ethyl acetate (30mL) and dried with $MgSO_4$. The crude product was dried *in-vacuo* and purified via flash chromatography to afford a yellow residue (7mg, 29%).

^{1}H NMR(500MHz, $CDCl_3$): 8.27 (2H, d, ArC**H**), 7.77(2H, d, ArC**H**), 7.57(1H, s, ArC**H**), 7.44(2H, d, ArC**H**), 6.65(2H, d, ArC**H**), 4.82(2H, dt, -CH_2C**H**$_2$F), 4.73(2H, dt, -C**H**$_2$$CH_2$F), 4.62(2H, s, OC**H**$_2$Ar), 4.17 (2H, q, CC**H**$_2$$CH_3$), 4.12(2H, s, -NC**H**$_2$C-), 3.74(2H, t, -NC**H**$_2$$CH_2$-), 3.64 (2H, t, -$CH_2$C**H**$_2$O-), 1.25 (3H, t, -$CH_2$C**H**$_3$)

Synthesis of 2.26

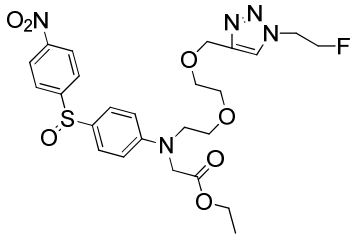

To a stirred solution of **2.25** (22.1mg, 0.046mmol) in acetonitrile, the prepared copper catalyst mixture was added. 2-[^{19}F]fluoroethyl azide solution (**2.72**) (3eq.) was then added and the reaction left to stir for 72 hours at room temperature. The majority of the solvent was removed in-vacuo and the remaining was diluted with water (3mL) before it was extracted with Ethyl acetate (3x 10mL). The organic phase was diluted with ethyl acetate (30mL) and dried with $MgSO_4$. The crude product was dried *in-vacuo* and purified via flash chromatography to afford a yellow residue (7.7mg, 29%).

^{1}H NMR(500MHz, $CDCl_3$): 8.29 (2H, d, ArC**H**), 7.76(2H, d, ArC**H**), 7.65(1H, s, ArC**H**), 7.43(2H, d, ArC**H**), 6.65(2H, d, ArC**H**), 4.84(2H, dt, -CH_2C**H**$_2$F), 4.75(2H, dt, -C**H**$_2$$CH_2$F), 4.66(2H, s, OC**H**$_2$Ar), 4.18 (2H, q, CC**H**$_2$$CH_3$), 4.13(2H, s, -NC**H**$_2$C-), 3.64(8H, m, -NC**H**$_2$C**H**$_2$OC**H**$_2$C**H**$_2$O-), 1.25 (3H, t, -CH_2C**H**$_3$)

Synthesis of 2.36

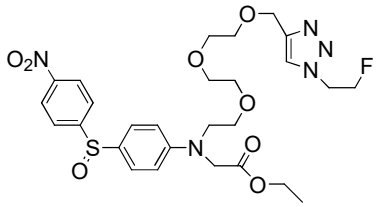

To a stirred solution of **2.35** (25.4mg, 0.049mmol) in acetonitrile, the prepared copper catalyst mixture was added. 2-[^{19}F]fluoroethyl azide solution (**2.72**) (3eq.) was then added and the reaction left to stir for 72 hours at room temperature. The majority of the solvent was removed in-vacuo and the remaining was diluted with water (3mL) before it was extracted with Ethyl acetate (3x 10mL). The organic phase was diluted with ethyl acetate (30mL) and dried with $MgSO_4$. The crude product was dried *in-vacuo* and purified via flash chromatography to afford a yellow residue (8.1mg, 27%).

^{1}H NMR(500MHz, $CDCl_3$): 8.30(2H, d, ArC**H**), 7.77(2H, d, ArC**H**), 7.69(1H, s, ArC**H**), 7.44(2H, d, ArC**H**), 6.65(2H, d, ArC**H**), 4.84(2H, dt, -CH_2C**H**$_2$F), 4.75(2H, dt, -C**H**$_2$$CH_2$F), 4.68(2H, s, OC**H**$_2$Ar), 4.18(2H, q, CC**H**$_2$$CH_3$), 4.14(2H, s, -NC**H**$_2$C-), 3.65(12H, m, -NC**H**$_2$C**H**$_2$(OC**H**$_2$C**H**$_2$)$_2$O-), 1.25 (3H, t, -CH_2C**H**$_3$)

Synthesis of 2.43

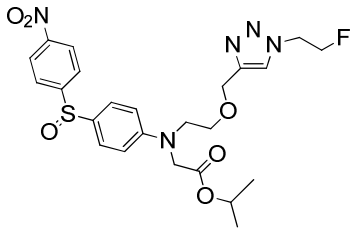

To a stirred solution of **2.42** (23.7mg, 0.053mmol) in acetonitrile, the prepared copper catalyst mixture was added. 2-[^{19}F]fluoroethyl azide solution (**2.72**) (3eq.) was then added and the reaction left to stir for 72 hours at room temperature. The majority of

the solvent was removed in-vacuo and the remaining was diluted with water (3mL) before it was extracted with Ethyl acetate (3x 10mL). The organic phase was diluted with ethyl acetate (30mL) and dried with $MgSO_4$. The crude product was dried *in-vacuo* and purified via flash chromatography to afford a yellow residue (6.3mg, 21%).

^{1}H NMR(500MHz, $CDCl_3$): 8.29(2H, d, ArC**H**), 7.76(2H, d, ArC**H**), 7.57(1H, s, ArC**H**), 7.43(2H, d, ArC**H**), 6.63(2H, d, ArC**H**), 5.02(1H, septet, CC**H**$(CH_3)_2$), 4.81(2H, dt, -CH-$_2$C**H**$_2$F), 4.73(2H, dt, -C**H**$_2$CH$_2$F), 4.63(2H, s, OC**H**$_2$Ar), 4.06(2H, s, -NC**H**$_2$C-), 3.73(2H, t, -NC**H**$_2$CH$_2$-), 3.63 (2H, t, -CH$_2$C**H**$_2$O-), 1.20 (6H, d, -CH(C**H**$_3$)$_2$)

Synthesis of 2.53

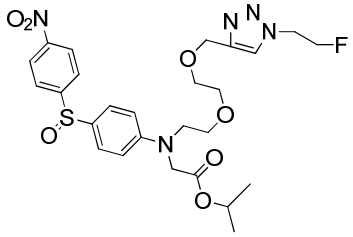

To a stirred solution of **2.52** (28.2mg, 0.058mmol) in acetonitrile, the prepared copper catalyst mixture was added. 2-[^{19}F]fluoroethyl azide solution (**2.15**) (3eq.) was then added and the reaction left to stir for 72 hours at room temperature. The majority of the solvent was removed in-vacuo and the remaining was diluted with water (3mL) before it was extracted with Ethyl acetate (3x 10mL). The organic phase was diluted with ethyl acetate (30mL) and dried with $MgSO_4$. The crude product was dried *in-vacuo* and purified via flash chromatography to afford a yellow residue (5.6mg, 17%)

^{1}H NMR(500MHz, $CDCl_3$): 8.29(2H, d, ArC**H**), 7.76(2H, d, ArC**H**), 7.66(1H, s, ArC**H**), 7.43(2H, d, ArC**H**), 6.64(2H, d, ArC**H**), 5.03(2H, septet, CC**H**$(CH_3)_2$), 4.84(2H, dt, -CH-

$_2$C**H**$_2$F), 4.75(2H, dt, -C**H**$_2$CH$_2$F), 4.67(2H, s, OC**H**$_2$Ar), 4.09(2H, s, -NC**H**$_2$C-), 3.65(8H, m, -NC**H**$_2$C**H**$_2$OC**H**$_2$C**H**$_2$O-) , 1.25 (6H, d, -CH(C**H**$_3$)$_2$)

Synthesis of 2.63

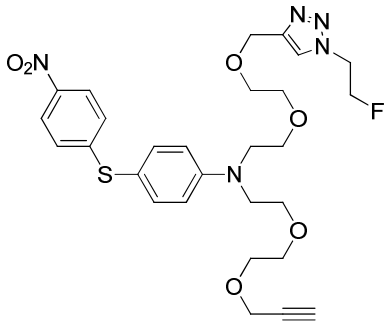

To a stirred solution of **2.62** (32.5mg, 0.063mmol) in acetonitrile, the prepared copper catalyst mixture was added. 2-[^{19}F]fluoroethyl azide solution (**2.15**) (3eq.) was then added and the reaction left to stir for 72 hours at room temperature. The product could not be isolated as the reaction had passed completion to form an unwanted by-product.

3 Radiosynthesis of Fluorine-18 Radiotracers

3.1 Introduction

With the synthesis of the precursors and their cold standards completed the next step was to utilise the precursors in radiolabelling experiments, to test the potential of the new imaging agents.

Radiolabelling experiments were carried out using the Fluorine-18 isotope produced from either the 18/18 or 10/5 cyclotron at Austin Health.

3.1.1 Production of Fluorine-18 radioisotopes

The [^{18}F]fluoride radioisotope was produced via the ^{18}O(p,n)^{18}F nuclear reaction using either a 18MeV or 10 MeV proton beam, generated by the IBA cyclone 18/18 cyclotron or 10/5 cyclotron respectively, in a titanium target using [^{18}O]H_2O.[52, 80] Irradiation typically took about 10 minutes on the 18/18 cyclotron and 30 minutes on the 10/5 cyclotron. The irradiation cycles typically produced around 200-300mCi (5.4-8.1 GBq) of [^{18}F]fluoride.[80] The [^{18}F]fluoride is transferred from the target in the cyclotron to the synthesis module using He gas. No Fluorine-19 is added during the production making it "no-carrier-added"; this helps with the specific activity as there is no competition between the fluorine isotopes that would be associated with [^{18}F]F_2 gas.[50]

[^{18}F]Fluoride is produced in the form of [^{18}F]HF in [^{18}O]H_2O, leaving it initially unsuitable for nucleophilic substitutions. [^{18}F]Fluoride must be isolated so that there is no competition with water during the labelling process; it must also be treated with base.[50, 81-82]

Isolation of $[^{18}F]F^-$ from the $[^{18}O]H_2O$ is achieved by trapping it onto a QMA ion exchange column.[50] The activated QMA column had previously been conditioned using a 0.1M potassium carbonate solution and 10mL of deionised water. The trapped $[^{18}F]F^-$ is eluted off the QMA column using a solution containing 3.5mg of potassium carbonate in 0.2mL of water and 20mg of kryptofix 2.2.2 in 0.4mL of acetonitrile. Krytopfix 2.2.2 acts as a chelating agent, forming the K^+/kryptofix complex as illustrated in Scheme 3-1: Kryptofix acting as a chelating agent for Fluorine-18 radiolabelling allowing the $^{18}F^-$ to be eluted in a organic solvent making it for radiolabelling.[50, 54, 83]

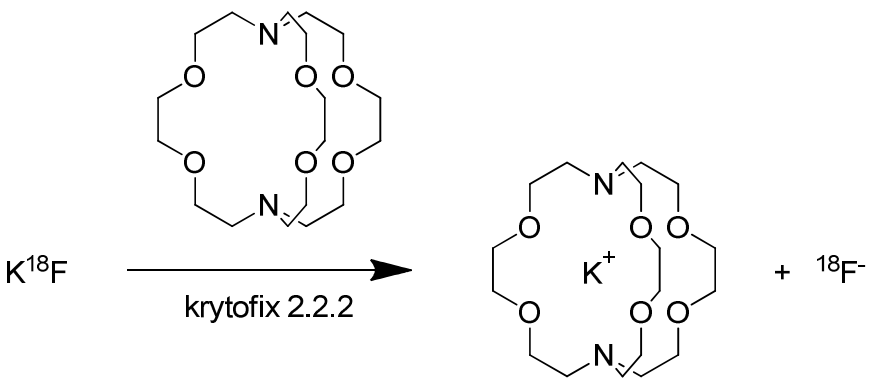

Scheme 3-1: Kryptofix acting as a chelating agent for Fluorine-18 radiolabelling

Once the Fluorine is extracted from the QMA by the eluent solution the water is removed by azeotropic distillation with acetonitrile. Repeated cycles of evaporative drying ensured that the fluoride ion was anhydrous for the following labelling experiments.[50-51, 80]

3.1.2 Radiolabelling methods

There are 2 methods of synthesis available for use at the Austin hospital for the incorporation of a fluorine-18 into the precursors; either a simple halogen exchange or via click chemistry. For the purposes of this project only click chemistry was used.

Radiolabelling experiments ideally have to be as short a time as possible with a maximum length of 120-150minutes including time for purification and reformulation, due to the constant decay of the Fluorine-18. Reactions were therefore optimised to in order to determine the most suitable conditions to maximise the yield of radiotracer.

3.1.3 Click Chemistry Radiolabelling

Many research groups have used click chemistry as a method of radiochemical synthesis.[79-80, 84-85] It offers several advantages over some conventional radiolabelling procedures including; compatibility with many functional groups, no deprotection steps, simple reaction conditions and less by-products formed.[79, 86]

There are several forms for click chemistry utilised for the introduction of [^{18}F]Fluoride into small molecules and biomolecules. The first type of click chemistry is the Copper(I)-catalysed azide-alkyne cycloaddition, this utilises a copper catalyst to overcome the activation barrier to allow the alkyne and azide to react under mild conditions for form a triazole. This allows for small molecules and biomolecules to be incorporated with one of the reactive groups followed by labelling with a prosthetic group containing the opposite moiety and the radioactive [^{18}F]Fluoride.[87] This is the type of click chemistry used in this thesis and will be explained in more detail later.

Another type of click chemistry is a strain-promoted azide-alkyne cycloaddition. This reaction relies on the reaction of a strained triple bond on a cyclooctyne with the azide without the copper catalyst of the previous type, an example of this is demonstrated in Scheme 3-2.

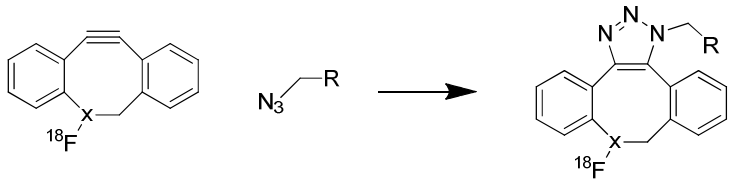

Scheme 3-2: An example of a strain-promoted azide-alkyne cycloaddition

Further types of click chemistry used in radiosynthesis include the Staudinger ligation and Tetrazine ligation. Staudinger ligations don't rely on metal catalysts and instead the reactions are carried out between an azide and phosphine via a iminophosphorane. The iminophosporane is stable in organic solvents, but in an aqueous solution it is rapidly hydrolysed to give the primary amine and phosphine oxide.[87] The ^{18}F labelled amide is easily separated from the phosphine oxide by-product.

Tetrazine ligations are based on an inverse electron demand Diels-Alder reaction of s-tetrazine and trans-cyclooctene moieties as a biorthogonal cycloaddition. Tetrazine ligations are characterised by a rapid reaction meaning they do not require a metal catalyst, can be effectively performed at low concentrations and are not dependant on the type of solvent allowing them to be carried out in water, cell media, cell lysates or organic solvents without comprising yields.[87]

For this project all the click chemistry involved the use of [^{18}F]fluoroethyl azide(**[^{18}F]2.72**) for the introduction of fluoroine-18 into the structure of the compound.[79] This was achieved through the 1,3 Huisgen cycloaddition of the [^{18}F]fluoroethyl azide(**[^{18}F]2.72**) and the terminal alkyne of the precursor.[78]

To ensure the correct product was formed a catalyst was used to promote the click reaction. The type of catalyst used will influence the yielded product.[88-90] In this case the use of Cu(I) catalyst resulted in the formation of 1,4 adducts while other catalysts or thermal promotion of the reaction would form the 1,5 adduct.[88, 91-92] This project solely focused on the 1,4 adduct so Cu(I) was used as the catalyst.

Figure 3-1: Iphase Flexlab for the automated synthesis of radiolabelled compounds

Radiolabelling for the click chemistry reactions is performed in an automated synthesis module Iphase Flexlab shown in Figure 3-1 . The Flexlab is contained in a lead lined hot cell designed to shield the operators from radiation, allowing for the safe handling of Fluorine-18 labelled compounds.

The Iphase Flexlab module contains 2 reaction vials, 2 heating apparatus and multiple vials for the holding of solvents or additional reactants, it also has 2 integrated HPLC loop loading systems, 2 HPLC columns and the ability to reformulate the product after

purification. It uses both vacuum and pressurisation with inert gasses to move reagents and solvents.

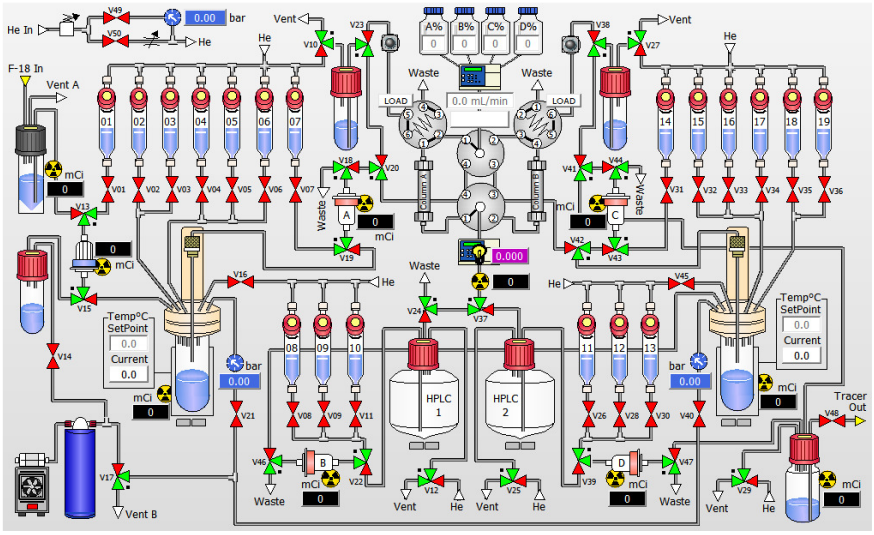

Figure 3-2: Schematic of the Iphase Flexlab

The synthesis module is controlled by a laptop which uses a recipe to determine what steps to take. Figure 3-2 shows the graphical user interface; from this screen the automated process can be interrupted with input from the operator if modifications to the synthesis are required. The only manual step usually required of the operator is the selection of the radioactive peak on the HPLC column for the output of the tracers being synthesised.

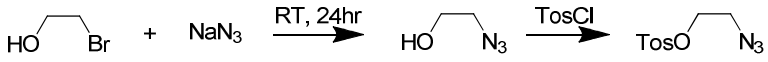

Scheme 3-3: Synthesis of tosylethyl azide

2-tosylethyl azide was prepared by Dr. Rachel Goh at the Austin Health using the method presented in Scheme 3-3. Starting with 2-bromoethanol reacted with sodium azide for 24hours at room temperate the 2-azido ethanol was formed. This is then reacted with tosylchloride forming 2-tosylethyl azide.

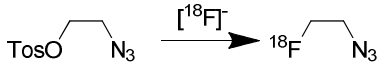

Scheme 3-4: Formation of [^{18}F]fluoroethyl azide

The prepared 2-tosylethyl azide was stored at -18°C until it was required. 2-tosylethyl azide was added into the reaction vessel containing the dried fluorine-18 forming [^{18}F]fluoroethyl azide (**[^{18}F]2.72**).[79] This was then distilled across to the second reaction flask removing it from any leftover free 18-fluoride. Although yield calculations were not carried out for this step in this thesis, the same reaction has been carried out with the method and module with a reported radiochemical yield of 87±5.3%.[93]

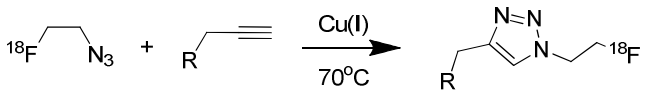

Scheme 3-5: Radiolabelling of a precursor in the presence of a copper catalyst

The alkyne precursor dissolved in DMF was present in the flask the **[^{18}F]2.72** was distilled to. To this a freshly made Cu(I) catalyst is added to instigate the click chemistry radiolabelling experiment. The catalyst has to be made immediately prior to the start of the synthesis to ensure that the copper does not degrade due to its susceptibility to oxidation. The conditions for radiolabelling for a 1,3 Huisgen cycloaddition had previously been optimised by Dr Evelyn Laurens showing an ideal reaction time of 20 minutes at 70°C.[1, 80]

3.1.4 Proposed approach for radiolabelling the precursor compounds

The precursors **2.15**, **2.25**, **2.35**, **2.42**, **2.52** and **2.62** will all be labelled using Click chemistry following the synthesis proposed in

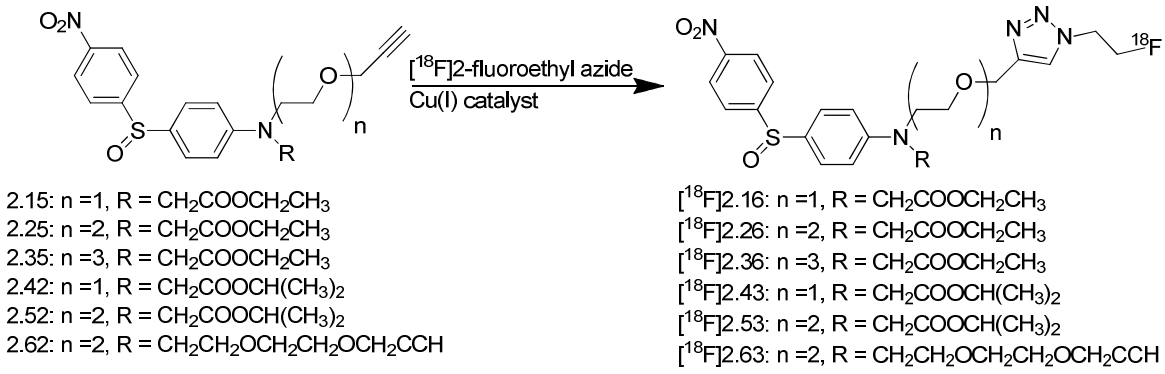

Figure **3-3**.

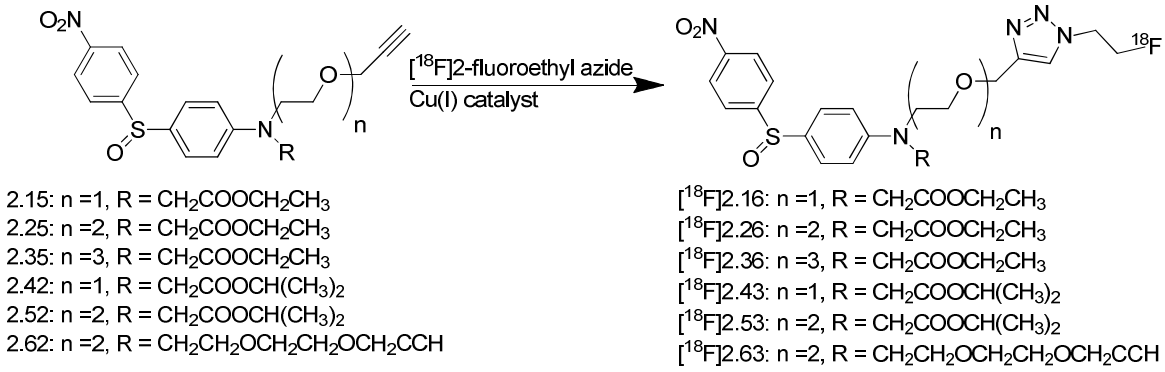

Figure 3-3: Summary of radiolabelling performed in this project

After the radiolabelling reactions were completed the fluorine-18 labelled radiotracer were isolated by semi-preparative HPLC and reformulated into a 10% EtOH/saline solution. The EtOH concentration could be adjusted through the addition of extra saline. HPLC verification would then be required to ensure the proper radiotracer was formed using the fluorine-19 cold standards.

3.1.5 Radiotracer cold standards

The cold standards that were synthesised in chapter 2 play a significant role in the validation of their radiolabelled isomers. The validation of a radiotracer is achieved by comparing its retention time with that of the corresponding cold standard. In this case it would be the radio-HLPC trace of the radiotracer to the UV HPLC trace of the cold standard using the same instrument, method, mobile phase and HPLC column. The characterisation must be performed by comparison because it would not be feasible to isolate the radiotracers due to their half-lives of 2 hours and the inherent dangers of working with radiation emitters. The tracers were injected separately from the cold standards and a comparison was made between the standards UV peak retention to the radio peak of the tracer to verify the identity of the later.

After the fluorine-18 labelled tracers are validated, they can then be used for further *in-vitro* and *in-vivo* studies

3.2 Results and Discussion

Table 3-1 lists the precursors and the successfully synthesised radiotracers together with their radio chemical yields (RCY).

The yields are calculated off the product/K[^{18}F]F. K[^{18}F]F is the recovery rate of F-18 from the QMA into the reaction vial before the synthesis of [^{18}F]fluoroethyl azide.

All yields are given as non-decay corrected unless otherwise specified.

Table 3-1: List of precursors and radiotracers with the corresponding RCY-Non decay corrected

Precursor	Radiotracer	RCY (non decay corrected)
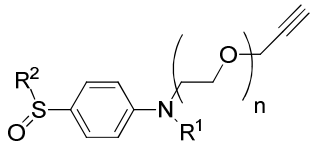	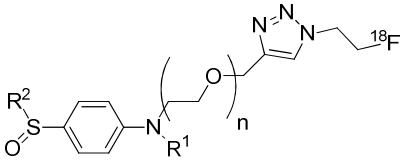	
2.15: n =1, $R^1 = CH_2COOCH_2CH_3$ $R^2 = p\text{-}NO_2C_6H_4$	**[^{18}F]2.16**: n =1, $R^1 = CH_2COOCH_2CH_3$ $R^2 = p\text{-}NO_2C_6H_4$	11%
2.25: n =2, $R^1 = CH_2COOCH_2CH_3$ $R^2 = p\text{-}NO_2C_6H_4$	**[^{18}F]2.26**: n =2, $R^1 = CH_2COOCH_2CH_3$ $R^2 = p\text{-}NO_2C_6H_4$	10%
2.35: n =3, $R^1 = CH_2COOCH_2CH_3$ $R^2 = p\text{-}NO_2C_6H_4$	**[^{18}F]2.36**: n =3, $R^1 = CH_2COOCH_2CH_3$ $R^2 = p\text{-}NO_2C_6H_4$	25%
2.42: n =1, $R^1 = CH_2COOCH(CH_3)_2$ $R^2 = p\text{-}NO_2C_6H_4$	**[^{18}F]2.43**: n =1, $R^1 = CH_2COOCH(CH_3)_2$ $R^2 = p\text{-}NO_2C_6H_4$	5%
2.52: n =2, $R^1 = CH_2COOCH(CH_3)_2$ $R^2 = p\text{-}NO_2C_6H_4$	**[^{18}F]2.53**: n =2, $R^1 = CH_2COOCH(CH_3)_2$ $R^2 = p\text{-}NO_2C_6H_4$	4%
2.62: n =2, $R^1 = CH_2CH_2OCH_2CH_2OC_2CCH$ $R^2 = p\text{-}NO_2C_6H_4$	**[^{18}F]2.63**: n =2, $R^1 = CH_2CH_2OCH_2CH_2OC_2CCH$ $R^2 = p\text{-}NO_2C_6H_4$	4%

Radiotracer	Reaction Conditions
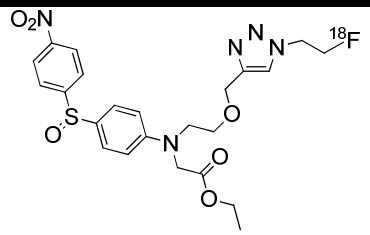 **[^{18}F]2.16**	20mins at 70°C
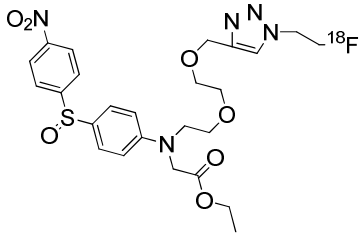 **[^{18}F]2.26**	20mins at 70°C
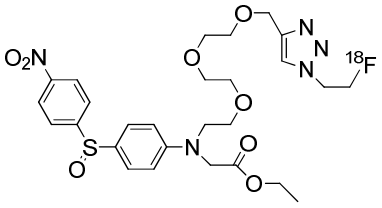 **[^{18}F]2.36**	20mins at 70°C
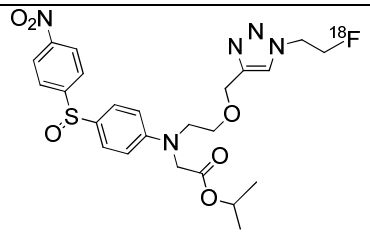 **[^{18}F]2.43**	20mins at 70°C
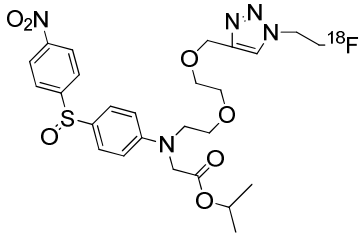 **[^{18}F]2.53**	20mins at 70°C

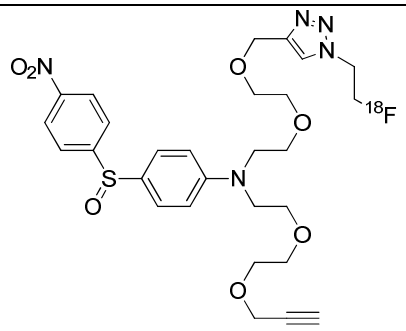 **[^{18}F]2.63**	20mins at 70°C

3.2.1 Radiolabelling of [18F]2.16

[^{18}F]2.16 was prepared by incorporating Fluorine-18 into the precursor **2.15** through click chemistry by using freshly distilled 2-[^{18}F]Fluoroethyl azide, **[^{18}F]2.72**.

The precursor **2.15** and the cold standard **2.16** were characterised in chapter 2 and were used for the validation of the radiotracer **[^{18}F]2.16**. HPLC tracers were obtained through reverse phase HPLC chromatography using acetonitrile (solvent A) and water with 0.1% formic acid(solvent B). 0 min, 5% A; 0-8min 5-90% A; 8-12min, 90% A; 12-15min: 90-5% A; 15-18min: 5% A.

Figure 3-4: UV spectrum of the cold standard 2.16 with a retention time of 13.059 minutes illustrates the UV HPLC trace of the cold standard **2.16**, having a single peak with a retention time of 13.059 minutes. As mention in chapter 2 the respective precursor **2.15** had a retention time of 13.946 minutes

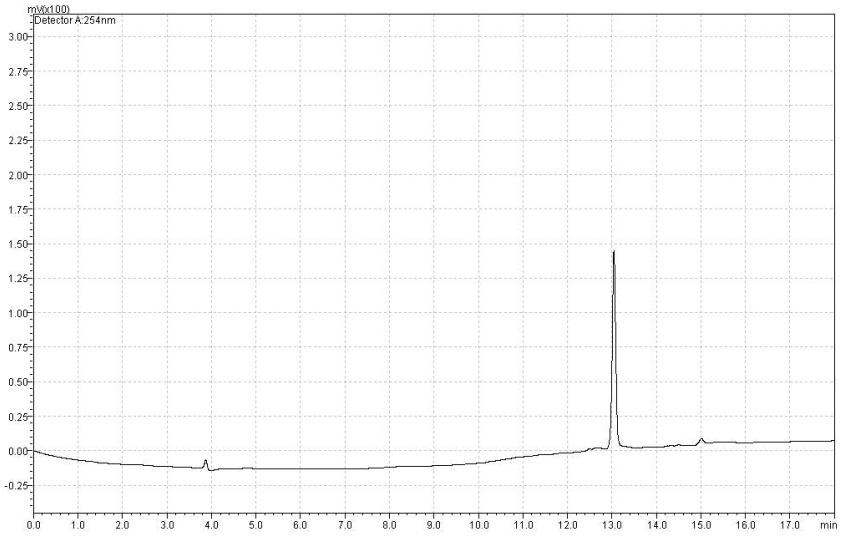

Figure 3-4: UV spectrum of the cold standard 2.16 with a retention time of 13.059 minutes

3.2.1.1 Radiochemistry

Click chemistry radiolabelling of **[^{18}F]2.16** comprised of a 2-step reaction. Firstly the 2-[^{18}F]fluoroethyl azide **[^{18}F]2.72** is prepared followed by its reaction with the precursor 2.15 to give the radiotracer **[^{18}F]2.16**.

The 2-[^{18}F]fluoroethyl azide **[^{18}F]2.72** was synthesised through the reaction of dried K[^{18}F]F Kryptofix complex and 2-azidoethyl 4-toulenesulfonate at 90°in dry acetonitrile. 2-[^{18}F]fluoroethyl azide **[^{18}F]2.72** was co-distilled with acetonitrile at 100°C to a second reaction vial containing 1.5mg of precursor **2.15** in 200µL of DMF. Once the distillation was completed a freshly made copper catalyst comprised of $Cu(CH_3CN)_4PF_6$ and TBTA in dry DMF (300µL). The reaction mixture was heated to 70°C for 20min. Scheme 3-6 illustrates the 2-step radiolabelling of **[^{18}F]2.16**.

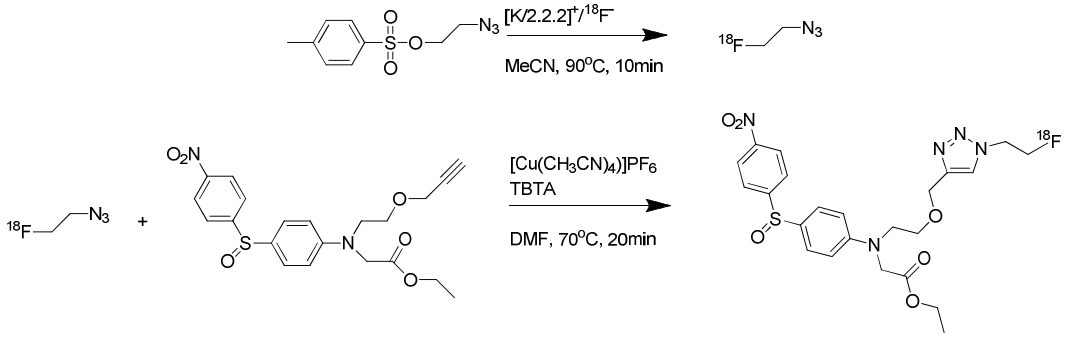

Scheme 3-6: Radiosynthesis of [18F]2.16

The radiolabelling was monitored using radiation detectors positioned throughout the module. Figure 3-5 demonstrates the movement of radioactivity through the iPhase Flexlab module. Starting with the transfer of activity from the Cyclotron, this is then trapped into a QMA ion exchange column. The activity is eluted from the QMA and transferred into the reactor 1 where 2-[^{18}F]fluoroethyl azide **[^{18}F]2.72** is produced. The distillation from reactor 1 to reactor 2 is shown by the rapid decline in intensity of the yellow trace followed by the increase for teal. Once the reaction was complete the contents of reactor 2 is transferred onto the HLPC where the radioisotope is isolated before been trapped onto seppak D. The final product is then eluted from seppak D to the product-out vial.

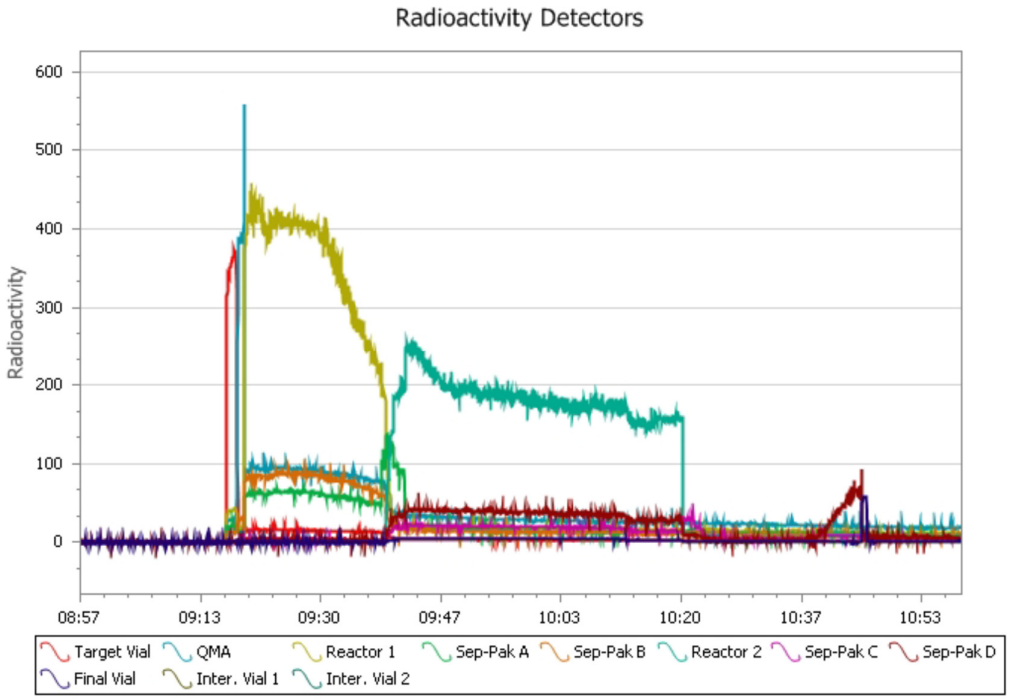

Figure 3-5: Radioactivity distribution in the Flexlab during the synthesis of [^{18}F]2.16

3.2.1.2 HPLC purification and reformulation

The radiotracer [^{18}F]2.16 was purified from the precursor 2.15 and any by-products using a semi-preparative HPLC. It had a retention time of 15.6 minutes as shown in Figure 3-6.

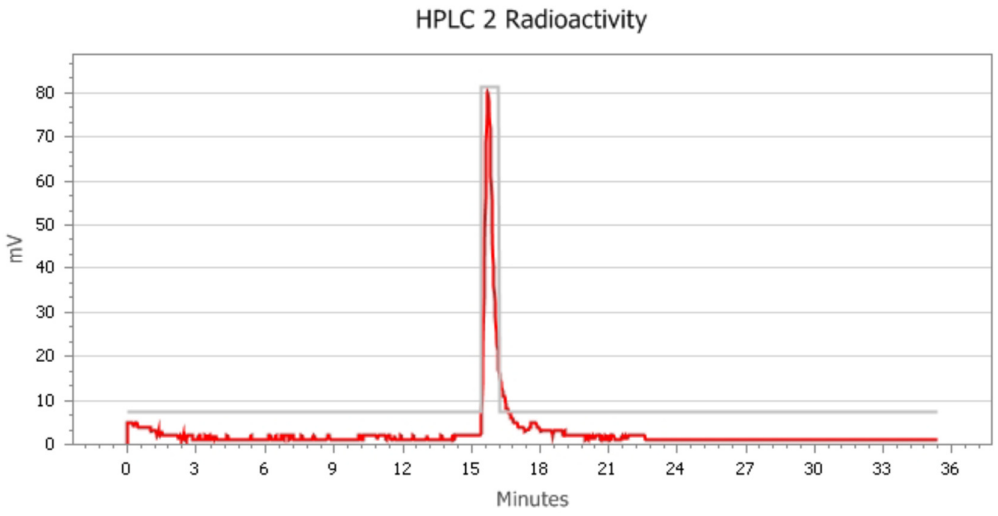

Figure 3-6: Radioactivity spectrum from the HPLC purification of [^{18}F]2.16

The purified [18F]2.16 was then reformulated into 10% ethanol/saline, closely following the C-18 seppak method. Total synthesis time including HPLC purification and reformulation was 90 minutes with a non-decay corrected yield of 12% based on K[^{18}F]F.

3.2.1.3 Quality Control

Quality control of radiotracer **[^{18}F]2.16** was performed on a Shimadzu LCMS system in ACPI mode using an analytical reverse phase C-18 column and a H_2O/CH_3CN gradient solvent system as mobile phase

The radiotracer was validated by correlating the retention time of the radiotracer peak **[^{18}F]2.16** with the retention time of the cold standard HPLC peak **2.16**. Figure 3-4 shows the retention time for the cold standard HPLC at 13.059 minutes, which is comparable with the retention time of the radiotracer **[^{18}F]2.16** shown in Figure 3-7 that had a retention time of 13.068 minutes.

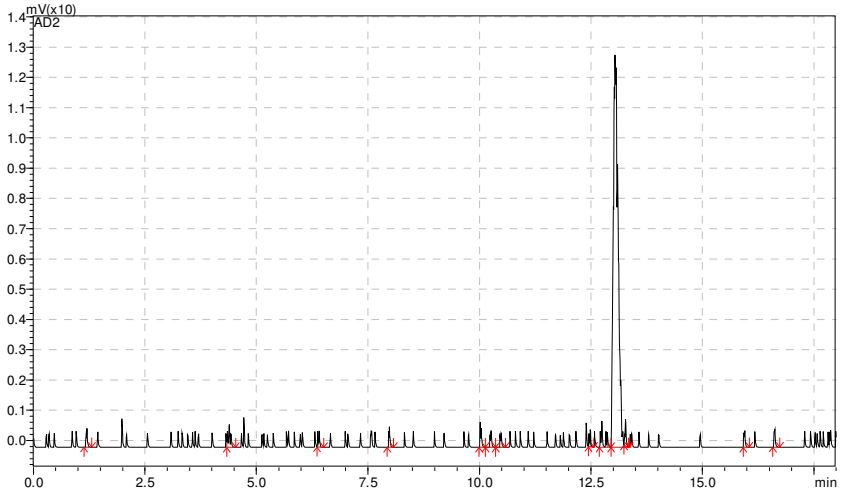

Figure 3-7: Radio Peak for [^{18}F]2.16 with a retention time of 13.068minutes

3.2.2 Radiolabelling of [^{18}F]2.26

[^{18}F]2.26 was prepared through a 2-step radiolabelling beginning with the formation of 2-[^{18}F]fluoroethyl azide **[^{18}F]2.72** followed by a click reaction with precursor compound **2.25**.

The precursor **2.25** and cold standard **2.26** used for the validation of radiotracer **[18F]2.26** are fully characterised in Chapter 2. HPLC tracers were obtained through reverse phase HPLC chromatography using acetonitrile (solvent A) and water with 0.1% formic acid(solvent B). 0 min, 5% A; 0-8min 5-90% A; 8-12min, 90% A; 12-15min: 90-5% A; 15-18min: 5% A.

Figure 3-8 shows the TIC spectrum from the LCMS of precursor 2.25 which reveals a primary peak at 13.928minutes with the $[M+H]^+$ ion (m/z= 475.1).

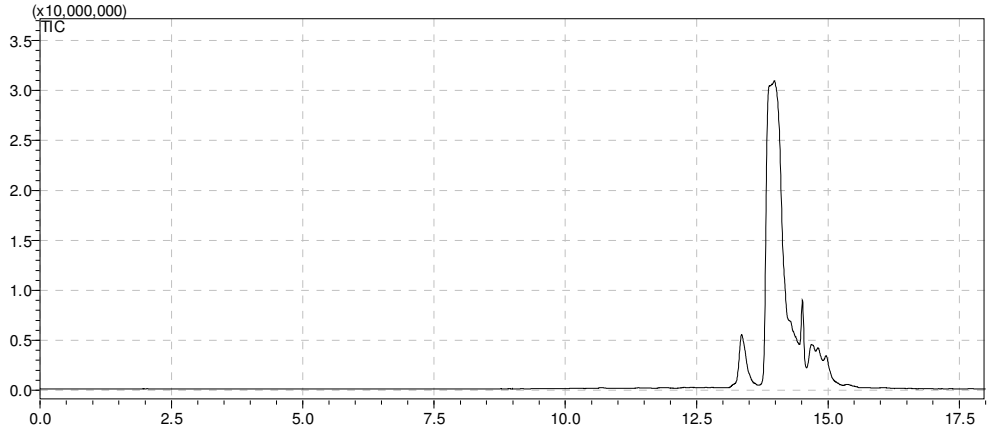

Figure 3-8: Total ion count LCMS for 2.25 with a retention time of 13.928mins

Figure 3-9 shows the UV HPLC tracer of cold standard **2.26** which displays a peak at 13.032 minutes. As shown in chapter 2, this was monitored by MS with the $[M+H]^+$ ion (m/z= 564.1).

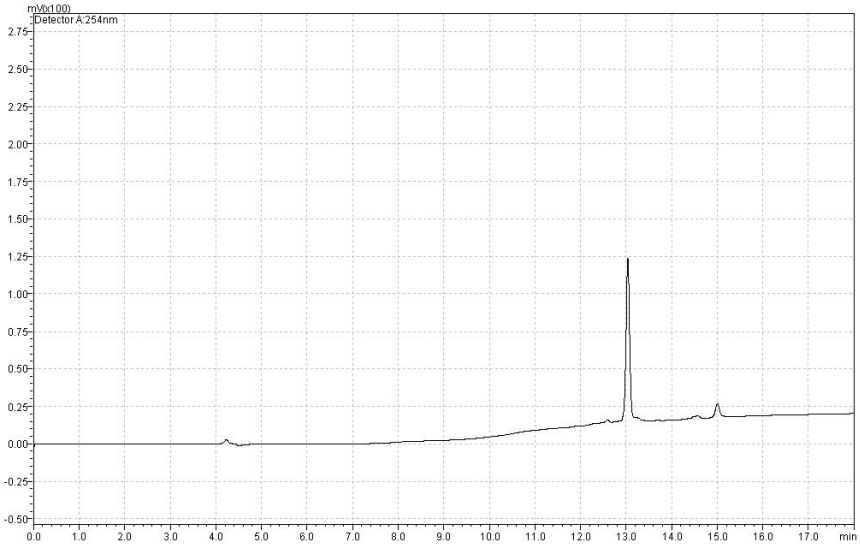

Figure 3-9:UV spectrum of the cold standard 2.26 with a retention time of 13.032 minutes

3.2.2.1 Radiochemistry

The click chemistry radiolabelling of **[^{18}F]2.26** was performed using the same method as the click labelling of **[^{18}F]2.16**. 2-[^{18}F]fluoroethyl azide **[^{18}F]2.72** was made and distilled into precursor **2.25.** The reaction was initiated by adding freshy prepared $Cu(CH_3CN)_4PF_6$ and TBTA catalyst. It was reacted for 20 minutes at 70°C.

Scheme 3-7 demonstrates the 2-step radiolabelling method used for the synthesis of radiotracer **[^{18}F]2.26**

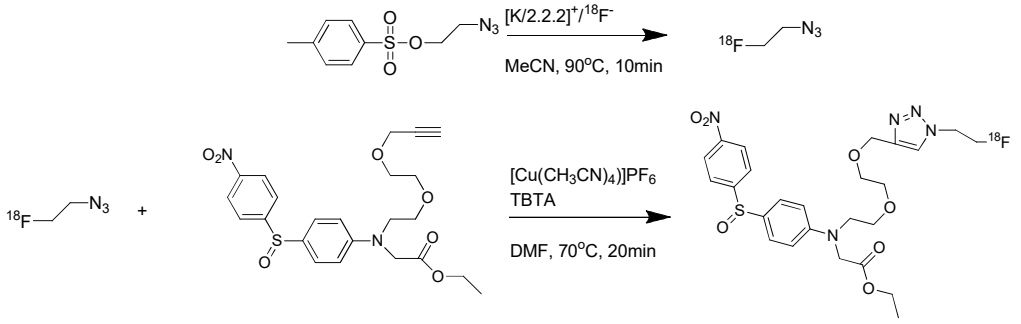

Scheme 3-7: Radiosynthesis of [^{18}F]2.26

The reaction was monitored by radiation detectors placed throughout the cell as shown by Figure 3-10 . Following the same method used for the production of **[^{18}F]2.16** activity was first transferred to the target vial from the cyclotron, it was then trapped onto the QMA. The activity was eluted from the QMA into reactor 1 where 2-[^{18}F]fluoroethyl azide **[^{18}F]2.72** was synthesised. 2-[^{18}F]fluoroethyl azide **[^{18}F]2.72** was then distilled from reactor 1 into reactor 2 which contained 1.5mg of precursor **2.25**. The catalyst was added and the reaction left to stir for 20minutes. It was transferred onto the semi-preparative Gemini column for purification.

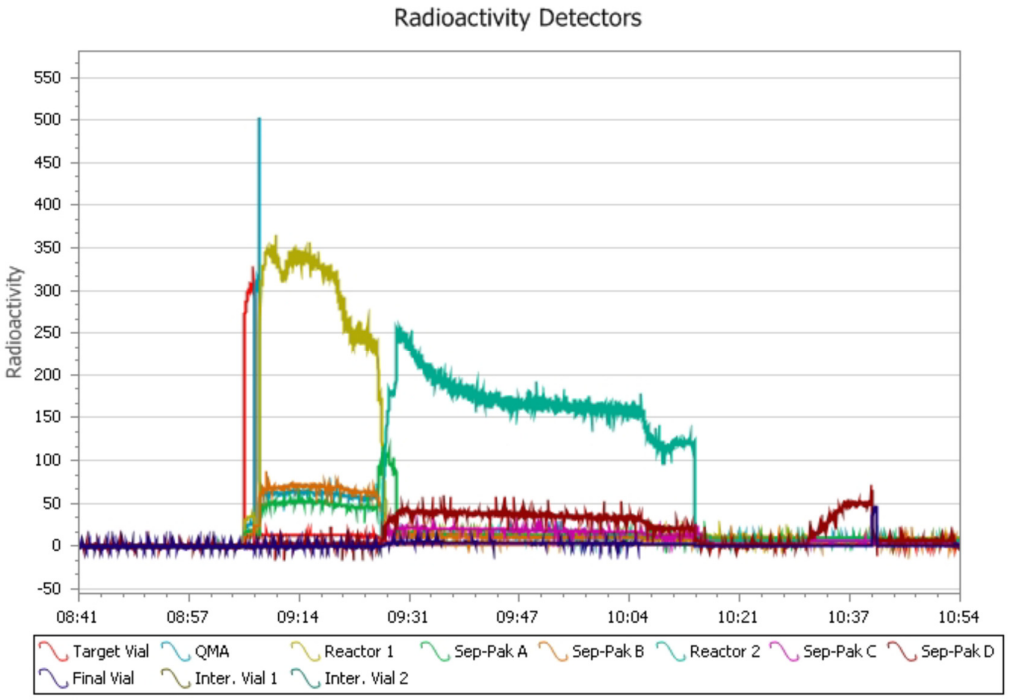

Figure 3-10: Radioactivity distribution in the Flexlab during the synthesis of [^{18}F]2.26

3.2.2.2 HPLC purification and reformulation

[^{18}F]2.26 was isolated from the precursor and any by-products using a semi-preparative HPLC system. It had a retention time of 15.7 minutes as shown in Figure 3-11.

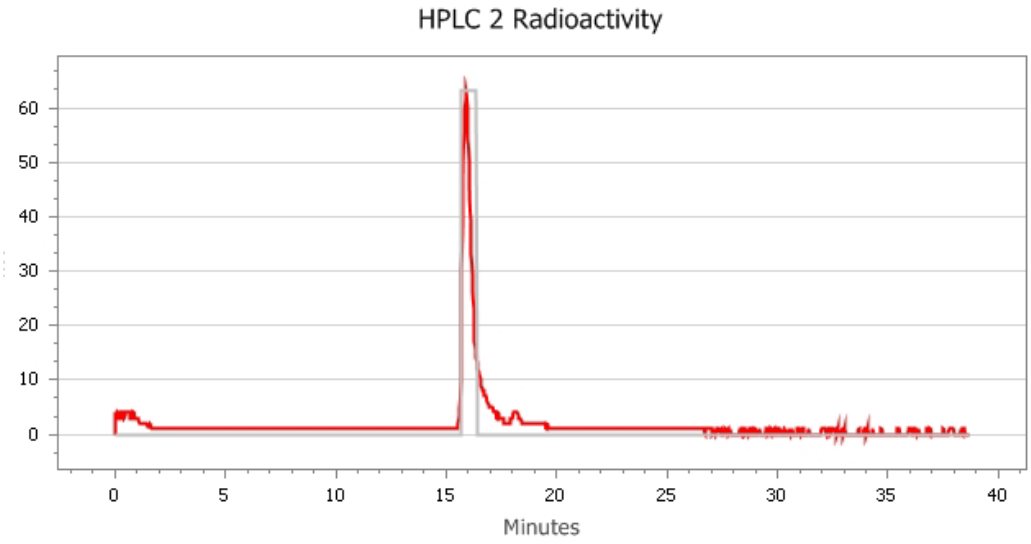

Figure 3-11: Purification of [^{18}F]2.26 via HPLC

The purified **[18F]2.26** was reformulated into 10% ethanol/saline, closely following the C-18 seppak method. Total synthesis time including HPLC purification and reformulation was 90 minutes with a non-decay corrected yield of 10% based on K[^{18}F]F.

3.2.2.3 Quality Control

Quality control of radiotracer **[^{18}F]2.26** was performed on a Shimadzu LCMS system in ACPI mode using an analytical reverse phase C-18 column and a H_2O/CH_3CN gradient solvent system as mobile phase

The radiotracer was validated by correlating the retention time of the radiotracer peak **[^{18}F]2.26** with the retention time of the cold standard HPLC peak **2.26**. Figure 3-9shows the retention time for the cold standard HPLC at 13.032 minutes, which is comparable with the retention time of the radiotracer **[^{18}F]2.26** shown in Figure 3-12 that had a retention time of 13.014 minutes.

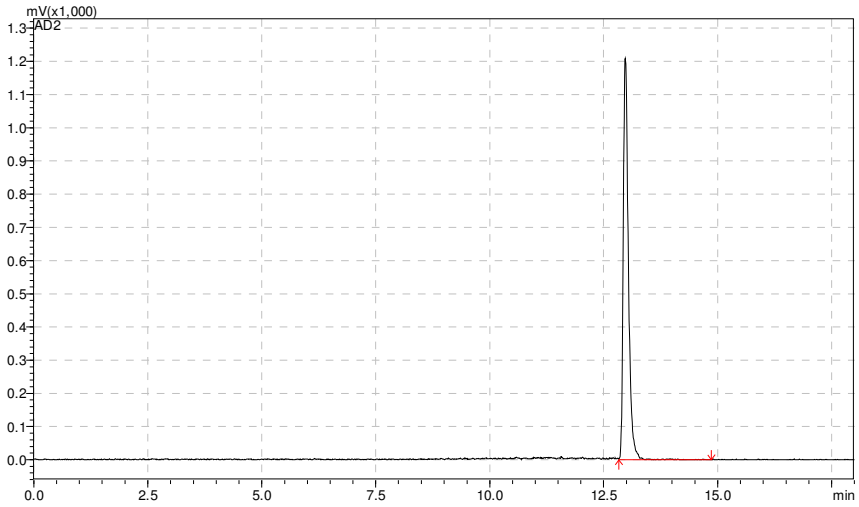

Figure 3-12: Radio Peak for [18F]2.26 with a retention time of 13.014minutes

3.2.3 Radiolabelling of [^{18}F]2.36

[^{18}F]2.36 was synthesised through the same 2-step radiolabelling as the previous 2 compounds. Firstly 2-[^{18}F]fluoroethyl azide **[^{18}F]2.72** was made followed by a click reaction with precursor compound **2.35**.

The precursor **2.35** and cold standard **2.36** used for the validation of radiotracer **[^{18}F]2.36** are fully characterised in Chapter 2. HPLC tracers were obtained through reverse phase HPLC chromatography using acetonitrile (solvent A) and water with 0.1%

formic acid(solvent B). 0 min, 5% A; 0-8min 5-90% A; 8-12min, 90% A; 12-15min: 90-5% A; 15-18min: 5% A.

Figure 3-13 shows the TIC spectrum from the LCMS of precursor **2.35** which reveals a primary peak at 13.873minutes with the $[M+H]^+$ ion (m/z= 518.1).

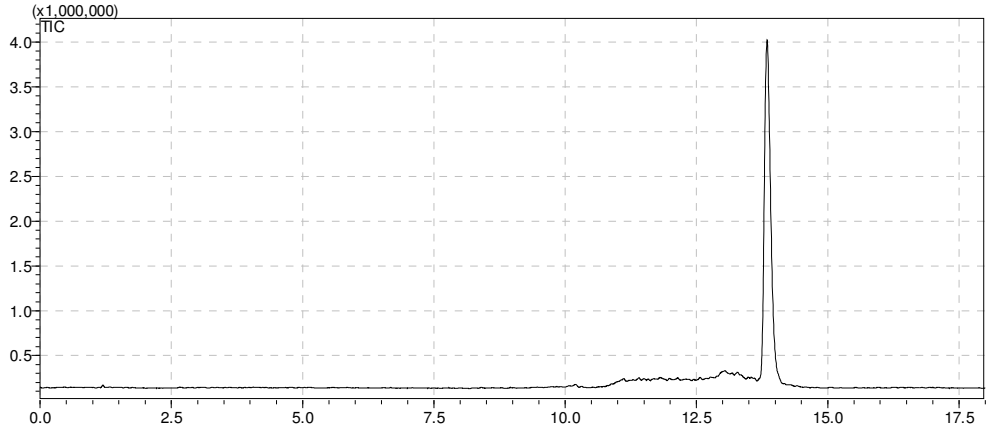

Figure 3-13: Total ion count LCMS for 2.35 with a retention time of 13.873mins

Figure 3-14 shows the UV HPLC tracer of cold standard **2.36** which displayed a peak at 13.032 minutes. As shown in chapter 2, this was monitored by MS with the $[M+H]^+$ ion (m/z= 608.1).

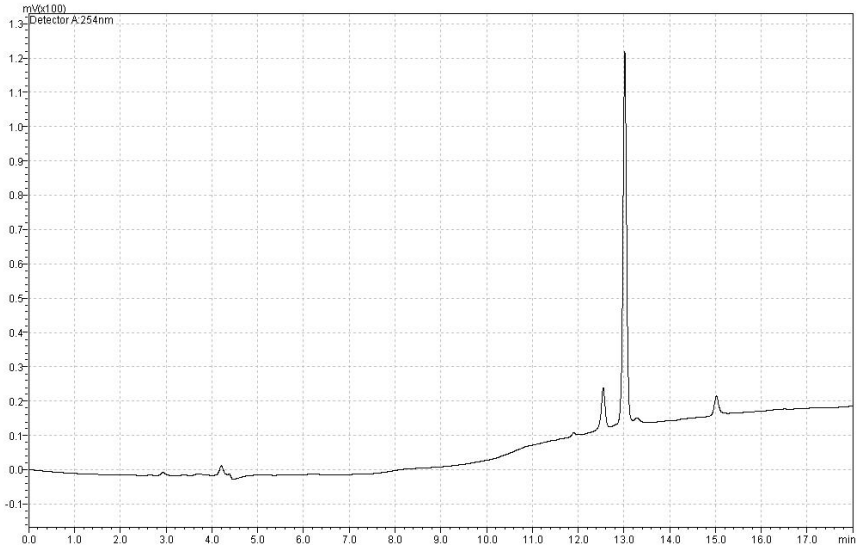

Figure 3-14: UV spectrum of the cold standard 2.36 with a retention time of 13.032 minutes

3.2.3.1 Radiochemistry

The click chemistry radiolabelling of **[^{18}F]2.36** was performed using the same method as the click labelling of **[^{18}F]2.16**. 2-[^{18}F]fluoroethyl azide **[^{18}F]2.72** was made and distilled into precursor **2.35.** The reaction was initiated by adding freshy prepared $Cu(CH_3CN)_4PF_6$ and TBTA catalyst. It was reacted for 20 minutes at 70°C.

Scheme 3-8 demonstrates the 2-step radiolabelling method used for the synthesis of radiotracer **[^{18}F]2.36**

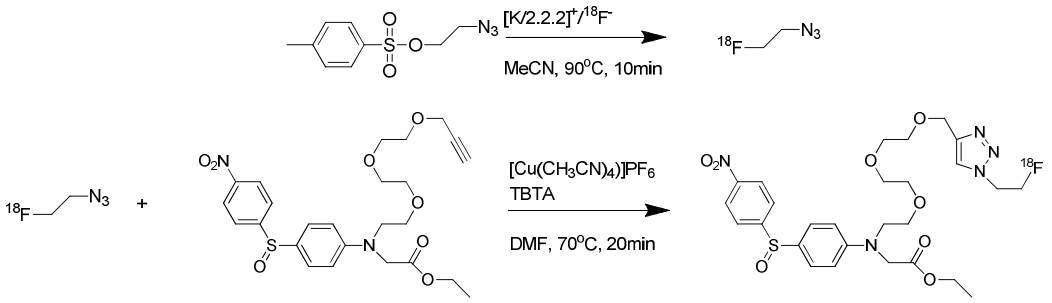

Scheme 3-8: Radiosynthesis of [^{18}F]2.36

The reaction was monitored by radiation detectors placed throughout the cell as shown by Figure 3-15. Following the same method used for the production of **[^{18}F]2.16** activity was first transferred to the target vial from the cyclotron, it is then trapped onto the QMA. The activity is eluted from the QMA into reactor 1 where 2-[^{18}F]fluoroethyl azide **[^{18}F]2.72** is synthesised. The 2-[^{18}F]fluoroethyl azide **[^{18}F]2.72** is then distilled from reactor 1 into reactor 2 which contained 1.5mg of precursor **2.36**. The catalyst was added and the reaction left to stir for 20minutes. It was then transferred onto the semi preparative Gemini column for purification.

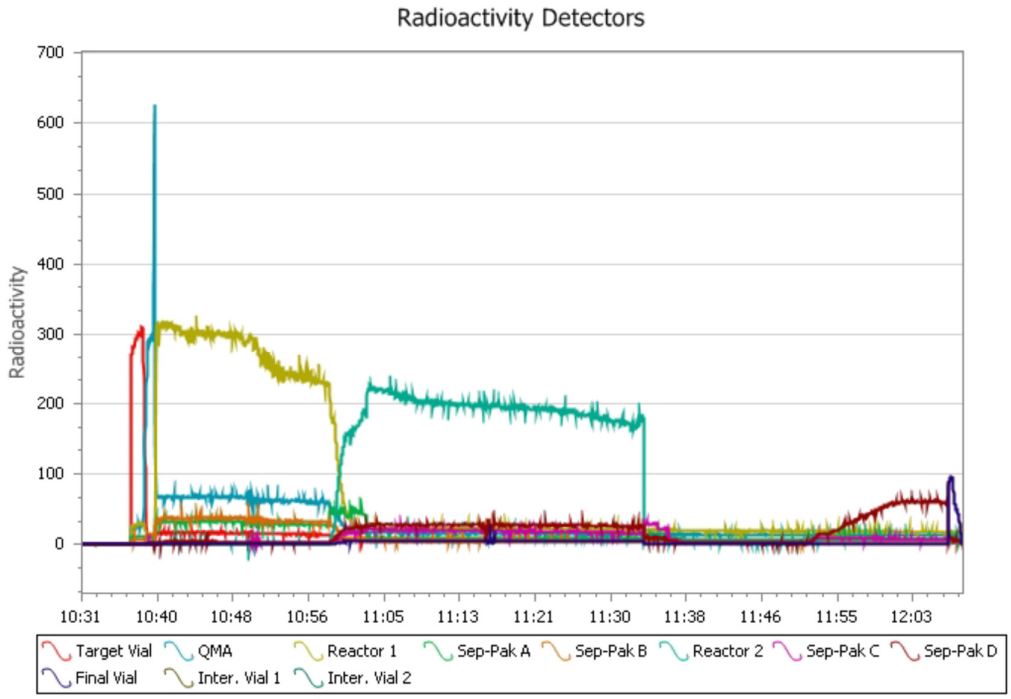

Figure 3-15: Radioactivity distribution in the Flexlab during the synthesis of [^{18}F]2.36

3.2.3.2 HPLC purification and reformulation

[^{18}F]2.36 was isolated from the precursor and any by-products using a semi-preparative HPLC system. It had a retention time of 15.5 minutes as shown in Figure 3-16

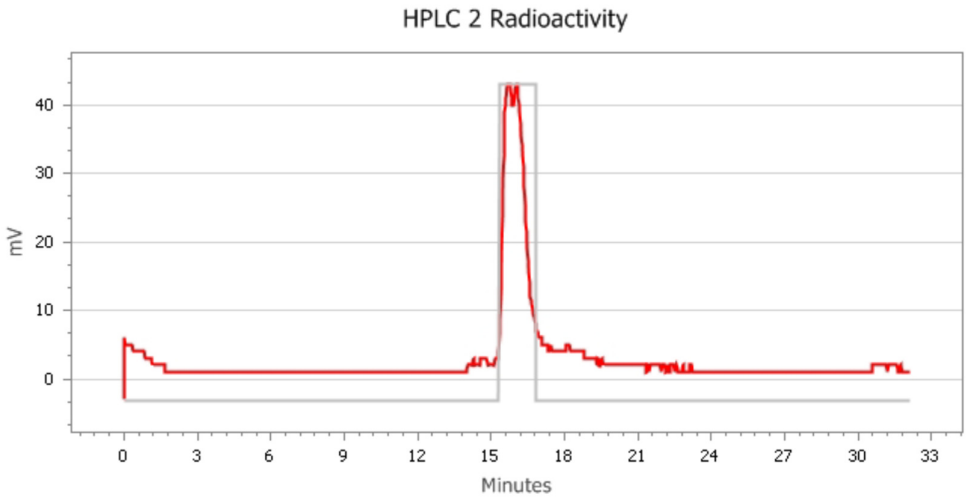

Figure 3-16: Purification of [^{18}F]2.36 via HPLC

The purified **[18F]2.36** was reformulated into 10% ethanol/saline, closely following the C-18 seppak method. Total synthesis time including HPLC purification and reformulation was 90 minutes with a non-decay corrected yield of 25% based on K[^{18}F]F.

3.2.3.3 Quality Control

Quality control of radiotracer **[^{18}F]2.36** was performed on a Shimadzu LCMS system in ACPI mode using an analytical reverse phase C-18 column and a H_2O/CH_3CN gradient solvent system as mobile phase

The radiotracer was validated by correlating the retention time of the radiotracer peak **[^{18}F]2.36** with the retention time of the cold standard HPLC peak **2.36**. Figure 3-14 shows the retention time for the cold standard HPLC at 13.032 minutes, which is comparable with the retention time of the radiotracer **[^{18}F]2.36** shown in Figure 3-17**,** which had a retention time of 13.041 minutes.

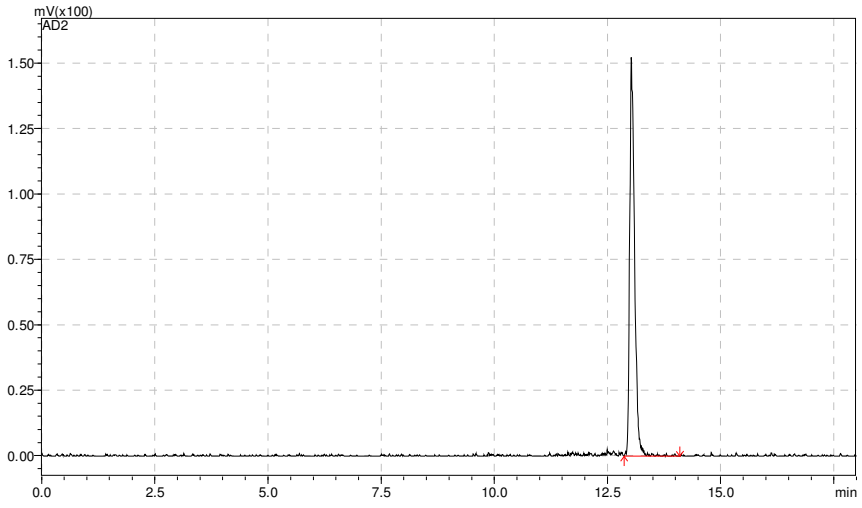

Figure 3-17:Radio Peak for [18F]2.36 with a retention time of 13.041minutes

3.2.4 Radiolabelling of [^{18}F]2.43

[^{18}F]2.43 was synthesised through the same 2-step radiolabelling as the previous 3 compounds. Firstly 2-[^{18}F]fluoroethyl azide **[^{18}F]2.72** was made followed by a click reaction with precursor compound **2.42**.

The precursor **2.42** and cold standard **2.43** used for the validation of radiotracer **[^{18}F]2.43** are fully characterised in Chapter 2. HPLC tracers were obtained through reverse phase HPLC chromatography using acetonitrile (solvent A) and water with 0.1% formic acid(solvent B). 0 min, 5% A; 0-8min 5-90% A; 8-12min, 90% A; 12-15min: 90-5% A; 15-18min: 5% A.

Figure 3-18 shows the TIC spectrum from the LCMS of precursor 2.42 which reveals a primary peak at 14.308minutes with the $[M+H]^+$ ion (m/z= 445.0).

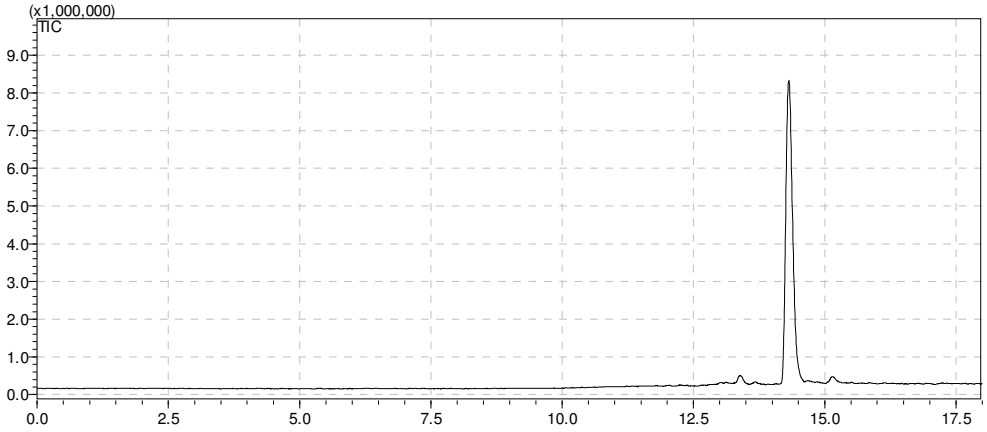

Figure 3-18: Total ion count LCMS for 2.42 with a retention time of 14.038mins

Figure 3-19 shows the UV HPLC tracer of cold standard **2.43** which displays a peak at 13.357 minutes. As shown in chapter 2, this was monitored by MS with the $[M+H]^+$ ion (m/z=534.0).

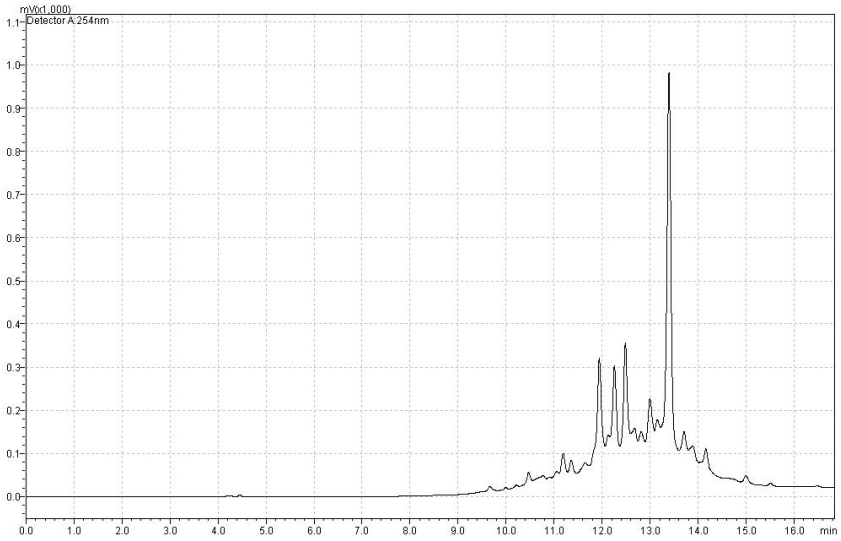

Figure 3-19: UV spectrum of the cold standard 2.43 with a retention time of 13.357 minutes

3.2.4.1 Radiochemistry

The click chemistry radiolabelling of **[^{18}F]2.43** was performed using the same method as the click labelling of **[^{18}F]2.16**. 2-[^{18}F]fluoroethyl azide **[^{18}F]2.72** was made and distilled into precursor **2.42.** The reaction was initiated by adding freshy prepared $Cu(CH_3CN)_4PF_6$ and TBTA catalyst. It was reacted for 20 minutes at 70°C.

Scheme 3-8 demonstrates the 2-step radiolabelling method used for the synthesis of radiotracer **[^{18}F]2.43**

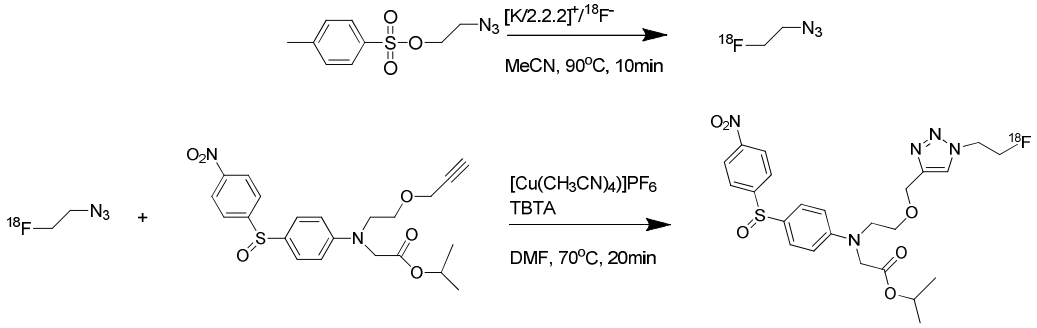

Scheme 3-9: Radiosynthesis of [^{18}F]2.43

The formation of **[^{18}F]2.43** was monitored by radiation detectors placed throughout the cell as shown by Figure 3-20. Following the same method used for the production of **[^{18}F]2.16** activity was first transferred to the target vial from the cyclotron, it is then trapped onto the QMA. The activity is eluted from the QMA into reactor 1 where 2-[^{18}F]fluoroethyl azide **[^{18}F]2.72** is synthesised. The 2-[^{18}F]fluoroethyl azide **[^{18}F]2.72** is then distilled from reactor 1 into reactor 2 which contained 1.5mg of precursor **2.42**. The catalyst was added and the reaction left to stir for 20minutes. It was then transferred onto the semi preparative Gemini column for purification.

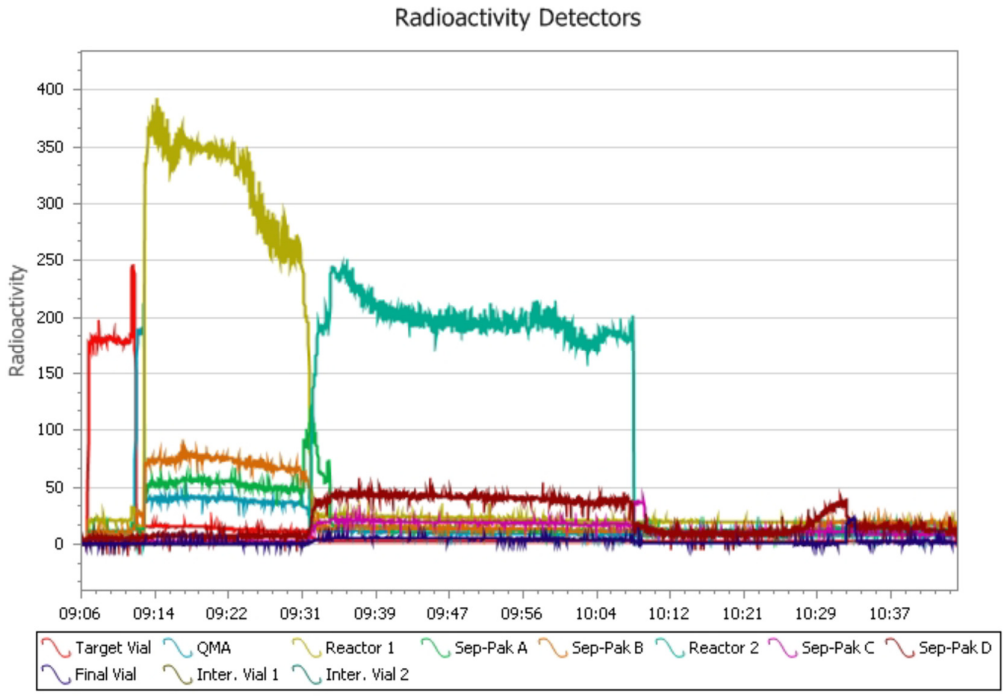

Figure 3-20: Radioactivity distribution in the Flexlab during the synthesis of [^{18}F]2.43

3.2.4.2 HPLC purification and reformulation

[^{18}F]2.43 was isolated from the precursor and any by-products using a semi-preparative HPLC system. It had a retention time of 16.2 minutes as shown in Figure 3-21.

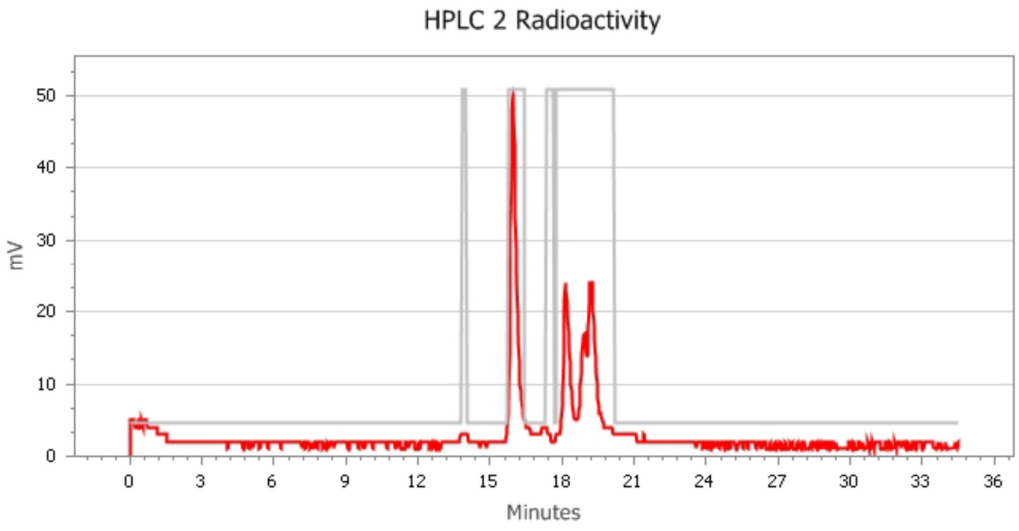

Figure 3-21: Purification of [^{18}F]2.43 via HPLC

The purified **[18F]2.43** was reformulated into 10% ethanol/saline, closely following the C-18 seppak method. Total synthesis time including HPLC purification and reformulation was 90 minutes with a non-decay corrected yield of 5% based on K[^{18}F]F.

3.2.4.3 Quality Control

Quality control of radiotracer **[^{18}F]2.43** was performed on a Shimadzu LCMS system in ACPI mode using an analytical reverse phase C-18 column and a H_2O/CH_3CN gradient solvent system as mobile phase.

The radiotracer was validated by correlating the retention time of the radiotracer peak **[^{18}F]2.43** with the retention time of the cold standard HPLC peak **2.43**. Figure 3-19 shows the retention time for the cold standard HPLC at 13.357 minutes, which is comparable with the retention time of the radiotracer **[^{18}F]2.43** shown in Figure 3-22**,** which had a retention time of 13.370 minutes.

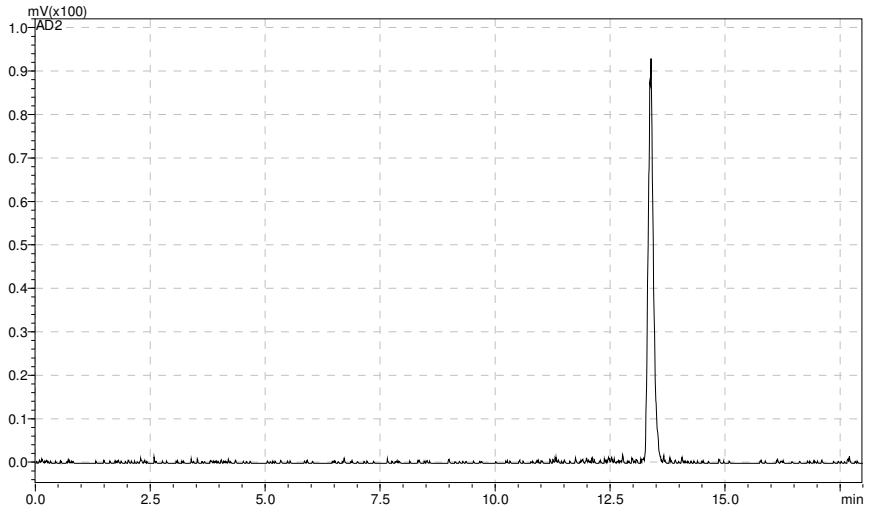

Figure 3-22:Radio Peak for [18F]2.43 with a retention time of 13.370minutes

3.2.5 Radiolabelling of [^{18}F]2.53

[^{18}F]2.53 was synthesised through the same 2-step radiolabelling as the previous 4 compounds. Firstly 2-[^{18}F]fluoroethyl azide **[^{18}F]2.72** was synthesised followed by a click reaction with precursor compound **2.52**.

The precursor **2.52** and cold standard **2.53** used for the validation of radiotracer **[^{18}F]2.53** are fully characterised in Chapter 2. HPLC tracers were obtained through reverse phase HPLC chromatography using acetonitrile (solvent A) and water with 0.1%

formic acid(solvent B). 0 min, 5% A; 0-8min 5-90% A; 8-12min, 90% A; 12-15min: 90-5% A; 15-18min: 5% A.

Figure 3-23 shows the TIC spectrum from the LCMS of precursor 2.52 which reveals a primary peak at 14.281 minutes with the $[M+H]^+$ ion (m/z= 488.1).

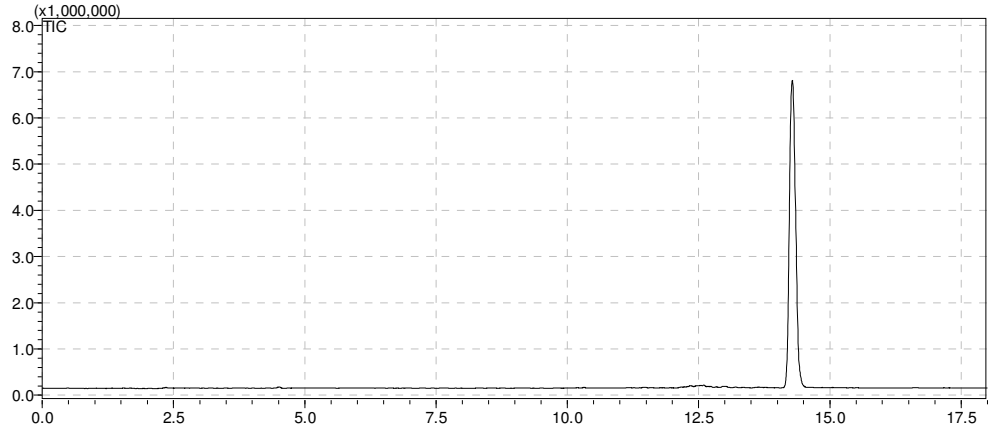

Figure 3-23: Total ion count LCMS for 2.52 with a retention time of 14.281mins

Figure 3-24 shows the UV HPLC tracer of cold standard **2.53** which displays a peak at 13.385 minutes. As shown in chapter 2, this was monitored by MS with the $[M+H]^+$ ion (m/z=578.1).

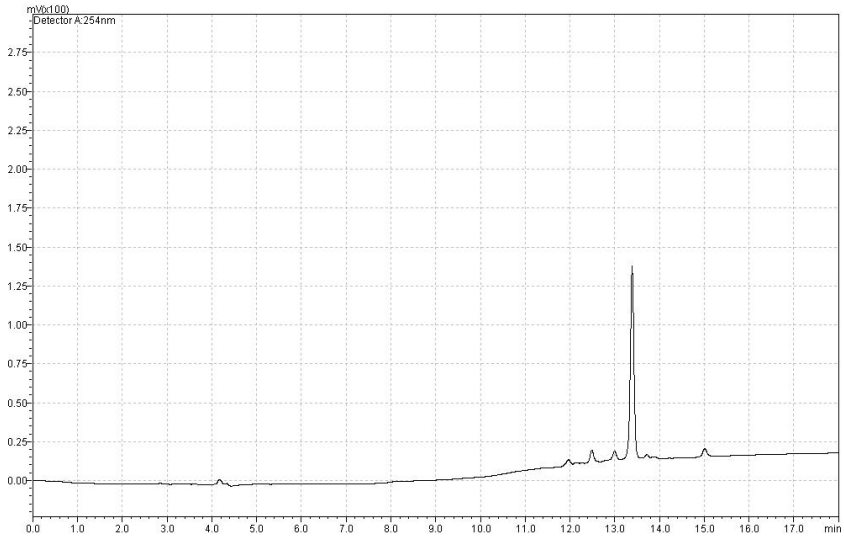

Figure 3-24: UV spectrum of the cold standard 2.53 with a retention time of 13.385 minutes

3.2.5.1 Radiochemistry

The click chemistry radiolabelling of **[^{18}F]2.53** was performed using the same method as the click labelling of **[^{18}F]2.16**. 2-[^{18}F]fluoroethyl azide **[^{18}F]2.72** was made and distilled into precursor **2.52.** The reaction was initiated by adding freshy prepared $Cu(CH_3CN)_4PF_6$ and TBTA catalyst. It was reacted for 20 minutes at 70°C.

Scheme 3-10 demonstrates the 2-step radiolabelling method used for the synthesis of radiotracer **[^{18}F]2.53**

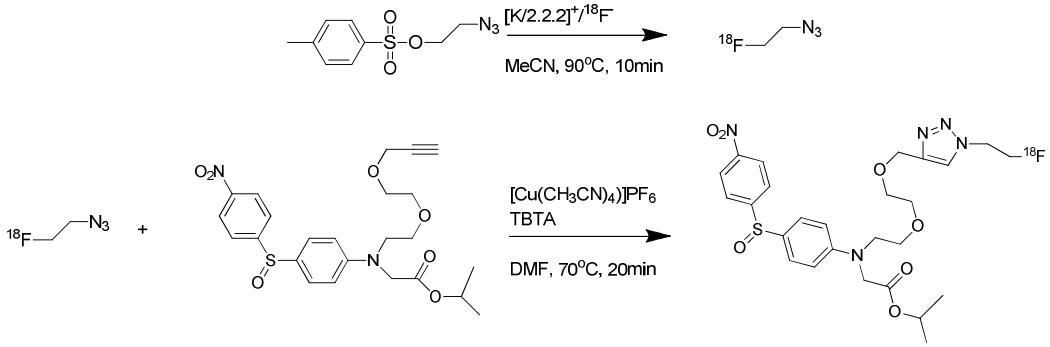

Scheme 3-10: Radiosynthesis of [^{18}F]2.53

The formation of **[^{18}F]2.53** was monitored by radiation detectors placed throughout the cell as shown by Figure 3-25. Following the same method used for the production of **[^{18}F]2.16** activity was first transferred to the target vial from the cyclotron, it was then trapped onto the QMA. The activity was eluted from the QMA into reactor 1 where 2-[^{18}F]fluoroethyl azide **[^{18}F]2.72** was synthesised. The 2-[^{18}F]fluoroethyl azide **[^{18}F]2.72** was then distilled from reactor 1 into reactor 2 which contained 1.5mg of precursor **2.52**. The catalyst was added and the reaction left to stir for 20minutes. It was then transferred onto the semi preparative Gemini column for purification.

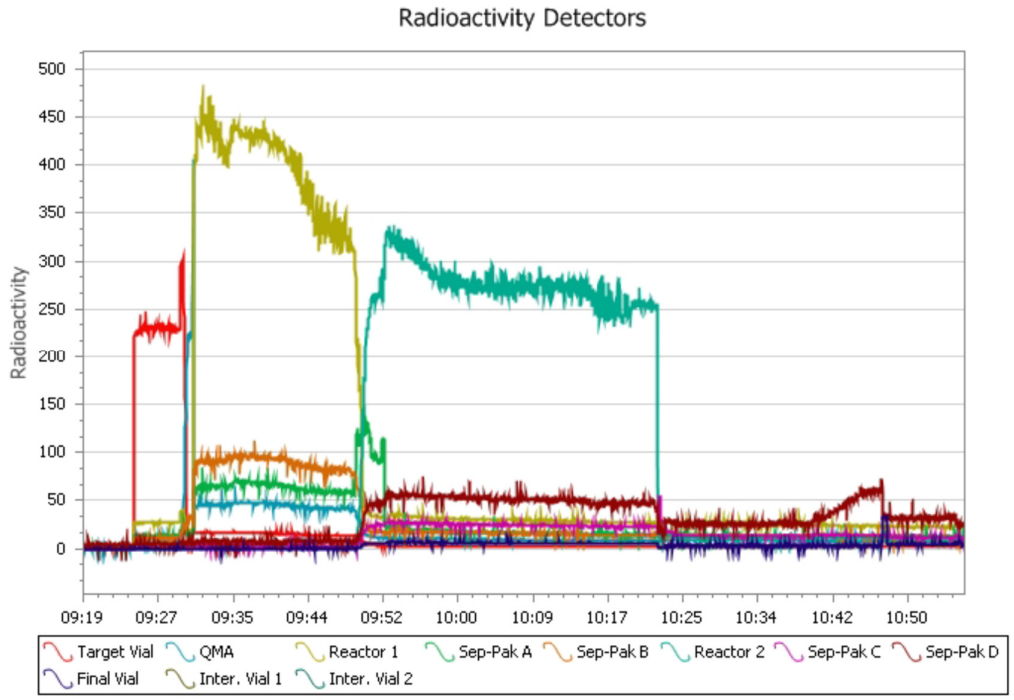

Figure 3-25: Radioactivity distribution in the Flexlab during the synthesis of [^{18}F]2.53

3.2.5.2 HPLC purification and reformulation

[^{18}F]2.53 was isolated from the precursor and any by-products using a semi-preparative HPLC system. It had a retention time of 16.2 minutes as shown Figure 3-26

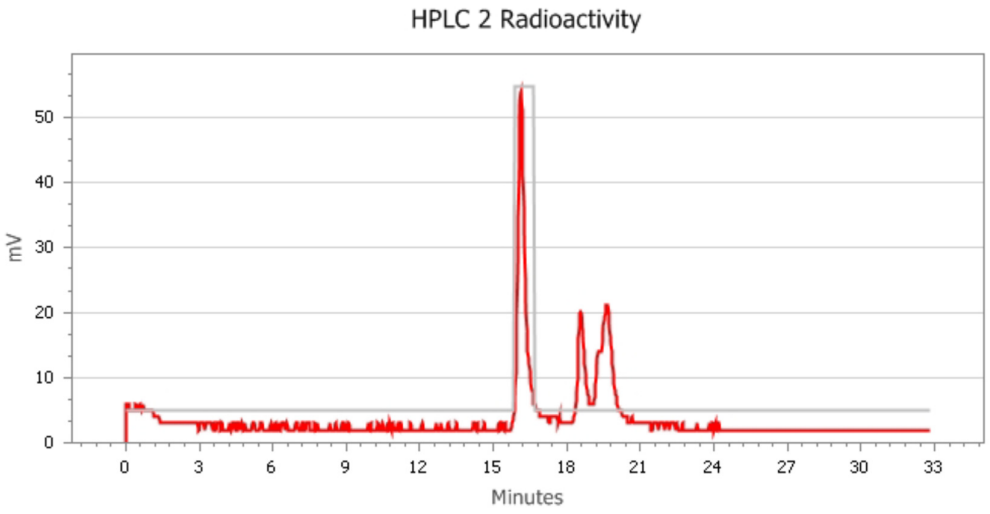

Figure 3-26: Purification of [^{18}F]2.53 via HPLC

The purified **[18F]2.53** was reformulated into 10% ethanol/saline, closely following the C-18 seppak method. Total synthesis time including HPLC purification and reformulation was 90 minutes with a non-decay corrected yield of 4% based on K[^{18}F]F.

3.2.5.3 Quality Control

Quality control of radiotracer **[^{18}F]2.53** was performed on a Shimadzu LCMS system in ACPI mode using an analytical reverse phase C-18 column and a H_2O/CH_3CN gradient solvent system as mobile phase

The radiotracer was validated by correlating the retention time of the radiotracer peak **[^{18}F]2.53** with the retention time of the cold standard HPLC peak **2.53**. Figure 3-24 shows the retention time for the cold standard **2.53** at 13.385 minutes, which is comparable with the retention time of the radiotracer **[^{18}F]2.53** shown in Figure 3-27**,** which had a retention time of 13.397 minutes.

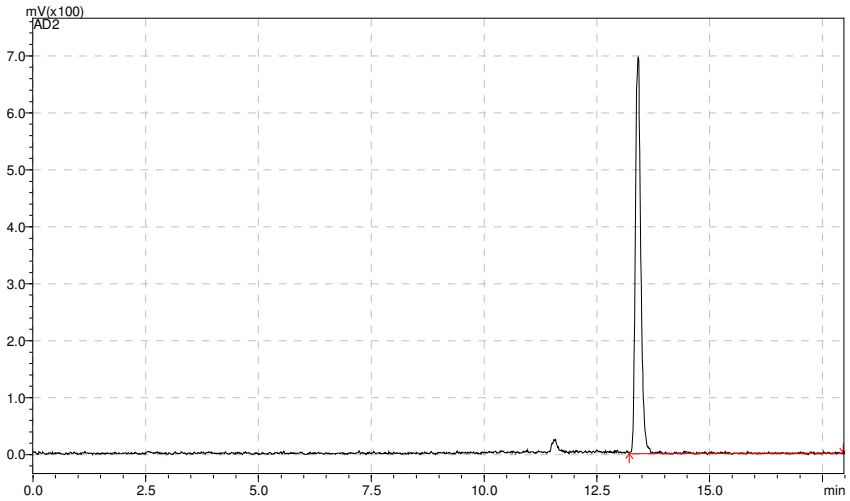

Figure 3-27:Radio Peak for [18F]2.53 with a retention time of 13.397minutes

3.2.6 Radiolabelling of [^{18}F]2.63

[^{18}F]2.63 was synthesised through the same 2-step radiolabelling as the previous 5 compounds. Firstly 2-[^{18}F]fluoroethyl azide **[^{18}F]2.72** was synthesised followed by a click reaction with precursor compound **2.62**.

The precursor **2.62** and cold standard **2.63** used for the validation of radiotracer **[^{18}F]2.53** are characterised in Chapter 2 . HPLC tracers were obtained through reverse phase HPLC chromatography using acetonitrile (solvent A) and water with 0.1% formic

acid(solvent B). 0 min, 5% A; 0-8min 5-90% A; 8-12min, 90% A; 12-15min: 90-5% A; 15-18min: 5% A.

Figure 3-28 shows the TIC spectrum from the LCMS of precursor 2.62 which reveals a primary peak at 14.003 minutes with the $[M+H]^+$ ion (m/z= 155.0).

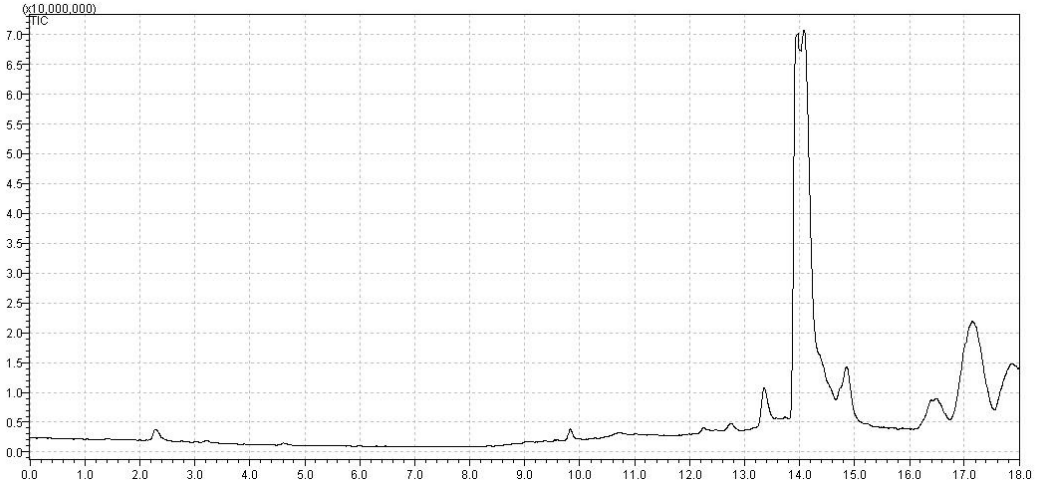

Figure 3-28: Total ion count LCMS for 2.62 with a retention time of 14.003mins

Figure 3-29 shows the UV HPLC tracer of cold standard **2.63** which displays a peak at 13.163 minutes. As shown in chapter 2, this was monitored by MS with the $[M+H]^+$ ion (m/z=604.0). The primary peak was unreacted cold standard showing the same mass as the precursor with the same retention time at 14.003minutes. An earlier peak in the spectrum at 12.437 minutes with an $[M+H]^+$ ion (m/z=693.0) relates to the doubly reacted compound **2.64**, this value lines up with data presented in chapter 2 where Figure 2-13 shows the doubly reacted precursor at 12.457 minutes.

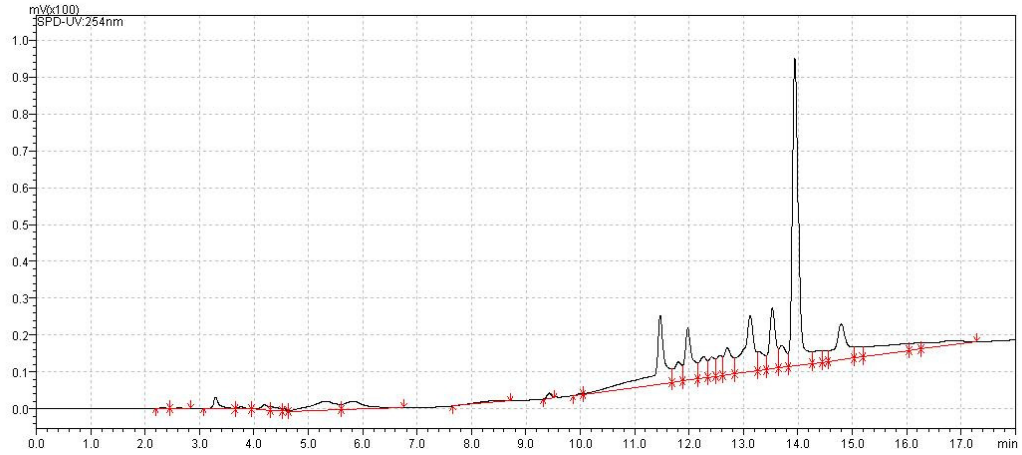

Figure 3-29: UV spectrum of the cold standard 2.63 with a retention time of 13.163 minutes

3.2.6.1 Radiochemistry

The click chemistry radiolabelling of **[^{18}F]2.63** was performed using the same method as the click labelling of **[^{18}F]2.16**. 2-[^{18}F]fluoroethyl azide **[^{18}F]2.72** was made and distilled into precursor **2.62.** The reaction was initiated by adding freshy prepared $Cu(CH_3CN)_4PF_6$ and TBTA catalyst. It was reacted for 20 minutes at 70°C.

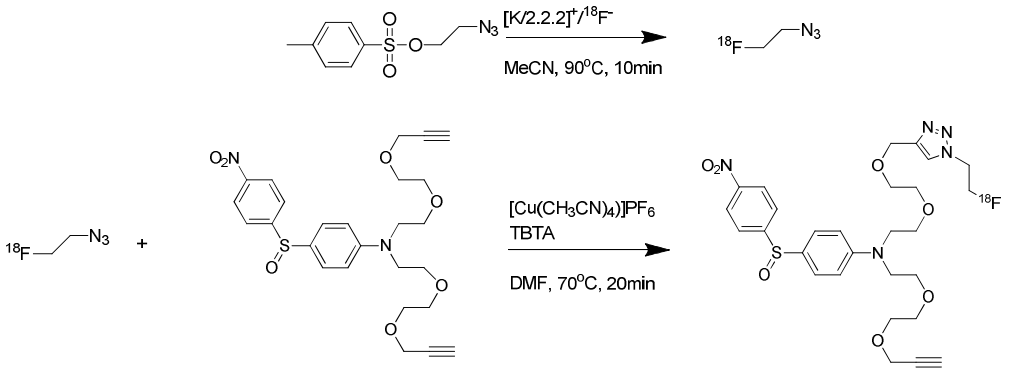

Scheme 3-11: Radiosynthesis of [18F]2.63

Scheme 3-11 demonstrates the 2-step radiolabelling method used for the synthesis of radiotracer **[^{18}F]2.63.** The formation of **[^{18}F]2.63** was monitored by radiation detectors

placed throughout the cell as shown by Figure 3-30. Following the same method used for the production of **[^{18}F]2.16** activity was first transferred to the target vial from the cyclotron, it is then trapped onto the QMA. The activity is eluted from the QMA into reactor 1 where 2-[^{18}F]fluoroethyl azide **[^{18}F]2.72** is synthesised. The 2-[^{18}F]fluoroethyl azide **[^{18}F]2.72** is then distilled from reactor 1 into reactor 2 which contained 1.5mg of precursor **2.62**. The catalyst was added and the reaction left to stir for 20minutes. It was then transferred onto the semi preparative Gemini column for purification.

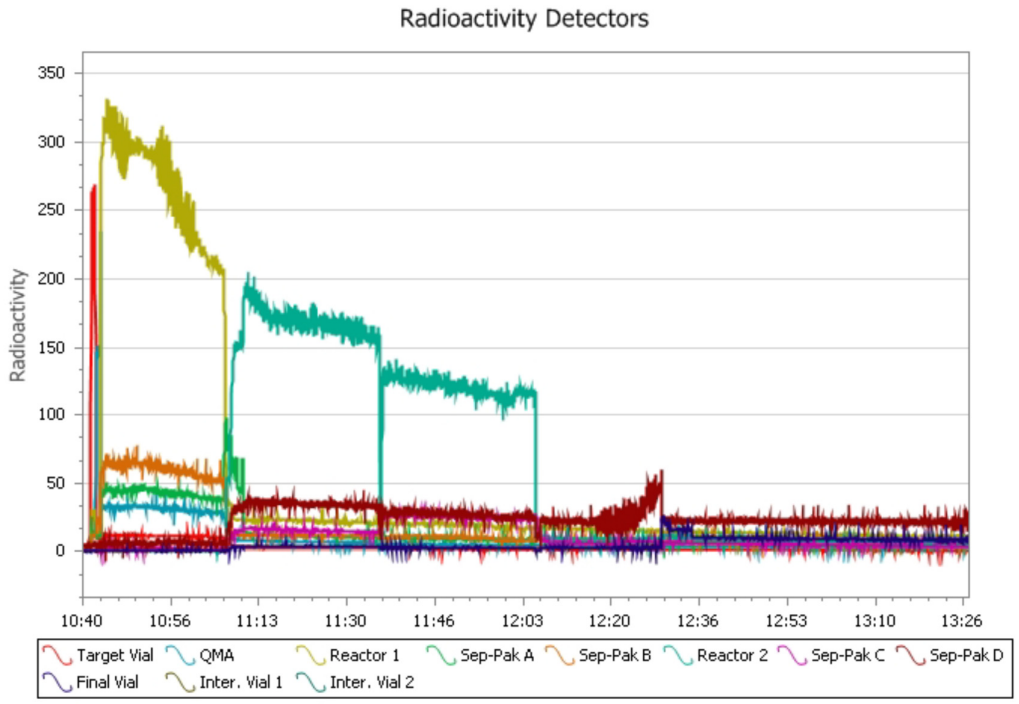

Figure 3-30: Radioactivity distribution in the Flexlab during the synthesis of [^{18}F]2.63

3.2.6.2 HPLC purification and reformulation

[^{18}F]2.63 was isolated from the precursor and any by-products using a semi-preparative HPLC system. It had a retention time of 15.5 minutes as shown Figure 3-31.

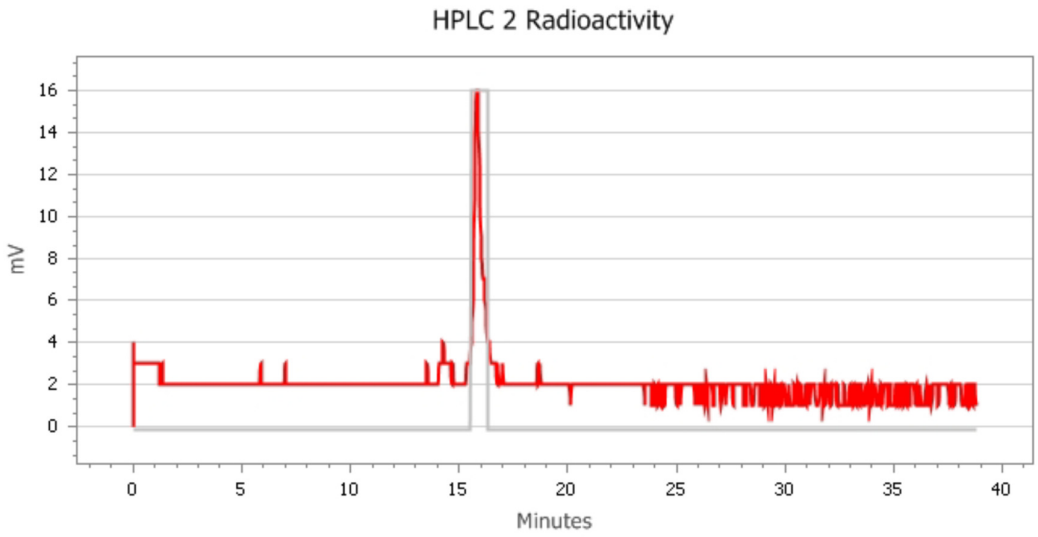

Figure 3-31: Purification of [^{18}F]2.63 via HPLC

The purified **[18F]2.63** was reformulated into 10% ethanol/saline, closely following the C-18 seppak method. Total synthesis time including HPLC purification and reformulation was 90 minutes with a non-decay corrected yield of 4% based on K[^{18}F]F.

3.2.6.3 Quality Control

Quality control of radiotracer **[^{18}F]2.63** was performed on a Shimadzu LCMS system in ACPI mode using an analytical reverse phase C-18 column and a H_2O/CH_3CN gradient solvent system as mobile phase.

The radiotracer was validated by correlating the retention time of the radiotracer peak **[^{18}F]2.63** with the retention time of the cold standard HPLC peak **2.63**. shows the retention time for the cold standard **2.63** at 13.163 minutes, which is comparable with

the retention time of the radiotracer **[^{18}F]2.63** shown in Figure 3-32**,** which had a retention time of 13.185 minutes.

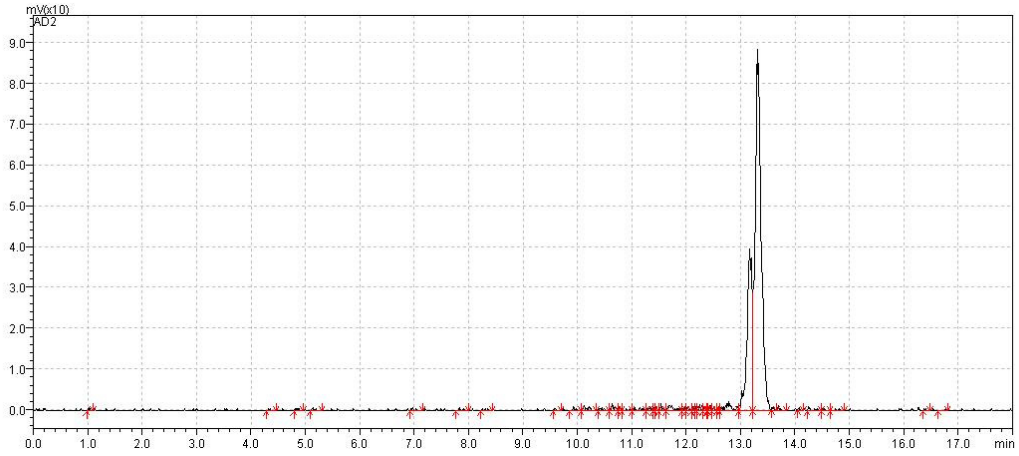

Figure 3-32:Radio Peak for [18F]2.63 with a retention time of 13.397minutes

3.3 Conclusion

The synthesis of the fluorine labelled radiotracers **[^{18}F]2.16**, **[^{18}F]2.26**, **[^{18}F]2.36**, **[^{18}F]2.43, [^{18}F]2.53** and **[^{18}F]2.63** from their respective precursors **2.15**, **2.25**, **2.35**, **2.42**, **2.52** and **2.62** was successfully achieved. Table 3-2 shows both the decay corrected and non-decay corrected RCYs for each radiotracer. While some radiotracers show good yields others still require some work. However, for preliminary biological studies the yields were sufficient. The suitability of these compounds as hypoxia imaging agents will be examined further in chapter 4 and 5 using in-vivo and in-vitro studies.

Table 3-2: List of radiotracers and their non-decay and decay corrected RCYs

Radiotracer	Non-decay corrected RCY	Decay corrected RCY
[^{18}F]2.16	11%	19%
[^{18}F]2.26	10%	18%
[^{18}F]2.36	25%	44%
[^{18}F]2.43	5%	9%
[^{18}F]2.53	4%	7%
[^{18}F]2.63	4%	7%

There were substantial loses of radioactivity during the production of the radiotracers, possible areas of loss include F-18 that is not distilled across from the first step, F-18 lost during the azeotropic drying and from side products that are formed but purified out during the HPLC purification of the final product. Product can also be lost due to getting stuck in the lines and during the HPLC collection step.

3.4 Experimental

3.4.1 Materials and methods

No-carrier added [^{18}F]fluoride was generated by the IBA cyclone 10/5 using a 10MeV proton beam and a titanium target containing [^{18}O]H_2O, utilising the $^{18}O(p,n)^{18}F$ nuclear reaction. Typical irradiation parameters involved running the cyclotron at 20μA for 45-60 minutes to generate 300-400mCi (11.1MBq to 14.8MBq) of [^{18}F]fluoride. These yields are only around 25% of the theoretical yield, which can be partially explained by the use of recycled [^{18}O]H_2O, previously used [^{18}O]H_2O that has been redistilled after use with an unknown isotopic enrichment. Isolation of [^{18}F]fluoride was achieved by trapping an

QMA ion exchange column separating it from the $[^{18}O]H_2O$. The column was eluted with a solution containing 3.45mg of anhydrous K_2CO_3 (0.025 mmol) and 20mg of Kryptofix 2.2.2 (0.53mmol) in 0.4mL of acetonitrile and 0.2mL of water. In the reactor vial the solvent was removed azeotropically with dry acetonitrile (750µL) to give the anhydrous $[^{18}F]$fluoride complex that was used in the labelling experiments.

Solvents were purchased Merck and used as received. Reagents were purchased from sigma Aldrich and used without further purification. 2-Azidoethyl 4-toluenesulfonate was synthesised following literature procedures.

Quality control was carried out on a Shimadzu 2010 LCMS system with a 5µL injection loop, SPD-20A UV-Vis detector and two LC-20AD solvent pumps for the mixing of the mobile phase system that was used. A Phenomenex Gemini C-18, 5µ RP column, 150 x 4.6mm acted as the stationary phase, while the mobile phase was acetonitrile (A) and 0.1%formic acid in water (B). The flow rate used was 0.5mL/min with a range of gradient elution technique used for analysis. A Bioscan FC-4000 dual BGO PET metabolite coincidence detector was used for the detection of radioactive compounds.

3.4.2 Procedure for radiolabelling

Preparation of the copper catalyst.

The copper catalyst was prepared by combining TBTA(4mg, 7.5µmol) and tetrakis(acetonitrile)copper(I) hexafluorophosphate (6mg, 16µmol) in DMF(500µL)

2-[^{18}F]Fluoroethyl azide ([^{18}F]2.72)

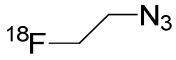

2-azodoethyl 4-toluenesulfonate (4µL, 12mg, 0.05mmol) in 750µL of acetonitrile was added to the dried [18F]KF/Kryptofix complex. The reaction mixture was heated at 95°C for 15minutes. Acetonitrile (1mL) was added and the temperature was increased to 100°C. The 2-[^{18}F]Fluoroethyl azide **([^{18}F]2.72)** was then distilled into a second reactor vial.

General method for click chemistry

The second reactor vial contained a solution of precursor compound (1mg) in 200µL of DMF. Once the transfer of 2-[^{18}F]fluoroethyl azide **([^{18}F]2.72)** was complete the copper catalyst (500µL) was added to the second reactor vial. The reaction mixture was heated at 70°C for 20 minutes before it was transferred to the semi-preparative HPLC system for purification. HPLC was performed using a Phenomenex Gemini C-18, 5µ RP column, 150 x 4.6mm with a gradient technique; Solvent A : Acetonitrile, Solvent B: 0.1M Ammonium Formate in distilled water; 0min: 20% A; 0-10min: 20-80% A; 10min-Collection: 80% A; Collection-End: 90% A, with a flow rate of 4mL/min . The collected radio peak was reformulated using the seppak method to give the desired radiotracer.

4 n-vivo Studies of radiolabelled tracers

4.1 Introduction

4.1.1 Developing novel hypoxia radiotracers

Hypoxic tissue plays an important role in many diseases including cancer, diabetes and stroke. Hypoxic tumours are often more resistant to radiotherapy and chemotherapy compared to non-hypoxic cancer cells.[94-95] High levels of tumour hypoxia are often connected with biologically aggressive tumours resulting in poor prognosis for the patients.[24-25] Hypoxia is therefore an important factor in determining local tumour control for radiotherapy and due to its prevalence in certain varieties of tumours it also provides a basis for tumour selectivity.[30, 48, 70]

Despite increased resistance to conventional therapies, hypoxia also provides an attractive target to chemotherapy by use of so-called hypoxia activated prodrugs. These prodrugs are designed to form cytotoxins after they are activated via metabolic reduction under hypoxic conditions.[6, 10, 27] Radiotherapy also has the possibility of being hypoxia directed with both conformal radiotherapy and intensity modulated radiotherapy.[5] To properly plan for the treatment of these cancers, it is therefore important to be able to measure the hypoxic fraction of these tumours.[33, 48]

Positron Emission Tomography (PET) is a nuclear imaging technique that allows non-invasive measurement and quantification of physiological processes *in-vivo*. As discussed in Chapter 1 [^{18}F]FMISO (**1.2**) is the most commonly used organic radiotracer.[65-68] However, the slow kinetics exhibited by [^{18}F]FMISO(**1.2**) results in relatively poor image quality prompted the development of several different hypoxia

selective tracers by Dr Cheryl Falzon in our research group.[55, 71] Compounds [^{18}F]SO101 (**1.9**) and [^{18}F]SO201 (**1.10**) both exhibited faster pharmacokinetics and higher contrast compared to [^{18}F]FMISO (**1.2**) in rat models for ischemic stroke. Despite this the nitrogen mustard analogues were deemed unsuitable for routine production and use in human patients due to the perceived toxicity. Later modifications by Dr Evelyn Laurens led to the tracer [^{18}F]SO501 (**1.15**).[1] This tracer displayed good uptake into hypoxic tumours during small animal imaging, however substitution-based radiolabelling does not provide consistent yields during the radiosynthesis.

In Chapters 2 and 3, syntheses and radiolabellings were reported for 6 radiotracers based of the structure of [^{18}F]SO501 (**1.15**). These 6 tracers were **[^{18}F]2.16**, **[^{18}F]2.26**, **[^{18}F]2.36**, **[^{18}F]2.43, [^{18}F]2.53** and **[^{18}F]2.63**. This chapter will investigate the in-vivo properties of these radiotracers in order to evaluate their potential for binding to hypoxic tissue. Animal models play an important role in biomedical research for the study of disease and physiological processes. Imaging of animal models was utilised to access the uptake of radiotracers in experimental tumour models.

4.1.2 PET and Small animal PET

PET can provide spatial and temporal measurements for the distribution of radiotracers within living systems due to its dynamic imaging capabilities.[96-97] Direct correlations can be drawn between animal models and human studies by utilising small animal PET.[96, 98-99] Due to the small size of animal models like mice, animal PET requires higher spatial resolution and sensitivity in order to achieve the same level of accuracy and detail as those for current human PET studies.[100-102] As such small animal PET scanners have been optimised to yield higher spatial resolution than human scanners.[100] In turn this improves the resolution of sensitivity of images.[103] Small animal PET can therefore

provide dynamic imaging, allowing for the kinetics of the tracer to be monitored over time providing radiotracer time activity curves (TACs) from a single animal.[53]

The utilisation of small animal PET also reduces the number of animals required for the experiments as each animal subject can be used for the entire course of repeated studies for the tracers.[53, 59, 103-104]

For this research project BALB/c nude mice xenografted with SK-RC-52 (renal tumours) were used to study the uptake of the synthesised radiotracers **[^{18}F]2.16**, **[^{18}F]2.26**, **[^{18}F]2.36**, **[^{18}F]2.43** and **[^{18}F]2.53.** Each tracer had a TAC acquired by using a 2h PET dynamic scanning.

4.2 Materials and Methods

All animal experiments were approved by the Austin Health animal ethics committee and carried out within the outlines for the ethics submission of this project. Animal handling and imaging were performed by Dr. Angela Rigopoulos from the Oliver Newton John Cancer Research Centre.

4.2.1 Transplants

SK-RC-52 tumours were first grown by subcutaneously injecting BALB/c nude mice in the flank with a suspension of 6x10^6 SK-RC-52 cells. Once the tumours had grown to a size of 300mm^3 they were cut into 40mm^3 pieces and transplanted into the shoulder of other BALB/c nude mice. When the tumours grew to at least 180mm imaging was started, when the studies were concluded the BALB/c nude mice were euthanised.

4.2.2 Imaging

Mice imaging studies were performed using the Mediso small animal PET/MRI system . Animals were injected with 9.25MBq (0.26mCi) of radiotracer in 100µL of the final formulation. Before the study animals were anaesthetised using isoflurane delivered by the Minerva Biovet system, the system also provides a temperature stable environment for the animals during uptake and imaging stages. The 2h dynamic imaging was performed by acquiring 12x10 min frames from the start of injection. A 10 minute static frame was acquired at the end of each study 2h post injection. Images were reconstructed using the RAMLA3D algorithm. The MRI was acquired at the same time as the PET scan. MRI and PET images were imported into the PMOD analysis software allowing for the spatial alignment of the animals and subsequent Volume of interest analysis. All imaging studies were performed at the Austin Animal House by qualified animal technicians.

Oxygen tension measurements previously been carried out by Dr. Evelyn Laurens and showed good correlation between tumour size and pO_2 mmHg. Table 4-1 shows the direct correlation between tumour sizes and the partial pressure of oxygen.[1]

Table 4-1: Partial pressure of oxygen for given tumour sizes

Tumour size	Volume	pO_2 (mmHg)
Small	<300mm^3	>14
Medium	300-500mm^3	8
Large	>500mm^3	4-5

4.3 Results and discussions

In-vivo testing of the compounds were tested using transplanted SK-RC-52 tumours. The tumours were xenografted on to the right shoulder of BABL/c nude mice, tumour sizes were measured using callipers. Animals were tested when the tumour growth had exceeded 400mm^3. Animals were imaged for 2 hours post tracer administration to obtain time activity curves.

Radiotracer	Retained	Number of Studies
[^{18}F]2.16	Yes	6
[^{18}F]2.26	No	4
[^{18}F]2.36	No	6
[^{18}F]2.43	No	4
[^{18}F]2.53	No	6

4.3.1 Imaging results for [^{18}F]2.16

Initial imaging studies of the radiotracer **[^{18}F]2.16** were carried out in smaller tumours. At 2 hours post injection the tumour to muscle ratio was 0.9 for the small tumour. This is reflected in the dynamic study over 2 hours as shown by the TAC in Figure 4-1 where the clearance rates for the tracer is similar for both the tumour and normoxic tissue. There is little to no retention of the radiotracer **[^{18}F]2.16** in small tumours.

(Note: Tumour size was not provided)

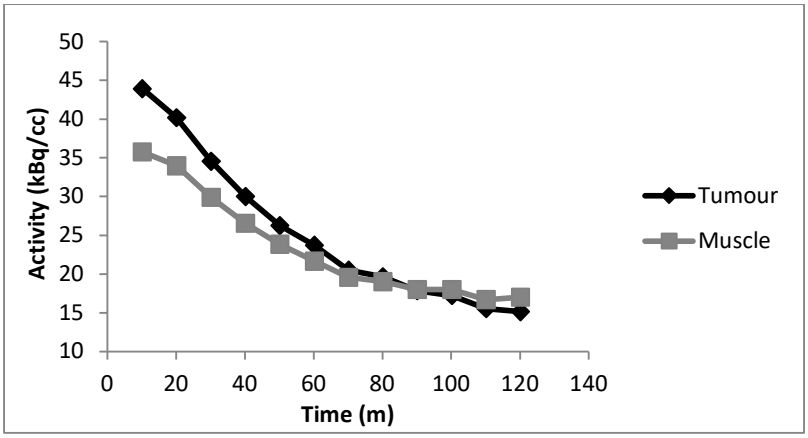

Figure 4-1: Time activity curve for [18F]2.16 for a small tumour

This is further reflected in the reconstructed image shown in Figure 4-2. The image has 3 rows representing the MRI, PET image and then the combined image with the PET image overlayed onto the MRI. The MRI provides an anatomical reference for the PET reconstruction. In Figure 4-2 the tumour on the right shoulder has a low uptake of **[^{18}F]2.16**, possibly indicating that the tumour is not yet hypoxic.

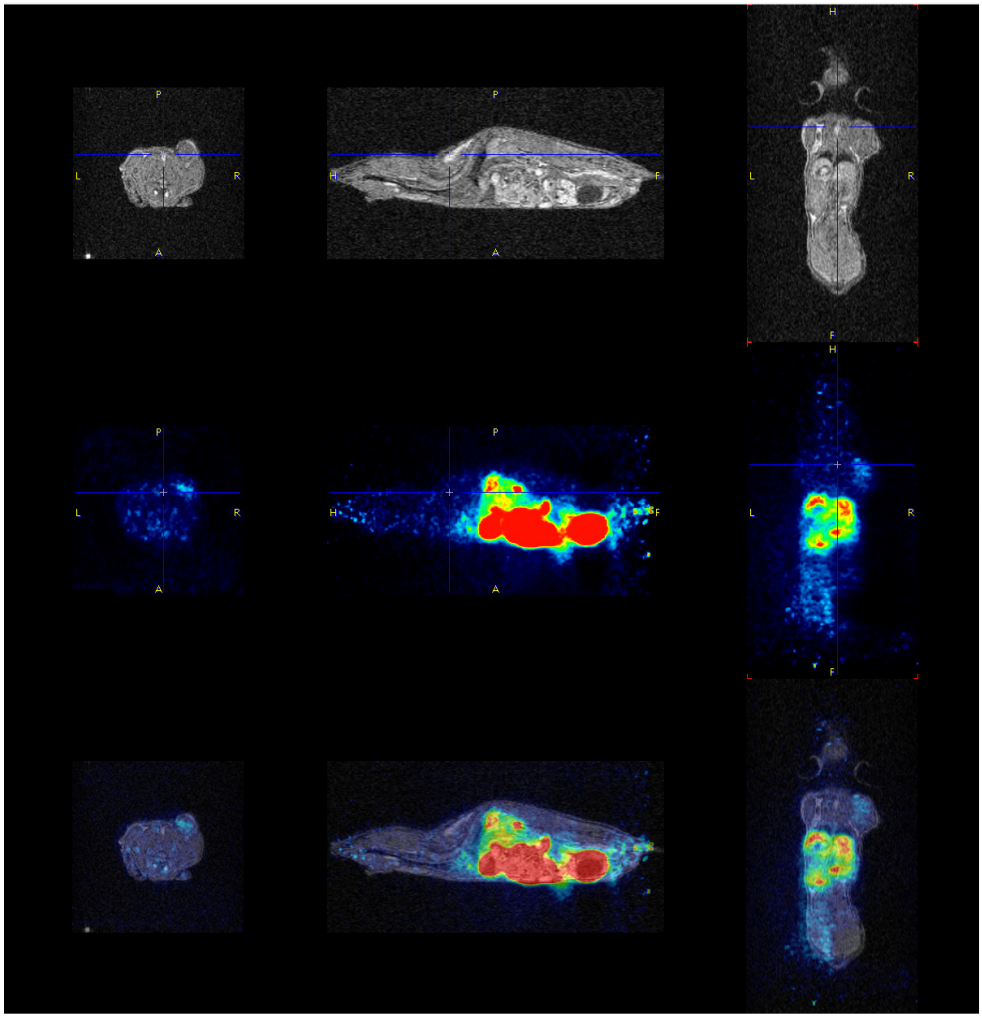

Figure 4-2: Compound image of [^{18}F]2.16 in a small SK-RC-52 tumour in a BALB/c Mouse, tumour located on right shoulder

For larger tumours the dynamic imaging of radiotracer **[^{18}F]2.16** shows retention in tumour tissue while maintaining the clearance rate for normoxic tissue. Figure 4-3 is the TAC for **[^{18}F]2.16** in a 904mm^3 tumour, the clearance from normoxic tissue is similar to that of Figure 4-1 but the tumour tissue is different showing very little initial uptake but over time the radioactivity is steady eventually reaching a tumour to muscle ratio of 2.06. It has an equilibrium time of 30 minutes where the average activity in the tumour and muscle are the same before reaching a maximum activity level at 80 minutes.

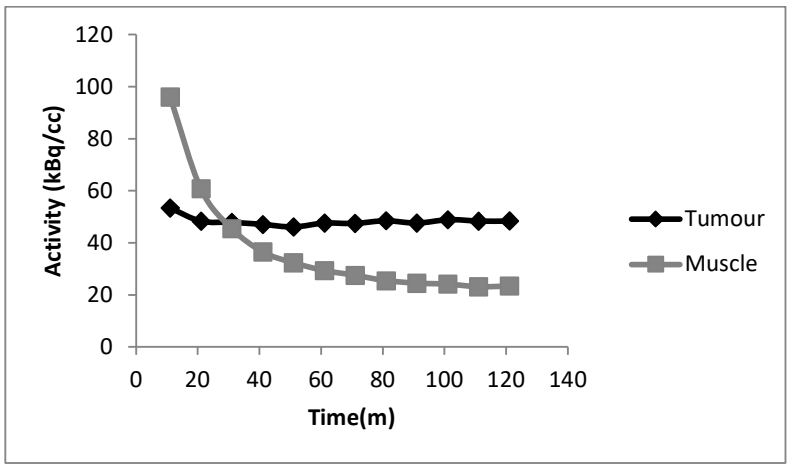

Figure 4-3: Time activity curve for [^{18}F]2.16 for a 904mm^3 tumour

The 626mm^3 tumour TAC shown in Figure 4-4 exbibits a similar retention pattern with fast clearance from normoxic tissue and uptake into the tumour, ending with a muscle to tumour ration of 2.34. The equilibrium time was similar to the larger 904mm^3 tumour at 33 minutes but reaching a maximum activity level at 70minutes.

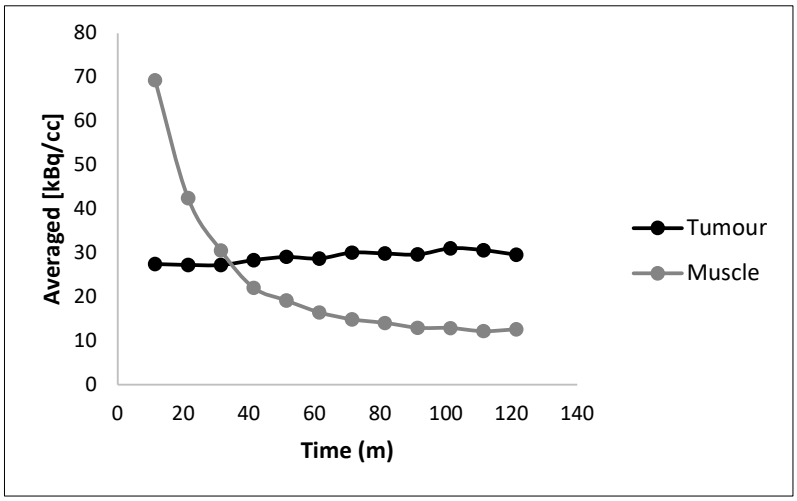

Figure 4-4: Time activity curve for [^{18}F]2.16 for a 626mm^3 tumour

PET/MRI imaging of the larger 904mm^3 tumour shows more favourable results compared to that of the small tumour. The tumour is more clearly visible in Figure 4-5 with it clearly visible on the right shoulder. The radiation is also lower in the urinary system compared to Figure 4-2.

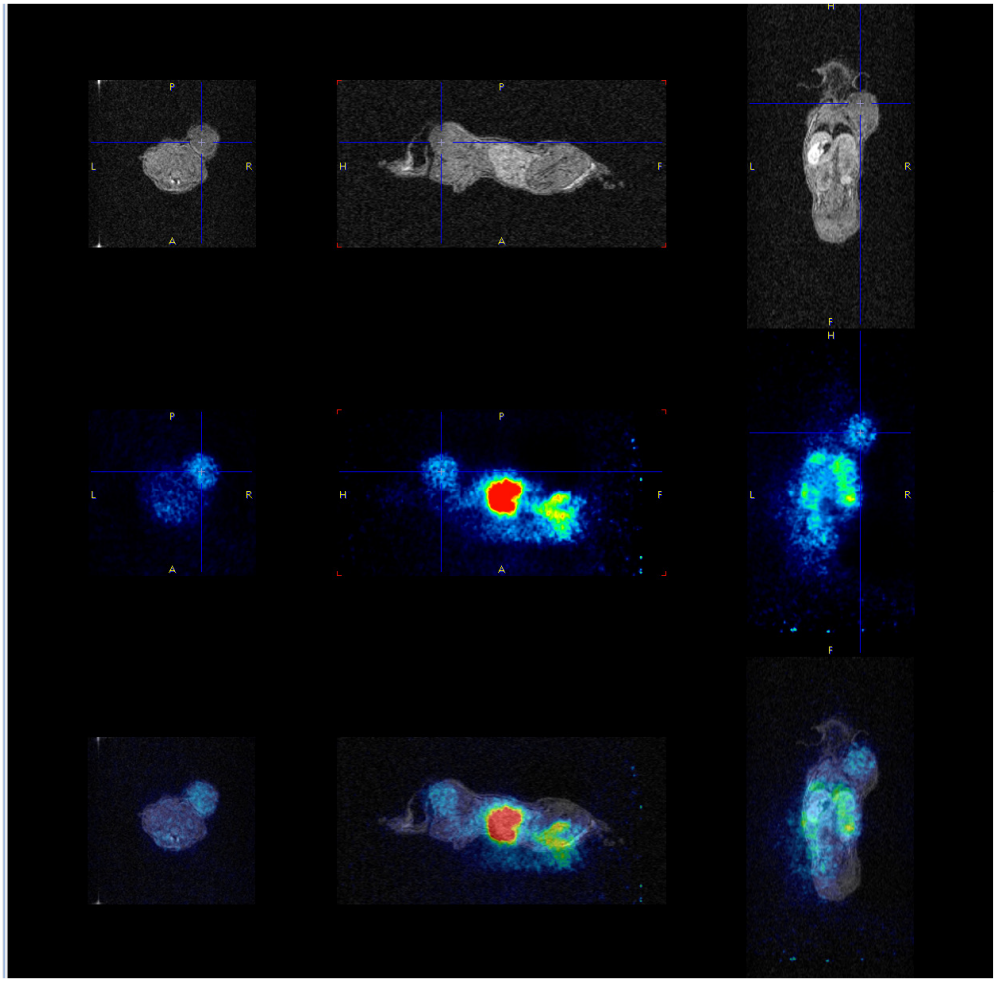

Figure 4-5: Compound image of [^{18}F]2.16 in a 904mm^3 SK-RC-52 tumour in a BALB/c Mouse, tumour located on right shoulder

4.3.2 Imaging results for [^{18}F]2.26

With quick clearance from small tumours for radiotracer **[^{18}F]2.16** the other tracers on this list were instead imaged directly into large tumours. **[^{18}F]2.26** was tested on larger tumours ranging from 881mm^3-1008mm^3. Results for **[^{18}F]2.26** showed fast clearance initially in both tumour and muscle with an end tumour to muscle ratio of 1.8. Figure 4-6 demonstrates the fast clearance in the TAC of **[^{18}F]2.26** showing no real uptake into hypoxic tissue with the levels of activity plateauing for both regions examined.

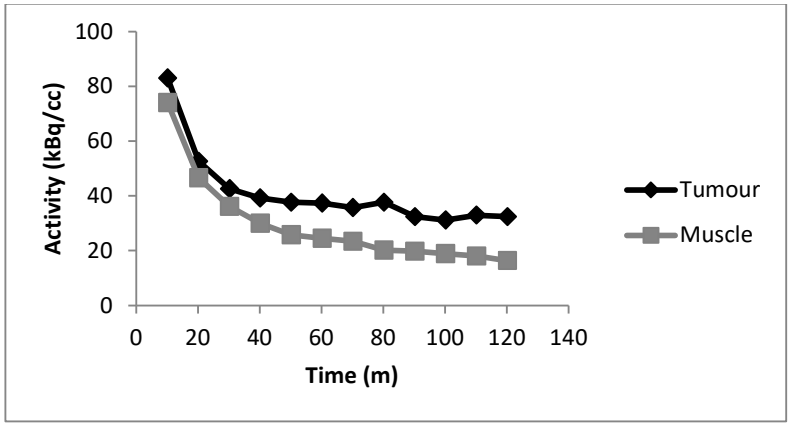

Figure 4-6: Time activity curve for [^{18}F]2.26 for an 881mm^3 tumour

Images for **[^{18}F]2.26** in the 881mm^3 tumour also show a lack of uptake into the tumour with the majority of the activity accumulated into the bladder to the BALB/c mouse. This is illustrated in Figure 4-7 where the tumour in the right shoulder is barely visible in the PET image despite the large growth clearly visible in the MRI.

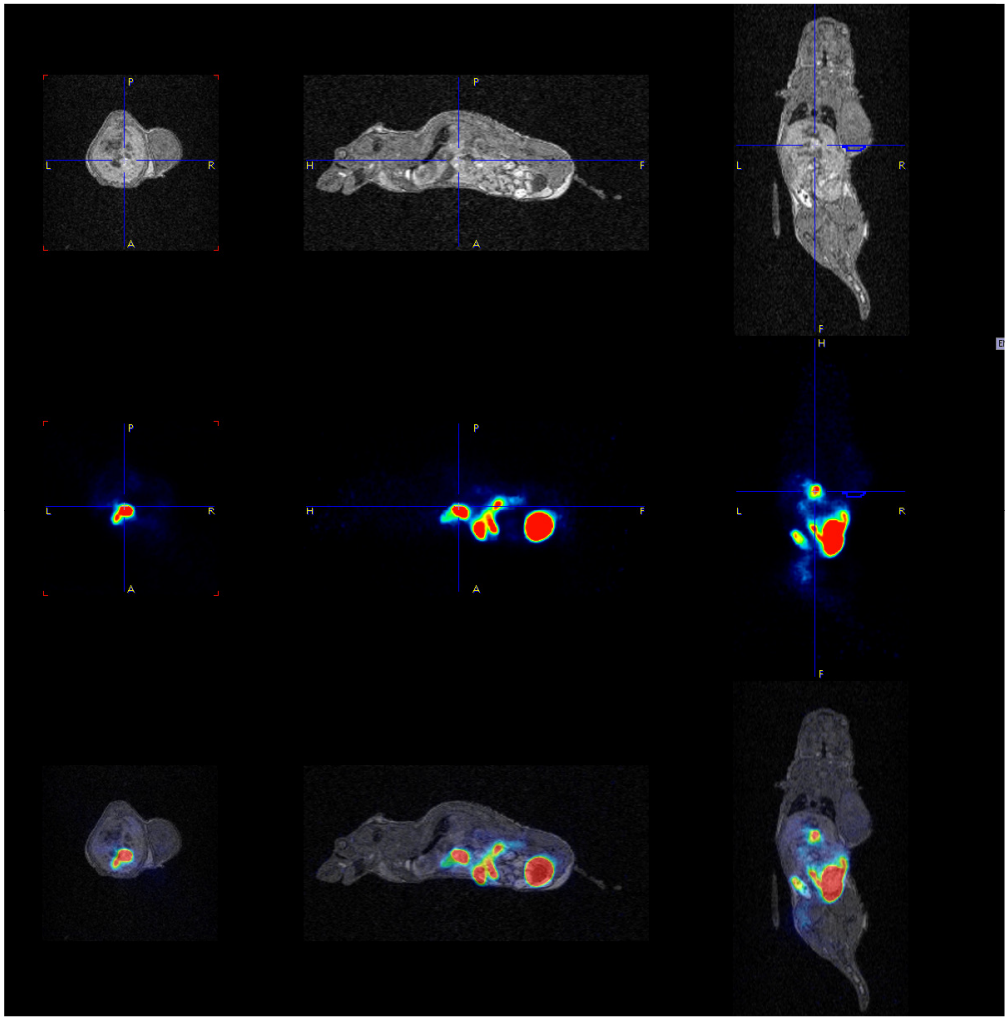

Figure 4-7: Compound image of [18F]2.26 in a 881mm3 SK-RC-52 tumour in a BALB/c Mouse, tumour located on right shoulder

4.3.3 Imaging results for [^{18}F]2.36

Imaging studies performed with radiotracer **[^{18}F]2.36** showed quick initial clearance from tumour and muscle in a 1551mm^3, shown in Figure 4-8, until the 40-minute mark where the rate of clearance slows. The activity of the hypoxic tissue starts to plateau while in normoxic tissue it still has a higher clearance rate. The final tumour to muscle ratio after 120 minutes was 1.35.

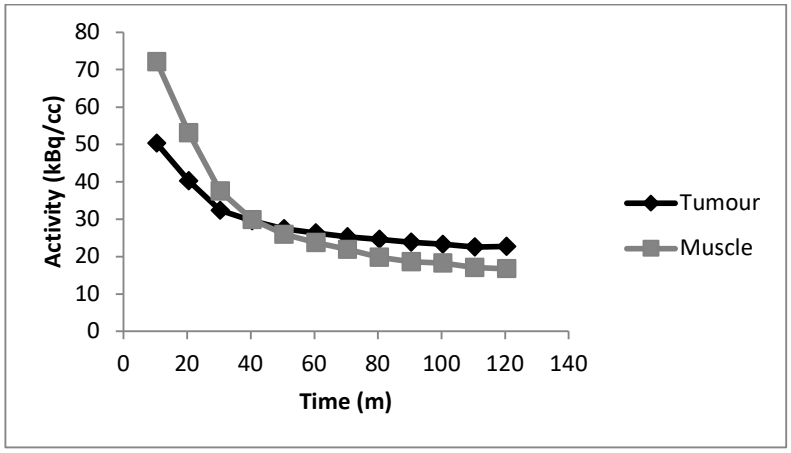

Figure 4-8: Time activity curve for [^{18}F]2.36 for a 1551mm^3 tumour

PET imaging could provide some insight for the low retention and uptake of the tracer in the large tumour. In Figure 4-9 the caudal to cranial view in the middle left image shows the tumour off the right shoulder of the BALB/c mouse, the centre of the tumour is dark indicating that the radiotracer **[^{18}F]2.36** has failed to penetrate into the tumour tissue suggesting that the tissue may have become necrotic. Other studies performed using [^{18}F]2.36 exhibited similar results to those shown despite not being necrotic.

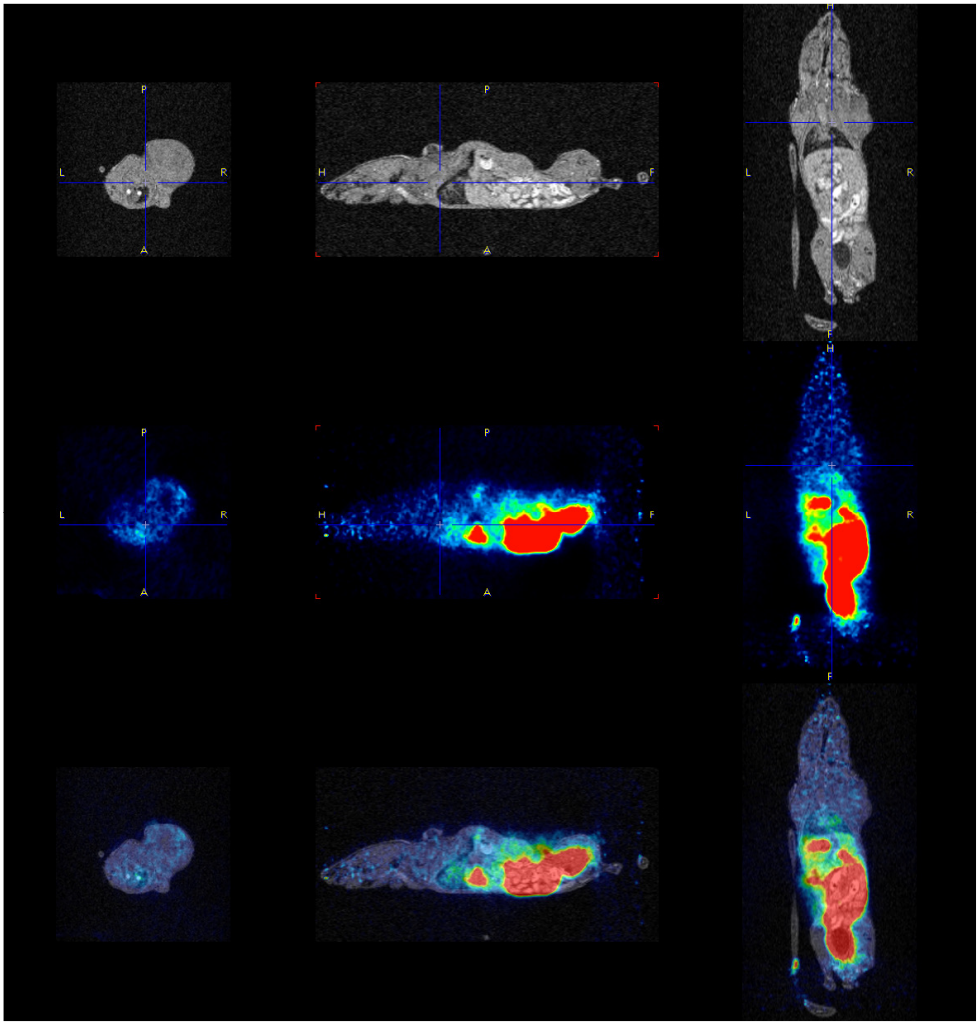

Figure 4-9: Compound image of [18F]2.36 in a 1551mm3 SK-RC-52 tumour in a BALB/c Mouse, tumour located on right shoulder

4.3.4 Imaging results for [^{18}F]2.43

Radiotracer **[^{18}F]2.43** had no uptake in either hypoxic or normoxic tissue. Figure 4-10 demonstrates the quick clearance from both the muscle and tumour before the activity plateaus with no real difference between the activity levels. The final Tumour to muscle ratio reflects this with a value of 0.96.

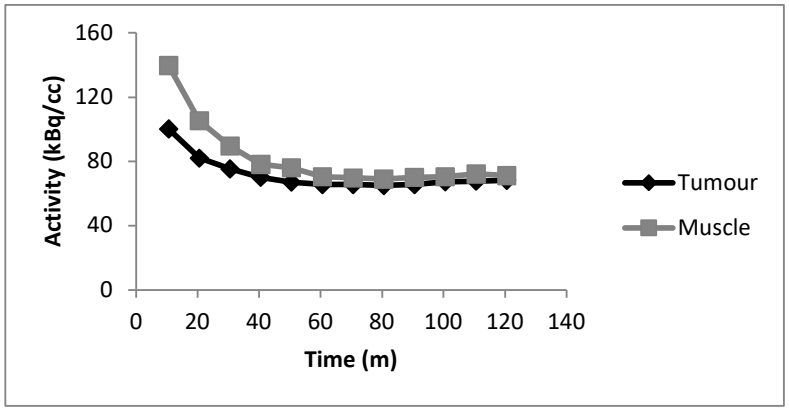

Figure 4-10: Time activity curve for [^{18}F]2.43 in a large tumour, exact size unknown

The tumour in Figure 4-11 showed signs of necrotic damage similar to Figure 4-9. It is visible in the caudal to cranial view as well as the lateral view, with the dark area indicating the absence of any [^{18}F]2.43 radiotracer in those areas.

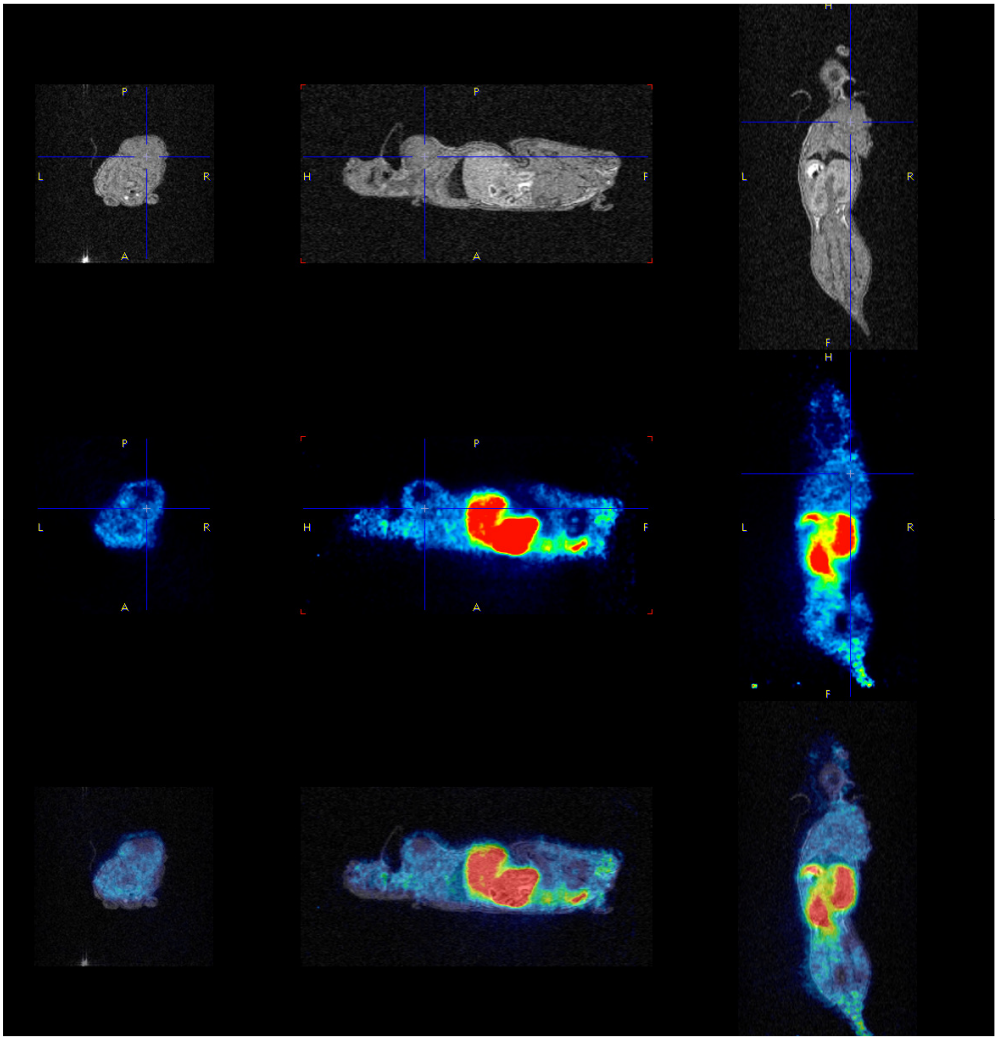

Figure 4-11: Compound image of [^{18}F]2.43 in a SK-RC-52 tumour in a BALB/c Mouse, tumour located on right shoulder

4.3.5 Imaging results for [^{18}F]2.53

Imaging of the radiotracer **[^{18}F]2.53** shows a TAC profile similar **[^{18}F]2.26** with high initial clearance from both muscle and tumour tissue which slows down after 40minutes where the rate of clearance drops. Figure 4-12 shows a maximal difference between activity in the muscle and tumour at 70 minutes. The final tumour to muscle ratio at 120minutes of 2.47.

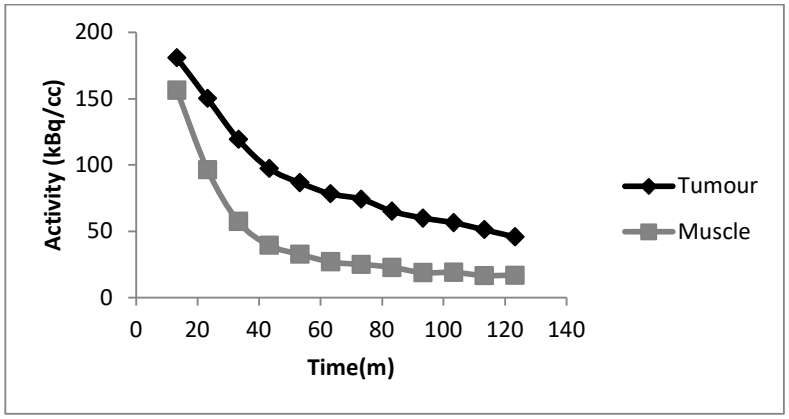

Figure 4-12: Time activity curve for [^{18}F]2.53

Figure 4-13 displays a clear tumour on the right shoulder of the BALB/c nude mouse, despite the high clearance of the radiotracer **[^{18}F]2.53.**

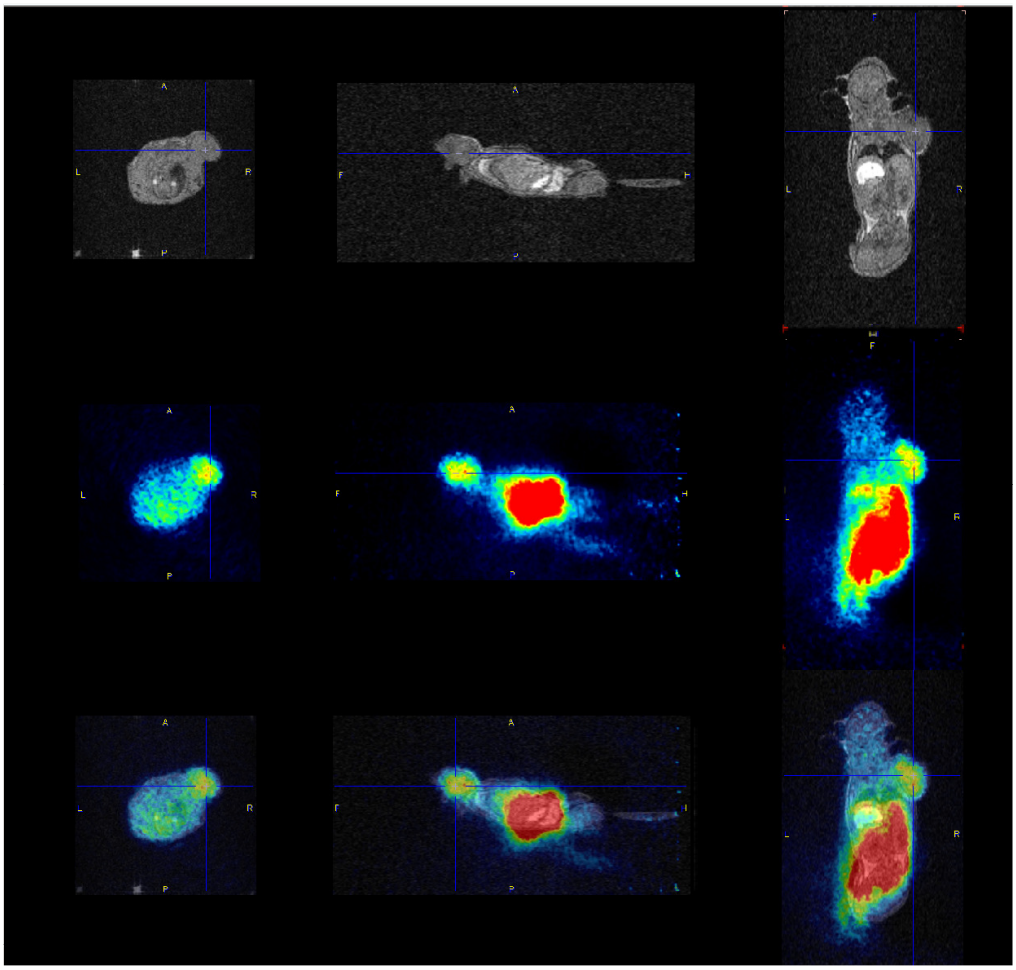

Figure 4-13: Compound image of [18F]2.53 in a SK-RC-52 tumour in a BALB/c Mouse, tumour located on right shoulder

4.4 Conclusion

The radiotracers **[^{18}F]2.16**, **[^{18}F]2.26**, **[^{18}F]2.36**, **[^{18}F]2.43** and **[^{18}F]2.53** were successfully imaged in BALB/c mice with SK_RC-52 tumours. Tracers **[^{18}F]2.16** and **[^{18}F]2.53** had the clearest PET images with the highest tumour to muscle ratios at 120minutes with a tumour to muscle ration of 2.34 and 2.47 respectively. Only the TAC of **[^{18}F]2.16** in a 626mm^3 tumour exhibited retention in the tumour over time, while all the other tracers displayed clearance from muscle and tumours at a similar rate.

From a structural perspective **[^{18}F]2.16** is the closest structurally to **1.15** with the shortest PEG chain. It would therefore have the least rotational variation and also it has the lowest molecular weight. Radiotracers **[^{18}F]2.26** and **[^{18}F]2.36** have longer PEG chains, while **[^{18}F]2.43** and **[^{18}F]2.53** are entirely different due to the presence of the iso-propyl ester. The changes to the structure reflect the results of the study with the higher the variation of the compound the quicker it cleared from the tumours.

5 In-vitro studies of radiolabelled tracers

5.1 Introduction

The synthesis and in-vivo imaging of the radiotracers **[^{18}F]2.16, [^{18}F]2.26, [^{18}F]2.36, [^{18}F]2.43** and **[^{18}F]2.53** have been described over chapter 2, 3 and 4, however since they are novel compounds little is known about their biological or pharmacokinetic properties.

Due to the results of the previous chapters compound **[^{18}F]2.16** underwent a stability study using S9 liver fractions as a model of liver metabolism. Additionally, the lipophilicity of the tracers **[^{18}F]2.16, [^{18}F]2.26, [^{18}F]2.36, [^{18}F]2.43** and **[^{18}F]2.53** was calculated.

5.1.1 Lipophilicity studies

Lipophilicity of radiotracer has an impact on its ability to cross membranes, directly effecting the ability to diffuse into tissues and cells. The lipophilicity is therefore important to the uptake of the radiotracer into tumours, clearance from the blood and non-specific binding.

The lipophilicity of a molecule is the logarithm of the octanol-water partition coefficient and is denoted as logP. High logP values indicate that a molecule will be highly lipophilic indicating that it will have poor water solubility and a low logP value will usually mean that the molecule is hydrophilic.[105] For a molecule to be able to diffuse through a cell membrane it must have a suitably high logP value, however a logP value that is too high may lead to undesirable qualities. These qualities could include: fast clearance from blood, accumulation in metabolic tissue and high non-specific binding in tumours.[105]

Based on previous studies the typical logP value that is desired for a molecule is between 1.5 to 3.[55, 105-106] To determine the logP value of the radiotracers in this study a modified octanol/water method was utilised.[1, 80, 85]

5.1.2 Metabolism Studies

Pharmacokinetic characterisation of a novel radiotracer is important to study the distribution of that radiotracer. The metabolism study of compound **[^{18}F]2.16** was conducted as a means to explore its stability in cells and as a method to predict its metabolism. In this case due to being a hypoxic tracer the ideal quality of **[^{18}F]2.16** would be stability to non-hypoxia dependant metabolism with the ability to be metabolised under hypoxic conditions *in-vivo*. Imaging quality could be affected by non-hypoxia dependent metabolism as it may lead to non-specific uptake of the radiotracer.

In-vivo metabolism studies of radiotracers would prove too costly as it would involve handling higher dosages of the radiotracer raising the costs associated with the handling of animal experiments.[107] *In-vitro* methods provide an alternative in order to elucidate the metabolic pathways of radiotracers more efficiently.[107] Many metabolic enzymes, including the cytochrome P450 enzymes, are located in the endoplasmic reticulum of liver cells and are directly responsible for the majority of drug metabolism.[108-109] The metabolic stability assay will utilise liver fractions extracted from the livers of animals.

The metabolic stability of **[^{18}F]2.16** was explored by subjecting it to phase 1 aerobic *in-vitro* metabolism. The metabolic stability of radiotracers refers to the percentage of the parent compound lost overtime while in the presence of a metabolically active test system.[80] For this study S9 liver fractions from rats were used due to their availability, cost and ease of storage.

In addition to the liver fraction, the metabolic system will also require a cofactor, NADPH generating system to allow reduction processes to occur.[110] The metabolic stability of the radiotracer **[^{18}F]2.16** was determined by analysing the supernatant of the metabolism system using radio-HPLC within a 2h time period. Analysis of the derived metabolites was not possible by LCMS due to the low levels of radioactivity during the study.

5.2 Results and discussions

5.2.1 Partition coefficients of radiolabelled tracers

The lipophilicity of the radiotracers **[^{18}F]2.16, [^{18}F]2.26, [^{18}F]2.36, [^{18}F]2.43** and **[^{18}F]2.53** were measured by using the octanol/saline partition co-efficient. Using the respective cold standards **2.16, 2.26, 2.36, 2.43** and **2.53** in a 1mg/mL solution the area under the curve was taken for each partition to give a formula: logP = log (area of octanol/area of water). This method was used to reduce the time critical nature associated with radioisotopes and to reduce exposure to radiation. LogP values of **2.16, 2.26, 2.36, 2.43** and **2.53** are presented in Table 5-1.

Table 5-1: LogP values of prepared standards

Cold Standard	**LogP Value**
2.16	0.95
2.26	1.77
2.36	1.90
2.43	1.66
2.53	0.89

The octanol/water coefficient was measured and the logP was calculated to be 0.95, 1.77 and 1.90 for **2.16, 2.26** and **2.36** respectively. This was expected as the primary difference between these three compounds is the increasing length of the PEG chain between the triazole and the diphenyl backbone. The logP increases as the length of the PEG chain increases. Compounds **2.43** and **2.53** exhibited the opposite effect where the shorter chain **2.43** had a logP of 1.66 while the longer chain **2.53** had a coefficient of 0.89.

While the three standards **2.26, 2.36** and **2.43** all had coefficients within the ideal range of 1.5-3.0 they were the tracers that showed clearance from both hypoxic and normoxic tissue. The standards **2.16** and **2.53** showed the best results in-vivo but both have logP values below the typical ideal range.

This clearly demonstrates while the LogP may have an ideal value of between 1.5 and 3 for crossing membranes that is not always strictly true and there are definitely other factors to consider, also the experimental method can also cause variations to calculated logP values making them even less reliable as a measure. [111]

5.2.2 Metabolism Study of Radiotracer [^{18}F]2.16

The metabolic stability of the radiotracer **[^{18}F]2.16** was determined by subjecting it to a phase 1 metabolism assay, in this case the S9 liver fraction from Sprague Dawley rats was used.

The phase 1 metabolism assay consisted of the following components: the radiotracer, phosphate buffer, S9 liver fraction and an NADPH generating system. The NADPH generating system was formed using magnesium chloride, glucose 6-phisohate, NADP

and glucose 6-phosphate dehydrogenase. Besides the metabolism assays an additional control assay was made, which included all the components except for the S9 liver fraction. All assays were incubated at 37°C in a thermo shaker were then quenched with methanol at designated time points (30, 60, 90 and 120 minutes). The resulting solutions were centrifuged to separate out the deactivated enzymes; the supernatants were analysed by radio-HPLC using a Shimadzu HPLC system with a UV detector(254nm) and BGO PET metabolite coincidence detector. The control assay was tested at 0 and 150minutes to ensure that any metabolism was a result of phase 1 metabolism and not due to other factors.

Analysis of the metabolism assays of **[^{18}F]2.16** revealed that it underwent phase 1 metabolism. Metabolites of **[^{18}F]2.16** started to form at 30 minutes, with at least 4 metabolites forming. At 60 minutes post incubation the metabolites continued to grow, however the changing ratio of the peak heights indicate that one of the metabolites could be due to secondary metabolism of one of the other metabolite products. For the 30minute time point the primary metabolite peak had a retention time of 7.9 minutes with a second large peak at 9.1 minutes, however at 60minutes the peak heights had been swapped. Following on at 90 and 120 minutes the peaks of the metabolites shift until almost all the metabolite peak area is under the peak at 9.1 minutes. Figure 5-1 displays the results of the metabolism and also shows the 2 control samples at 0 and 150minutes. From the control samples we can determine that all the metabolites are due to interactions with the enzymes in the S9 liver fraction and not a result of chemical instability.

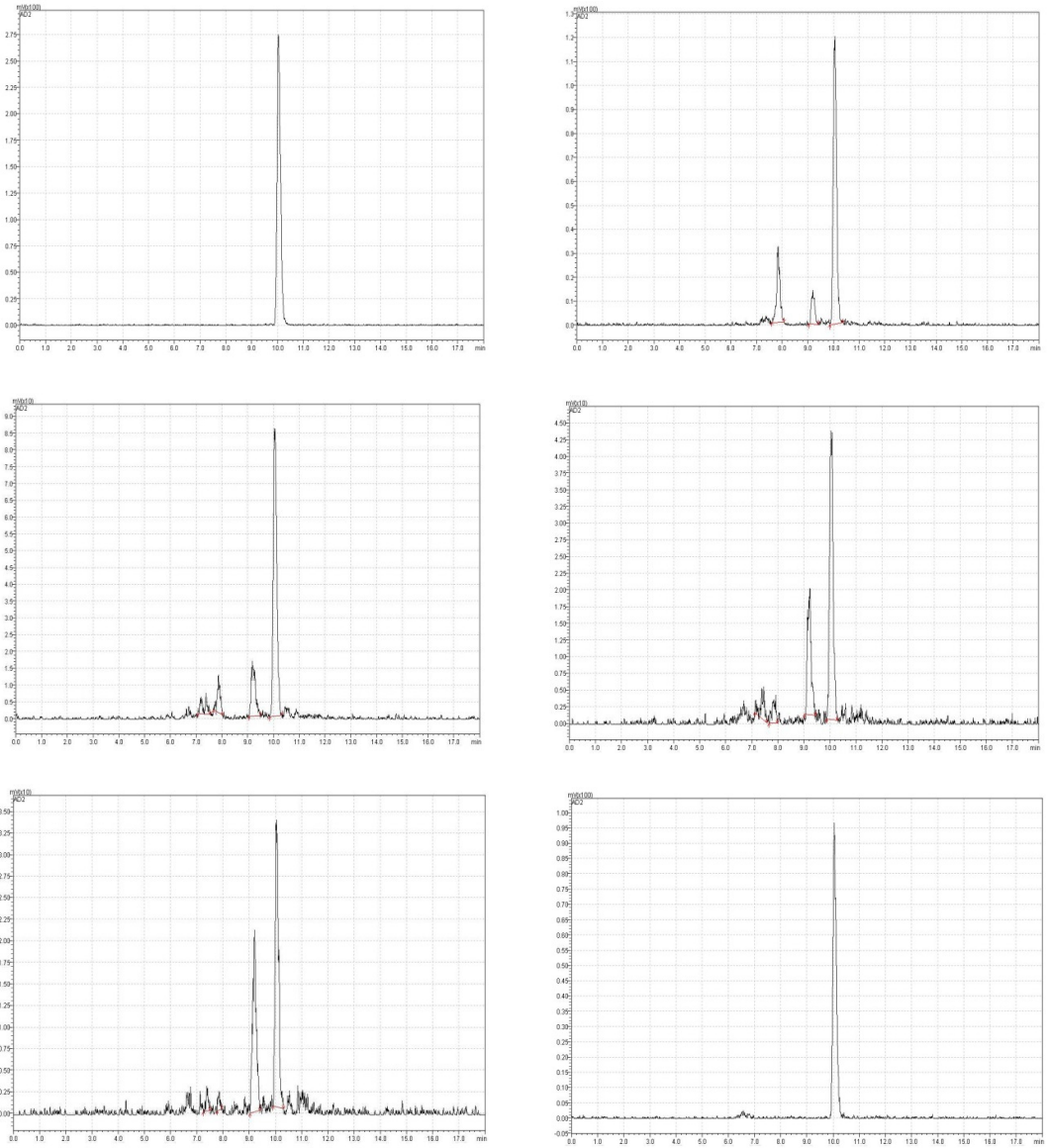

Figure 5-1: UV tracers from the HPLC, top left: 0 minutes, top right: 30 minutes, middle left: 60minutes, middle right: 90 minutes, bottom left: 120 minutes, bottom right: control at 150 minutes

The total peak area was taken and compared to the peak area of the parent compound **[^{18}F]2.16** to give Peak Area % = (area of [^{18}F]2.16/total area of peaks) x 100. Table 5-2 summarises the results for the study.

Table 5-2: [^{18}F]2.16 peak area left vs total area under peaks

Time	[^{18}F]2.16 Peak Area %
0	100
30	77.25
60	72.465
90	61.8
120	57.465

Using excel the data was plotted to generate a graph of intact parent compound as a percentage of **[^{18}F]2.16** vs time in minutes since the start of the experiment resulting in Figure 5-2. The data of this single exponential was found to have an R^2 value of 0.919. The half-life of **[^{18}F]2.16** in the S9 liver metabolism assay exceeded the 2-hour incubation period, giving it an estimated metabolic half-life of 148minutes.

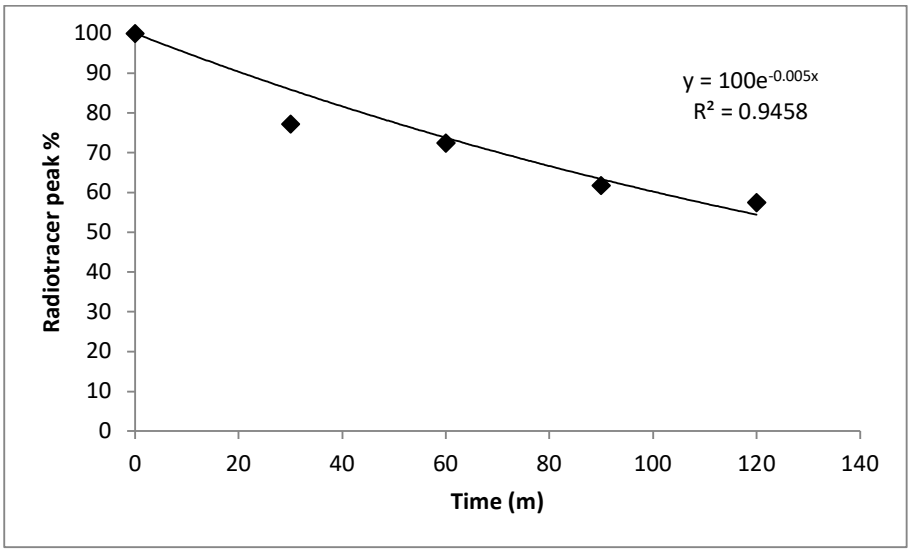

Figure 5-2: Percentage of intact parent compound [^{18}F]2.16 vs time in rat S9 liver fractions

Given the structure of the molecule and that there is a 2-stage metabolism that is seemingly exhibited it suggests at least 1 metabolism pathway most likely through a reduction of the nitro group to an amine via a hydroxylamine. This is demonstrated in Scheme 5-1 and would likely be facilitated through nitro reductase enzymes.

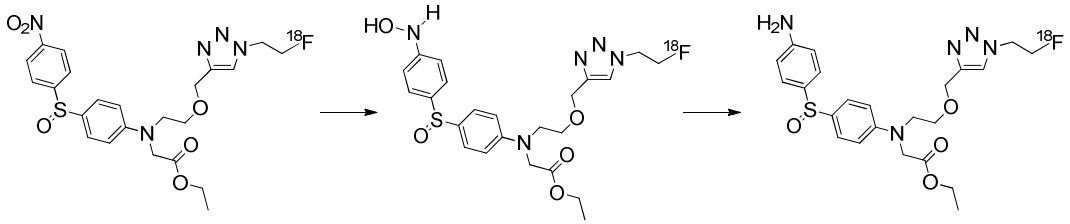

Scheme 5-1: Possible reduction pathway of [^{18}F]2.16

5.3 Experimental

5.3.1 Materials and methods

Solvents were purchased from MERCK and used as received. Reagents were purchased from Sigma-Aldrich and used without further purification.

For metabolism studies the rat S9 liver fractions were bought from Sigma-Aldrich and were stored at -78°C. For the analysis a Shimadzu HPLC with a 20µL injection loop was used. The UV was measured using a SPD-20A UV-Vis detector set at 254nm and the radioactivity was detected using a Bioscan FC-4000 dual BGO PET metabolite coincidence detector. Two LC-20AD solvent pumps were used for high pressure mixing of the mobile phase. The stationary phase was a Phenomenex Gemini NX C-18, 5µ RP column, 150x4.6mm. The mobile phases used were acetonitrile (A) and water (B) with 0.1% formic acid. The flow rate was 0.5mL/min with a gradient elution technique used

for analysis: 0 min, 5% A; 0-8min 5-90% A; 8-12min, 90% A; 12-15min: 90-5% A; 15-18min: 5% A.

5.3.2 Lipophilicity studies

LogP values were measure by mixing 1mg of cold standard into 1 gram each of water and octanol in a test tube. The test tube was vortexed for 3 minutes at room temperature before they were centrifuged for 5 minutes at 10,000 rpm. A 5µL aliquot from each layer was injected onto the HPLC system and the partition coefficient was calculated from the ratio of the peak areas from the octanol compared to that of the water.

5.3.3 Metabolism studies in S9 liver fractions

Four time points (30, 60, 90 and 120 minutes) were used to measure the tracer stability in the assay. For each time point a solution of 300µL was used, consisting of the S9 liver fraction, an NADPH generating system and the reformulated radiotracer was incubated at 37°C in an eppendorf tube. Once the required incubation time was reached the reaction was quenched using methanol, the solution was centrifuged and analysed by metabolite HPLC. Experiments were performed in duplicate.

The NADPH generating system was produced by dissolving of glucose 6-phosphate (37.2mg, 0.132mmol), NADP (39.8mg, 0.052mmol) and 11.5U of glucose 6 phosphate dehydrogenase in potassium phosphate (4mL, 100mM, pH 7.4). Magnesium chloride hexahydrate (26.8mg, 0.132mmol) in water (1mL) was added to this solution and the mixture was stored on ice.

The 300µL solution used for the time point consisted of 15µL of rat S9 liver fraction (20mg/mL), 40µL of the NADPH generating system, 15µL of the reformulated

radiotracer and 230µL of 100mM potassium phosphate buffer at pH 7.4. To neutralise quench the reaction after incubation 300µL of Methanol was added. The sample was then centrifuged for 10min at 11, 000rpm and 20µLof the supernatant was injected into the metabolite HPLC system.

6 Conclusion

The structural modification made to the lead compound SO501 (**1.15**) developed by Dr. Evelyn Laurens including the incorporation of propargyl groups, PEG chains and different ester groups was successfully complete. The modifications allowed the compounds to be click chemistry radiolabelled. The radiotracers **[^{18}F]2.16, [^{18}F]2.26, [^{18}F]2.36, [^{18}F]2.43, [^{18}F]2.53** and **[^{18}F]2.63** were successfully prepared from their respective precursors **2.15**, **2.25**, **2.35**, **2.42**, **2.52** and **2.62.** The cold standards were also prepared from the same precursors allowing for the identification of the radiotracers.

The radiolabelling experiments utilised click chemistry with the compound **[^{18}F]2.72** and a copper catalyst to form the radiotracers **[^{18}F]2.16, [^{18}F]2.26, [^{18}F]2.36, [^{18}F]2.43, [^{18}F]2.53** and **[^{18}F]2.63** from the precursors **2.15**, **2.25**, **2.35**, **2.42**, **2.52** and **2.62** with yields of 11%, 10%, 25%, 5%, 4% and 4%.

In-vivo studies using SK-RC-52 tumours implanted into BALB/c nude mice showed that only the radiotracer **[^{18}F]2.16** had retention over time in large tumours, with the other 4 tracers **[^{18}F]2.26, [^{18}F]2.36, [^{18}F]2.43** and **[^{18}F]2.53** exhibiting fast clearance. **[^{18}F]2.16** and **[^{18}F]2.53** were the only radiotracers to have an ending tumour to muscle ratio over 2 during the 120minutes PET imaging studies.

Partition coefficient studies revealed that the radiotracers **[^{18}F]2.16, [^{18}F]2.26, [^{18}F]2.36, [^{18}F]2.43** and **[^{18}F]2.53** had logP values of 0.95, 1.77, 1.90, 1.66 and 0.89. The three tracers **[^{18}F]2.26, [^{18}F]2.36** and **[^{18}F]2.43** had logP values between the ideal range of 1.5 to 3 however, it was the 2 tracers **[^{18}F]2.16** and **[^{18}F]2.53** that exhibited the best performance *in-vivo.*

A metabolism study performed on **[^{18}F]2.16** showed that it underwent phase 1 metabolism in the presence of S9 rat liver fractions and an NADPH generating system, with metabolic half-life of 148minutes.

6.1 Comparison to [^{18}F]SO501 (1.15)

The aim of the project was to improve upon the radiolabelling reliability of **[^{18}F]1.15** by changing its radiolabelling method from substitution-based radiochemistry to click chemistry. This aim was achieved with yields that were up to 25% non-decay corrected compared to 2.5% for **[^{18}F]1.15**.

Despite the improvement in radiolabelling yields the in-vivo imaging did not maintain the same results compared to those of **[^{18}F]1.15**. **[^{18}F]1.15** had a maximum tumour to muscle ratio of 3.3 compared to **[^{18}F]2.16** and **[^{18}F]2.53** with ratios of 2.06 and 2.34

respectively. **[^{18}F]2.16** was the only radiotracer that showed uptake in its TACs however the rate of uptake was lower than **[^{18}F]1.15**.

This project therefore achieved one of it's aims of increasing the radiochemical yields of the lead compound **[^{18}F]1.15**, however it failed to achieve the second aim of maintaining imaging quality and radiotracer uptake. This is most likely due to the triazole group utilised in click chemistry which has had a negative impact on the uptake of the radiotracers into hypoxic tissue.

7 References

1. Laurens, E. Synthesis and biological analysis of novel Fluorine-18 positron emission tomography (PET) imaging agents for hypoxic tissues in tumours. The University of Melbourne, 2012.
2. Lewis, J. S.; Welch, M. J., PET imaging of hypoxia. *Q J Nucl Med* **2001,** *45* (2), 183-188.
3. Vaupel, P.; Höckel, M.; Mayer, A., Detection and Characterization of Tumor Hypoxia Using pO2 Histography. *Antioxidants & Redox Signaling* **2007,** *9* (8), 1221-1236.
4. Bruehlmeier, M.; Roelcke, U.; Schubiger, P. A.; Ametamey, S. M., Assessment of hypoxia and perfusion in human brain tumors using PET with 18F-fluoromisonidazole and 15O-H2O. *Journal of nuclear medicine : official publication, Society of Nuclear Medicine* **2004,** *45 11*, 1851-9.
5. Padhani, A. R.; Krohn, K. A.; Lewis, J. S.; Alber, M., Imaging oxygenation of human tumours. *European Radiology* **2007,** *17* (4), 861-72.
6. Thomson, P.; Naylor, M. A.; Stratford, M. R. L.; Lewis, G.; Hill, S.; Patel, K. B.; Wardman, P.; Davis, P. D., Hypoxia-driven elimination of thiopurines from their nitrobenzyl prodrugs. *Bioorganic & Medicinal Chemistry Letters* **2007,** *17* (15), 4320-4322.
7. Wyss, M. T.; Honer, M.; Schubiger, P. A.; Ametamey, S. M., NanoPET imaging of [(18)F]fluoromisonidazole uptake in experimental mouse tumours. *European journal of nuclear medicine and molecular imaging* **2006,** *33* (3), 311-8.

8. Brizel, D. M.; Sibley, G. S.; Prosnitz, L. R.; Scher, R. L.; Dewhirst, M. W., Tumor hypoxia adversely affects the prognosis of carcinoma of the head and neck. *International journal of radiation oncology, biology, physics* **1997,** *38* (2), 285-9.
9. Eschmann, S. M.; Paulsen, F.; Reimold, M.; Dittmann, H.; Welz, S.; Reischl, G.; Machulla, H. J.; Bares, R., Prognostic impact of hypoxia imaging with 18F-misonidazole PET in non-small cell lung cancer and head and neck cancer before radiotherapy. *J Nucl Med* **2005,** *46* (2), 253-60.
10. Denny, W. A., The role of hypoxia-activated prodrugs in cancer therapy. *The Lancet. Oncology* **2000,** *1* (1), 25-9.
11. Bentzen, L.; Keiding, S.; Horsman, M. R.; Gronroos, T.; Hansen, S. B.; Overgaard, J., Assessment of hypoxia in experimental mice tumours by [18F]fluoromisonidazole PET and pO2 electrode measurements. Influence of tumour volume and carbogen breathing. *Acta oncologica (Stockholm, Sweden)* **2002,** *41* (3), 304-12.
12. Gronroos, T.; Bentzen, L.; Marjamaki, P.; Murata, R.; Horsman, M. R.; Keiding, S.; Eskola, O.; Haaparanta, M.; Minn, H.; Solin, O., Comparison of the biodistribution of two hypoxia markers [18F]FETNIM and [18F]FMISO in an experimental mammary carcinoma. *European journal of nuclear medicine and molecular imaging* **2004,** *31* (4), 513-20.
13. Krause, B. J.; Beck, R.; Souvatzoglou, M.; Piert, M., PET and PET/CT studies of tumor tissue oxygenation. *Q J Nucl Med M* **2006,** *50* (1), 28-43.
14. Vaupel, P.; Schlenger, K.; Knoop, C.; Hockel, M., Oxygenation of human tumors: evaluation of tissue oxygen distribution in breast cancers by computerized O2 tension measurements. *Cancer research* **1991,** *51* (12), 3316-22.
15. Al-Waili, N. S.; Butler, G. J., A combination of radiotherapy, nitric oxide and a hyperoxygenation sensitizing protocol for brain malignant tumor treatment. *Medical hypotheses* **2007,** *68* (3), 528-37.
16. Minn, H.; Gronroos, T. J.; Komar, G.; Eskola, O.; Lehtio, K.; Tuomela, J.; Seppanen, M.; Solin, O., Imaging of tumor hypoxia to predict treatment sensitivity. *Current pharmaceutical design* **2008,** *14* (28), 2932-42.
17. Zimny, M.; Gagel, B.; DiMartino, E.; Hamacher, K.; Coenen, H. H.; Westhofen, M.; Eble, M.; Buell, U.; Reinartz, P., FDG--a marker of tumour hypoxia? A comparison with [18F]fluoromisonidazole and pO2-polarography in metastatic head and neck cancer. *European journal of nuclear medicine and molecular imaging* **2006,** *33* (12), 1426-31.
18. Rockwell, S.; Dobrucki, I. T.; Kim, E. Y.; Marrison, S. T.; Vu, V. T., Hypoxia and radiation therapy: past history, ongoing research, and future promise. *Curr Mol Med* **2009,** *9* (4), 442-458.
19. Keyer, K.; Imlay, J. A., Superoxide accelerates DNA damage by elevating free-iron levels. *Proc Natl Acad Sci U S A* **1996,** *93* (24), 13635-13640.
20. Piert, M.; Machulla, H. J.; Picchio, M.; Reischl, G.; Ziegler, S.; Kumar, P.; Wester, H. J.; Beck, R.; McEwan, A. J.; Wiebe, L. I.; Schwaiger, M., Hypoxia-specific tumor imaging with 18F-fluoroazomycin arabinoside. *J Nucl Med* **2005,** *46* (1), 106-13.
21. Gagel, B.; Reinartz, P.; Dimartino, E.; Zimny, M.; Pinkawa, M.; Maneschi, P.; Stanzel, S.; Hamacher, K.; Coenen, H. H.; Westhofen, M.; Bull, U.; Eble, M. J., pO(2) Polarography versus positron emission tomography ([(18)F] fluoromisonidazole, [(18)F]-2-fluoro-2'-deoxyglucose). An appraisal of radiotherapeutically relevant

hypoxia. *Strahlentherapie und Onkologie : Organ der Deutschen Rontgengesellschaft ... [et al]* **2004,** *180* (10), 616-22.
22. Tercel, M.; Lee, A. E.; Hogg, A.; Anderson, R. F.; Lee, H. H.; Siim, B. G.; Denny, W. A.; Wilson, W. R., Hypoxia-Selective Antitumor Agents. 16. Nitroarylmethyl Quaternary Salts as Bioreductive Prodrugs of the Alkylating Agent Mechlorethamine. *Journal of Medicinal Chemistry* **2001,** *44* (21), 3511-3522.
23. Gronroos, T.; Minn, H., Imaging of tumour hypoxia using PET and 18F-labelled tracers: biology meets technology. *European journal of nuclear medicine and molecular imaging* **2007,** *34* (10), 1563-5.
24. Graeber, T. G.; Osmanian, C.; Jacks, T.; Housman, D. E.; Koch, C. J.; Lowe, S. W.; Giaccia, A. J., Hypoxia-mediated selection of cells with diminished apoptotic potential in solid tumours. *Nature* **1996,** *379* (6560), 88-91.
25. Shweiki, D.; Itin, A.; Soffer, D.; Keshet, E., Vascular endothelial growth factor induced by hypoxia may mediate hypoxia-initiated angiogenesis. *Nature* **1992,** *359* (6398), 843-5.
26. Hockel, M.; Vaupel, P., Tumor hypoxia: definitions and current clinical, biologic, and molecular aspects. *Journal of the National Cancer Institute* **2001,** *93* (4), 266-76.
27. Sun, Z. Y.; Botros, E.; Su, A. D.; Kim, Y.; Wang, E.; Baturay, N. Z.; Kwon, C. H., Sulfoxide-containing aromatic nitrogen mustards as hypoxia-directed bioreductive cytotoxins. *J Med Chem* **2000,** *43* (22), 4160-8.
28. Ang, K. K., More Lessons Learned From the Suffocation of Hypoxia. *Journal of Clinical Oncology* **2010,** *28* (18), 2941-2943.
29. Hay, M. P.; Wilson, W. R.; Moselen, J. W.; Palmer, B. D.; Denny, W. A., Hypoxia-selective antitumor agents. 8. Bis(nitroimidazolyl)alkanecarboxamides: a new class of hypoxia-selective cytotoxins and hypoxic cell radiosensitizers. *Journal of Medicinal Chemistry* **1994,** *37* (3), 381-391.
30. Brown, J. M., Exploiting the hypoxic cancer cell: mechanisms and therapeutic strategies. *Molecular medicine today* **2000,** *6* (4), 157-62.
31. Stone, H. B.; Brown, J. M.; Phillips, T. L.; Sutherland, R. M., Oxygen in human tumors: correlations between methods of measurement and response to therapy. Summary of a workshop held November 19-20, 1992, at the National Cancer Institute, Bethesda, Maryland. *Radiation research* **1993,** *136* (3), 422-34.
32. Hockel, M.; Knoop, C.; Schlenger, K.; Vorndran, B.; Knapstein, P. G.; Vaupel, P., Intratumoral pO2 histography as predictive assay in advanced cancer of the uterine cervix. *Advances in experimental medicine and biology* **1994,** *345*, 445-50.
33. Rajendran, J. G.; Hendrickson, K. R.; Spence, A. M.; Muzi, M.; Krohn, K. A.; Mankoff, D. A., Hypoxia imaging-directed radiation treatment planning. *European journal of nuclear medicine and molecular imaging* **2006,** *33 Suppl 1*, 44-53.
34. Parliament, M. B.; Chapman, J. D.; Urtasun, R. C.; McEwan, A. J.; Golberg, L.; Mercer, J. R.; Mannan, R. H.; Wiebe, L. I., Non-invasive assessment of human tumour hypoxia with 123I-iodoazomycin arabinoside: preliminary report of a clinical study. *British journal of cancer* **1992,** *65* (1), 90-5.
35. Tochon-Danguy, H. J.; Sachinidis, J. I.; Chan, F.; Chan, J. G.; Hall, C.; Cher, L.; Stylli, S.; Hill, J.; Kaye, A.; Scott, A. M., Imaging and quantitation of the hypoxic cell fraction of viable tumor in an animal model of intracerebral high grade glioma using [18F]fluoromisonidazole (FMISO). *Nuclear medicine and biology* **2002,** *29* (2), 191-7.

36. Parliament, M. B.; Wiebe, L. I.; Franko, A. J., Nitroimidazole adducts as markers for tissue hypoxia: mechanistic studies in aerobic normal tissues and tumour cells. *British journal of cancer* **1992,** *66* (6), 1103-8.
37. Chapman, J. D.; Engelhardt, E. L.; Stobbe, C. C.; Schneider, R. F.; Hanks, G. E., Measuring hypoxia and predicting tumor radioresistance with nuclear medicine assays. *Radiotherapy and oncology : journal of the European Society for Therapeutic Radiology and Oncology* **1998,** *46* (3), 229-37.
38. Czernin, J.; Weber, W. A.; Herschman, H. R., Molecular imaging in the development of cancer therapeutics. *Annual review of medicine* **2006,** *57*, 99-118.
39. Burdette, D. J. Very High Resolution Small Animal PET. 2005.
40. Rischin, D.; Hicks, R. J.; Fisher, R.; Binns, D.; Corry, J.; Porceddu, S.; Peters, L. J., Prognostic significance of [18F]-misonidazole positron emission tomography-detected tumor hypoxia in patients with advanced head and neck cancer randomly assigned to chemoradiation with or without tirapazamine: a substudy of Trans-Tasman Radiation Oncology Group Study 98.02. *Journal of clinical oncology : official journal of the American Society of Clinical Oncology* **2006,** *24* (13), 2098-104.
41. Vikram, D. S.; Zweier, J. L.; Kuppusamy, P., Methods for noninvasive imaging of tissue hypoxia. *Antioxid Redox Signal* **2007,** *9* (10), 1745-56.
42. Lodge, M. A.; Braess, H.; Mahmoud, F.; Suh, J.; Englar, N.; Geyser-Stoops, S.; Jenkins, J.; Bacharach, S. L.; Dilsizian, V., Developments in nuclear cardiology: transition from single photon emission computed tomography to positron emission tomography-computed tomography. *The Journal of invasive cardiology* **2005,** *17* (9), 491-6.
43. Czernin, J.; Phelps, M. E., Positron emission tomography scanning: current and future applications. *Annual review of medicine* **2002,** *53*, 89-112.
44. Shreve, P. D.; Steventon, R. S.; Deters, E. C.; Kison, P. V.; Gross, M. D.; Wahl, R. L., Oncologic diagnosis with 2-[fluorine-18]fluoro-2-deoxy-D-glucose imaging: dual-head coincidence gamma camera versus positron emission tomographic scanner. *Radiology* **1998,** *207* (2), 431-7.
45. Chatziioannou, A. F., Instrumentation for molecular imaging in preclinical research: Micro-PET and Micro-SPECT. *Proceedings of the American Thoracic Society* **2005,** *2* (6), 533-6, 510-11.
46. Ter-Pogossian, M. M., Cyclotron produced short-lived radioactive isotopes in nuclear medicine. *J Nucl Med* **1967,** *8* (5), 374.
47. Imam, S.; El-Maghraby, T.; Alavi, A.; Basu, S., Advances in PET radiopharmaceuticals. *World Journal of Nuclear Medicine* **2009,** *8* (1), 5-24.
48. Bache, M.; Kappler, M.; Said, H. M.; Staab, A.; Vordermark, D., Detection and specific targeting of hypoxic regions within solid tumors: current preclinical and clinical strategies. *Current medicinal chemistry* **2008,** *15* (4), 322-38.
49. B., B. E. F. R., *Table of radioactive isotopes*. John Wiley and Sons: New York, 1986.
50. Wester, H. J., *Munich Molecular Imaging Handbook Series*. Scintomics Print Media and Publishing: Furstenfeldbruck, Germany, 2010; Vol. 1.
51. McBride, W. J.; Sharkey, R. M.; Karacay, H.; D'Souza, C. A.; Rossi, E. A.; Laverman, P.; Chang, C. H.; Boerman, O. C.; Goldenberg, D. M., A novel method of 18F radiolabeling for PET. *J Nucl Med* **2009,** *50* (6), 991-8.
52. Kilbourn, M. R., *Fluorine-18 Labeling of Radiopharmaceuticals*. National Academy Press: Ann Arbor, Michigan, 1990.

53. Myers, R., The biological application of small animal PET imaging. *Nuclear medicine and biology* **2001,** *28* (5), 585-593.
54. Hamacher, K.; Coenen, H. H.; Stocklin, G., Efficient stereospecific synthesis of no-carrier-added 2-[18F]-fluoro-2-deoxy-D-glucose using aminopolyether supported nucleophilic substitution. *J Nucl Med* **1986,** *27* (2), 235-8.
55. Falzon, C. L. Synthesis, Radiolabelling and Evaluation of Novel Imaging Agents for Hypoxic Tissue. The University of Melbourne, 2006.
56. Clark, J. C.; Silvester, D. J., A cyclotron method for the production of fluorine-18. *The International journal of applied radiation and isotopes* **1966,** *17* (3), 151-4.
57. Chitneni, S. K.; Palmer, G. M.; Zalutsky, M. R.; Dewhirst, M. W., Molecular imaging of hypoxia. *J Nucl Med* **2011,** *52* (2), 165-8.
58. Chapman, J. D.; Lee, J.; Meeker, B. E., Keynote address: cellular reduction of nitroimidazole drugs: potential for selective chemotherapy and diagnosis of hypoxic cells. *International journal of radiation oncology, biology, physics* **1989,** *16* (4), 911-7.
59. Chatziioannou, A. F., Molecular imaging of small animals with dedicated PET tomographs. *European journal of nuclear medicine and molecular imaging* **2002,** *29* (1), 98-114.
60. Anderson, C. J.; Connett, J. M.; Schwarz, S. W.; Rocque, P. A.; Guo, L. W.; Philpott, G. W.; Zinn, K. R.; Meares, C. F.; Welch, M. J., Copper-64-labeled antibodies for PET imaging. *J Nucl Med* **1992,** *33* (9), 1685-91.
61. Fujibayashi, Y.; Cutler, C. S.; Anderson, C. J.; McCarthy, D. W.; Jones, L. A.; Sharp, T.; Yonekura, Y.; Welch, M. J., Comparative studies of Cu-64-ATSM and C-11-acetate in an acute myocardial infarction model: ex vivo imaging of hypoxia in rats. *Nuclear medicine and biology* **1999,** *26* (1), 117-21.
62. Fujibayashi, Y.; Taniuchi, H.; Yonekura, Y.; Ohtani, H.; Konishi, J.; Yokoyama, A., Copper-62-ATSM: a new hypoxia imaging agent with high membrane permeability and low redox potential. *J Nucl Med* **1997,** *38* (7), 1155-60.
63. Lewis, J. S.; McCarthy, D. W.; McCarthy, T. J.; Fujibayashi, Y.; Welch, M. J., Evaluation of 64Cu-ATSM in vitro and in vivo in a hypoxic tumor model. *J Nucl Med* **1999,** *40* (1), 177-83.
64. Lewis, J. S.; Sharp, T. L.; Laforest, R.; Fujibayashi, Y.; Welch, M. J., Tumor uptake of copper-diacetyl-bis(N(4)-methylthiosemicarbazone): effect of changes in tissue oxygenation. *J Nucl Med* **2001,** *42* (4), 655-61.
65. Markus, R.; Donnan, G. A.; Kazui, S.; Read, S.; Hirano, T.; Scott, A. M.; O'Keefe, G. J.; Tochon-Danguy, H. J.; Sachinidis, J. I.; Reutens, D. C., Statistical parametric mapping of hypoxic tissue identified by [(18)F]fluoromisonidazole and positron emission tomography following acute ischemic stroke. *NeuroImage* **2002,** *16* (2), 425-33.
66. Brady, F.; Luthra, S. K.; Brown, G. D.; Osman, S.; Aboagye, E.; Saleem, A.; Price, P. M., Radiolabelled tracers and anticancer drugs for assessment of therapeutic efficacy using PET. *Current pharmaceutical design* **2001,** *7* (18), 1863-92.
67. Nunn, A.; Linder, K.; Strauss, H. W., Nitroimidazoles and imaging hypoxia. *European journal of nuclear medicine* **1995,** *22* (3), 265-80.
68. Foo, S. S.; Abbott, D. F.; Lawrentschuk, N.; Scott, A. M., Functional imaging of intratumoral hypoxia. *Molecular imaging and biology : MIB : the official publication of the Academy of Molecular Imaging* **2004,** *6* (5), 291-305.

69. Lee, S. T.; Scott, A. M., Hypoxia positron emission tomography imaging with 18f-fluoromisonidazole. *Seminars in nuclear medicine* **2007,** *37* (6), 451-61.
70. Krohn, K. A.; Link, J. M.; Mason, R. P., Molecular imaging of hypoxia. *J Nucl Med* **2008,** *49 Suppl 2*, 129s-48s.
71. Read, S. J.; Hirano, T.; Abbott, D. F.; Markus, R.; Sachinidis, J. I.; Tochon-Danguy, H. J.; Chan, J. G.; Egan, G. F.; Scott, A. M.; Bladin, C. F.; McKay, W. J.; Donnan, G. A., The fate of hypoxic tissue on 18F-fluoromisonidazole positron emission tomography after ischemic stroke. *Annals of neurology* **2000,** *48* (2), 228-35.
72. Friedman, O. M.; Boger, E., New Nitrogen Mustards for "Toxagenic" Anti-cancer Agents1a,b. *Journal of the American Chemical Society* **1956,** *78* (18), 4659-4662.
73. Valu, K. K.; Gourdie, T. A.; Boritzki, T. J.; Gravatt, G. L.; Baguley, B. C.; Wilson, W. R.; Wakelin, L. P. G.; Woodgate, P. D.; Denny, W. A., DNA-directed alkylating agents. 3. Structure-activity relationships for acridine-linked aniline mustards: consequences of varying the length of the linker chain. *Journal of Medicinal Chemistry* **1990,** *33* (11), 3014-3019.
74. Johansson, E.; Parkinson, G. N.; Denny, W. A.; Neidle, S., Studies on the nitroreductase prodrug-activating system. Crystal structures of complexes with the inhibitor dicoumarol and dinitrobenzamide prodrugs and of the enzyme active form. *J Med Chem* **2003,** *46* (19), 4009-20.
75. Anlezark, G. M.; Melton, R. G.; Sherwood, R. F.; Wilson, W. R.; Denny, W. A.; Palmer, B. D.; Knox, R. J.; Friedlos, F.; Williams, A., Bioactivation of dinitrobenzamide mustards by an E. coli B nitroreductase. *Biochemical pharmacology* **1995,** *50* (5), 609-18.
76. Kwon, C. H.; Blanco, D. R.; Baturay, N., p-(Methylsulfinyl)phenyl nitrogen mustard as a novel bioreductive prodrug selective against hypoxic tumors. *J Med Chem* **1992,** *35* (11), 2137-9.
77. Falzon, C. L.; Ackermann, U.; Spratt, N.; Tochon-Danguy, H. J.; White, J.; Howells, D.; Scott, A. M., F-18 labelled N,N-bis-haloethylamino-phenylsulfoxides — a new class of compounds for the imaging of hypoxic tissue. *Journal of Labelled Compounds and Radiopharmaceuticals* **2006,** *49* (12), 1089-1103.
78. Rowe, C. C.; Ackerman, U.; Browne, W.; Mulligan, R.; Pike, K. L.; O'Keefe, G.; Tochon-Danguy, H.; Chan, G.; Berlangieri, S. U.; Jones, G.; Dickinson-Rowe, K. L.; Kung, H. P.; Zhang, W.; Kung, M. P.; Skovronsky, D.; Dyrks, T.; Holl, G.; Krause, S.; Friebe, M.; Lehman, L.; Lindemann, S.; Dinkelborg, L. M.; Masters, C. L.; Villemagne, V. L., Imaging of amyloid beta in Alzheimer's disease with 18F-BAY94-9172, a novel PET tracer: proof of mechanism. *The Lancet. Neurology* **2008,** *7* (2), 129-35.
79. Glaser, M.; Årstad, E., "Click Labeling" with 2-[18F]Fluoroethylazide for Positron Emission Tomography. *Bioconjugate Chemistry* **2007,** *18* (3), 989-993.
80. Laurens, E.; Yeoh, S. D.; Rigopoulos, A.; Cao, D.; Cartwright, G. A.; O'Keefe, G. J.; Tochon-Danguy, H. J.; White, J. M.; Scott, A. M.; Ackermann, U., Radiolabelling and evaluation of novel haloethylsulfoxides as PET imaging agents for tumor hypoxia. *Nuclear medicine and biology* **2012,** *39* (6), 871-82.
81. McMurray, J., *Organic Chemistry 4th Ed*. 4th Ed ed.; Brooks/Cole Publishing Companu: 1995.
82. Bruckenstein, S. K., M.; Elving, P. J., *Treatise on Analytical Chemistry*. Wiley International: New York, 1959.

83. Adams, D.; Clark, J., *Nucleophilic Routes to Selectively Fluorinated Aromatics*. 1999; Vol. 28, p 225-231.
84. Walsh, J. C.; Kolb, H. C., Applications of click chemistry in radiopharmaceutical development. *Chimia* **2010,** *64* (1-2), 29-33.
85. Ackermann, U.; O'Keefe, G.; Lee, S.-T.; Rigopoulos, A.; Cartwright, G.; Sachinidis, J. I.; Scott, A. M.; Tochon-Danguy, H. J., Synthesis of a [18F]fluoroethyltriazolylthymidine radiotracer from [18F]2-fluoroethyl azide and 5-ethynyl-2'-deoxyuridine. *Journal of Labelled Compounds and Radiopharmaceuticals* **2011,** *54* (5), 260-266.
86. Kolb, H. C.; Finn, M. G.; Sharpless, K. B., Click Chemistry: Diverse Chemical Function from a Few Good Reactions. *Angewandte Chemie (International ed. in English)* **2001,** *40* (11), 2004-2021.
87. Jacobson, O.; Kiesewetter, D. O.; Chen, X., Fluorine-18 Radiochemistry, Labeling Strategies and Synthetic Routes. *Bioconjugate Chemistry* **2015,** *26* (1), 1-18.
88. Moses, J. E.; Moorhouse, A. D., The growing applications of click chemistry. *Chemical Society reviews* **2007,** *36* (8), 1249-62.
89. Sharpless, K. B.; Manetsch, R., In situ click chemistry: a powerful means for lead discovery. *Expert opinion on drug discovery* **2006,** *1* (6), 525-38.
90. Rostovtsev, V. V.; Green, L. G.; Fokin, V. V.; Sharpless, K. B., A stepwise huisgen cycloaddition process: copper(I)-catalyzed regioselective "ligation" of azides and terminal alkynes. *Angewandte Chemie (International ed. in English)* **2002,** *41* (14), 2596-9.
91. Zhang, L.; Chen, X.; Xue, P.; Sun, H. H.; Williams, I. D.; Sharpless, K. B.; Fokin, V. V.; Jia, G., Ruthenium-catalyzed cycloaddition of alkynes and organic azides. *J Am Chem Soc* **2005,** *127* (46), 15998-9.
92. Becer, C. R.; Hoogenboom, R.; Schubert, U. S., Click chemistry beyond metal-catalyzed cycloaddition. *Angewandte Chemie (International ed. in English)* **2009,** *48* (27), 4900-8.
93. Ackermann, U.; Plougastel, L.; Goh, Y. W.; Yeoh, S. D.; Scott, A. M., Improved synthesis of [18F]FLETT via a fully automated vacuum distillation method for [18F]2-fluoroethyl azide purification. *Applied Radiation and Isotopes* **2014,** *94*, 72-76.
94. Lara, P. C.; Lloret, M.; Clavo, B.; Apolinario, R. M.; Henríquez-Hernández, L. A.; Bordón, E.; Fontes, F.; Rey, A., Severe hypoxia induces chemo-resistance in clinical cervical tumors through MVP over-expression. *Radiation oncology (London, England)* **2009,** *4*, 29.
95. Sasabe, E.; Zhou, X.; Li, D.; Oku, N.; Yamamoto, T.; Osaki, T., The involvement of hypoxia-inducible factor-1alpha in the susceptibility to gamma-rays and chemotherapeutic drugs of oral squamous cell carcinoma cells. *International journal of cancer* **2007,** *120* (2), 268-77.
96. Myers, R.; Hume, S., Small animal PET. *European neuropsychopharmacology : the journal of the European College of Neuropsychopharmacology* **2002,** *12* (6), 545-55.
97. Cherry, S. R., The 2006 Henry N. Wagner Lecture: Of mice and men (and positrons)--advances in PET imaging technology. *J Nucl Med* **2006,** *47* (11), 1735-45.
98. Koo, V.; Hamilton, P. W.; Williamson, K., Non-invasive in vivo imaging in small animal research. *Cellular oncology : the official journal of the International Society for Cellular Oncology* **2006,** *28* (4), 127-39.

99. Tornai, M.; J Jaszczak, R.; Turkington, T.; Coleman, E., *Small-animal PET: Advent of a new era of PET research*. 1999; Vol. 40, p 1176-9.
100. Tai, Y. C.; Laforest, R., Instrumentation aspects of animal PET. *Annual review of biomedical engineering* **2005,** *7*, 255-85.
101. Cutler, P. D.; Cherry, S. R.; Hoffman, E. J.; Digby, W. M.; Phelps, M. E., Design features and performance of a PET system for animal research. *J Nucl Med* **1992,** *33* (4), 595-604.
102. Ziegler, S. I.; Pichler, B. J.; Boening, G.; Rafecas, M.; Pimpl, W.; Lorenz, E.; Schmitz, N.; Schwaiger, M., A prototype high-resolution animal positron tomograph with avalanche photodiode arrays and LSO crystals. *European journal of nuclear medicine* **2001,** *28* (2), 136-43.
103. Hume, S. P.; Myers, R., Dedicated small animal scanners: a new tool for drug development? *Current pharmaceutical design* **2002,** *8* (16), 1497-511.
104. Wessels, J. T.; Busse, A. C.; Mahrt, J.; Dullin, C.; Grabbe, E.; Mueller, G. A., In vivo imaging in experimental preclinical tumor research--a review. *Cytometry. Part A : the journal of the International Society for Analytical Cytology* **2007,** *71* (8), 542-9.
105. Dissoki, S.; Eshet, R.; Billauer, H.; Mishani, E., Modified PEG-anilinoquinazoline derivatives as potential EGFR PET agents. *Journal of Labelled Compounds and Radiopharmaceuticals* **2009,** *52* (2), 41-52.
106. Yamamoto, F.; Aoki, M.; Furusawa, Y.; Ando, K.; Kuwabara, Y.; Masuda, K.; Sasaki, S.; Maeda, M., Synthesis and evaluation of 4-bromo-1-(3-[18F]fluoropropyl)-2-nitroimidazole with a low energy LUMO orbital designed as brain hypoxia-targeting imaging agent. *Biological & pharmaceutical bulletin* **2002,** *25* (5), 616-21.
107. Lee, S. Y.; Choe, Y. S.; Kim, D. H.; Park, B. N.; Kim, S. E.; Choi, Y.; Lee, K. H.; Lee, J.; Kim, B. T., A simple and efficient in vitro method for metabolism studies of radiotracers. *Nuclear medicine and biology* **2001,** *28* (4), 391-5.
108. Minchin, R. F.; Ho, P. C.; Boyd, M. R., Reductive metabolism of nitrofurantoin by rat lung and liver in vitro. *Biochemical pharmacology* **1986,** *35* (4), 575-80.
109. Delaforge, M., Importance of metabolism in pharmacological studies: possible in vitro predictability. *Nuclear medicine and biology* **1998,** *25* (8), 705-9.
110. Forti, G. C.; Paolini, M.; Hrelia, P.; Corsi, C.; Biagi, G. L.; Bronzetti, G., NADPH-generating system: influence on microsomal mono-oxygenase stability during incubation for the liver-microsomal assay with rat and mouse S9 fractions. *Mutation research* **1984,** *129* (3), 281-97.
111. Vraka, C.; Nics, L.; Wagner, K.-H.; Hacker, M.; Wadsak, W.; Mitterhauser, M., LogP, a yesterday's value? *Nuclear medicine and biology* **2017,** *50*.